



UNIL | Université de Lausanne

Unicentre

CH-1015 Lausanne

<http://serval.unil.ch>

---

*Year : 2017*

## Fluorine, chlorine, and OH content in biotites during contact metamorphism

Siron Guillaume

Siron Guillaume, 2017, Fluorine, chlorine, and OH content in biotites during contact metamorphism

Originally published at : Thesis, University of Lausanne

Posted at the University of Lausanne Open Archive <http://serval.unil.ch>

Document URN : urn:nbn:ch:serval-BIB\_9053B21514AE5

### **Droits d'auteur**

L'Université de Lausanne attire expressément l'attention des utilisateurs sur le fait que tous les documents publiés dans l'Archive SERVAL sont protégés par le droit d'auteur, conformément à la loi fédérale sur le droit d'auteur et les droits voisins (LDA). A ce titre, il est indispensable d'obtenir le consentement préalable de l'auteur et/ou de l'éditeur avant toute utilisation d'une oeuvre ou d'une partie d'une oeuvre ne relevant pas d'une utilisation à des fins personnelles au sens de la LDA (art. 19, al. 1 lettre a). A défaut, tout contrevenant s'expose aux sanctions prévues par cette loi. Nous déclinons toute responsabilité en la matière.

### **Copyright**

The University of Lausanne expressly draws the attention of users to the fact that all documents published in the SERVAL Archive are protected by copyright in accordance with federal law on copyright and similar rights (LDA). Accordingly it is indispensable to obtain prior consent from the author and/or publisher before any use of a work or part of a work for purposes other than personal use within the meaning of LDA (art. 19, para. 1 letter a). Failure to do so will expose offenders to the sanctions laid down by this law. We accept no liability in this respect.



UNIL | Université de Lausanne

Faculté des géosciences et de l'environnement  
Institut des Sciences de la Terre

# **Fluorine, chlorine, and OH content in biotites during contact metamorphism**

Thèse de doctorat

Présenté à la Faculté des géosciences et de l'environnement de  
l'Université de Lausanne par

Guillaume Siron

Master VTESS  
Université de Franche-comté 2012

Jury

Directeur de thèse : Prof. Lukas Baumgartner

Expert interne : Prof. Othmar Müntener

Expert externe: Prof. Simon Harley

Expert externe : Prof. Darrell Henry

Président du jury: Prof. Jean-Luc Epard

Lausanne 2017



## IMPRIMATUR

Vu le rapport présenté par le jury d'examen, composé de

Président de la séance publique :	M. le Professeur Jean-Luc Epard
Président du colloque :	M. le Professeur Jean-Luc Epard
Directeur de thèse :	M. le Professeur Lukas Baumgartner
Expert interne:	M. le Professeur Othmar Müntener
Expert externe :	M. le Professeur Darrell Henry
Expert externe :	M. le Professeur Simon Harley

Le Doyen de la Faculté des géosciences et de l'environnement autorise l'impression de la thèse de

### **Monsieur Guillaume SIRON**

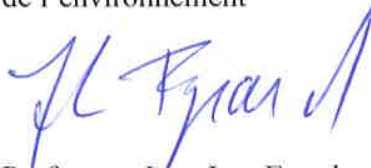
Titulaire d'un  
*Master Vie Terre Environnement Santé Société*  
*de l'Université de Lausanne*

intitulée

### **FLUORINE, CHLORINE, AND OH CONTENT IN BIOTITES DURING CONTACT METAMORPHISM**

Lausanne, le 12 mai 2017

Pour le Doyen de la Faculté des géosciences et  
de l'environnement



Professeur Jean-Luc Epard



## Table of contents

1	Introduction.....	15
1.1	Fluid-rock interactions.....	16
1.1.1	Stable isotopes.....	17
1.1.2	Fluorine and chlorine in metamorphism.....	18
1.2	Water content and the stoichiometry of the hydroxyl site.....	21
1.3	Geological settings.....	22
1.4	New in-situ methods.....	24
1.5	Outline of the thesis.....	26
1.6	References.....	27
2	Biotite Reference Materials for SIMS oxygen isotopes analysis.....	33
2.1	Introduction.....	35
2.2	Biotite reference material.....	36
2.3	Analytical techniques.....	37
2.3.1	Sample preparation.....	37
2.3.2	Electron Microprobe analysis (EPMA).....	38
2.3.3	Laser-heating fluorination.....	39
2.3.4	Secondary Ions Mass Spectrometry (SIMS).....	41
2.4	Results and discussion.....	41
2.4.1	Test for orientation dependent fractionation effects.....	41
2.4.2	$\delta^{18}\text{O}$ homogeneity tests for the 6 biotite RMs for in-situ analyses.....	43
2.4.3	Investigation of the matrix effect on IMF.....	46
2.4.4	Uncertainties.....	51
2.5	Conclusion.....	52
2.6	Acknowledgements.....	53
2.7	References.....	53
3	Channelized igneous fluid infiltration documented in the Torres del Paine contact aureole.....	57
3.1	Introduction.....	59
3.2	Geological setting.....	60
3.3	Methods.....	63
3.4	Sampling strategy.....	64
3.5	Results.....	66
3.5.1	Metamorphism.....	66
3.5.2	Field observations of fluid flow.....	72
3.5.3	Stable isotopes.....	74
3.6	Discussion.....	82
3.6.1	Fluid flow evidences.....	82
3.6.2	Timing of fluid infiltration.....	87
3.7	Conclusion.....	89
3.8	References.....	90
4	Accurate biotite OH-F-Cl determination using Secondary Ion Mass Spectrometry.....	97
4.1	Introduction.....	99
4.2	Analytical techniques.....	100
4.2.1	Electron Probe Micro Analysis (EPMA).....	100

4.2.2	Thermal Conversion Elemental Analyzer (TC/EA) .....	102
4.2.3	Secondary Ion Mass Spectrometry (SIMS) .....	103
4.3	Results and discussion .....	107
4.3.1	Homogeneity test of the RMs .....	107
4.3.2	Crystal orientation test .....	110
4.3.3	Vacuum test .....	113
4.3.4	F and Cl calibration.....	114
4.3.5	H <sub>2</sub> O calibration .....	116
4.3.6	Precision and accuracy for H <sub>2</sub> O, F and Cl measurement.....	118
4.4	Conclusion .....	119
4.5	References.....	120
5	Significance of OH, F and Cl content in biotite during metamorphism of the Western Adamello contact aureole .....	123
5.1	Introduction.....	125
5.2	Geological setting .....	126
5.3	Analytical methods .....	128
5.3.1	Electron Probe Micro-analysis (EPMA).....	128
5.3.2	Secondary Ion Mass Spectrometry (SIMS) .....	129
5.4	Results.....	130
5.4.1	Petrography .....	130
5.4.2	X-ray maps of F and Cl.....	134
5.4.3	H <sub>2</sub> O, F and Cl content of biotite by SIMS analysis .....	137
5.4.4	Variations of Cl and F content .....	140
5.4.5	Substitution for OH content .....	144
5.5	Discussion .....	147
5.6	Conclusion .....	151
5.7	References.....	152
6	Conclusion – Perspectives .....	155
6.2	Summary .....	156
6.3	Perspectives.....	158
7	Appendix.....	161
7.1	Sample description for reference material .....	162
7.2	List of supplementary data in the dropbox link: .....	162
7.3	Water activity – OH content in biotite link in metacarbonates from the Ubehebe Peak contact aureole .....	163
7.3.1	Introduction.....	163
7.3.2	Geological setting .....	163
7.3.3	H <sub>2</sub> O content in phlogopite .....	164
7.3.4	Conclusion .....	166

## Abstract

Fluids play an important role during metamorphism, they are good transport agent and have thus a strong impact on the kinetics of development of metamorphic reactions. The fluid composition is also one of the key parameter to understand the stability of various mineral assemblages. This thesis focus on the in-situ determination of both isotopic and minor element composition of biotite and the equilibrium between the fluid phase and biotite during metamorphism.

This has required the development of a set of biotite reference material of known oxygen isotope and OH-F-Cl composition for in-situ measurement using Secondary Ion Mass Spectrometry. This technique is known to be hampered by instrumental matrix effect for both elemental and isotopic determination. Matrix effect for oxygen isotopes is a function of  $X_{Mg}$  and  $X_F$  and requires a multivariate analysis to accurately determined  $\delta^{18}O$  values of unknown biotites. This can be done with an uncertainty of 0.4‰ (2s) for biotite of the same major element composition (i.e. less than 0.05 deviations in  $X_{Mg}$  from the closest Reference Material (RM)) and 0.5‰ (2s) for biotites of different compositions.  $H_2O$ , fluorine and chlorine content are also hampered by matrix effect. Nevertheless, the last two can be measured using only a second order polynomial fit using measured ion-intensities ( $^{19}F/^{28}Si$  and  $^{35}Cl/^{30}Si$ , respectively) and reference values.  $H_2O$  content exhibit a more complex pattern since the determination of the absolute value involves  $X_{Mg}$  as additional variable to the ion-intensities ( $^{16}O^1H/^{28}Si$ ). It requires a multivariate analysis to properly model the reference value of the set of reference materials (RMs). Both oxygen isotopes and OH-F-Cl measurements does not exhibit variations due to crystal orientation, this allow the determination of these variables in randomly oriented biotites from natural samples.

The similar OH-F-Cl content in biotite from biotite in anhydrous mineral (andalusite) and in the matrix indicate that the O(4) site composition of biotite is maintained after peak evolution and is not reset during cooling. In the case of the Western Adamello contact aureole low grade samples have higher variations than high grade samples. This homogenization trend is explained by the very low kinetic for Cl-OH exchange at low temperature. This low kinetics is in good agreement with the observation of very different absolute values for Cl content of the 5 selected samples. The homogenization of the higher-grade samples is possible since the biotites recrystallize. In particular, Cl seems to be very retentive since the Cl content represent the initial availability of Cl at the grain boundary of the growing biotite from chlorite breakdown reaction, this content cannot be changed unless biotite recrystallize in equilibrium with a fluid of completely different salinity. Fluorine content show quite the same behavior, with the absence of trend related to temperature for absolute value. Nevertheless, it does not exhibit the same homogenization trend than Cl content, this is interpreted has a faster kinetics, supported by the relative comparable size of the F and OH anions

radii (1.33 and 1.38 Ångström, respectively), compare to the large Cl<sup>-</sup> (1.81 Ångström). Both F and Cl content does not show any correlation to X<sub>Mg</sub>, Al<sup>iv</sup> or Ti, we conclude that at these low concentrations (between 0.01 and 0.06wt%) no crystallographic control is exerted. Variations for the OH content in biotite is traditionally interpreted as the consequence of the incorporation of highly coordinated cations in the octahedral site (Ti<sup>4+</sup>, Fe<sup>3+</sup> or Al<sup>3+</sup>), O<sup>2-</sup> being substitute to OH<sup>-</sup> in order to maintain neutral charge. The variations for OH content in the graphite free rocks of the Western Adamello contact aureole does not show any trend related to these cations, here we interpret the OH content in biotite as a function of the water activity during recrystallization of biotites. The biotites with filled O(4) site have been equilibrated under fluid saturated conditions whereas the non-stoichiometric biotites are in samples that have been equilibrated in under-saturated conditions ( $a_{\text{H}_2\text{O}} < 1$ ).

The knowledge of the Cl-OH exchange has been used to track fluid flow in the Torres del Paine contact aureole. The chlorine content in the contact aureole is constant at low values (around 0.01 wt%) but show significantly higher values for some samples close to the intrusion (0.1 - 0.2 wt%). Again, no correlation with X<sub>Mg</sub>, Al<sup>iv</sup> or Ti is observed, crystallographic control is then excluded to explain such variations. Hydrogen isotopes also exhibit change close to the intrusion, with increasing values of the δD to more magmatic signatures (about 80‰). The position of the infiltration front for hydrogen isotopes allow us to calculate, using transport theory, a volume of fluid that infiltrated the surrounding rocks of 4m<sup>3</sup>/m<sup>2</sup> of contact of intrusion. This low amount of fluid is in good agreement with the absence of variations in the oxygen isotopes. We interpret this infiltration of fluid as the result of the crystallization of the first of the three granite, this granite has evidences of saturation such as miarolitic cavities, especially close to the contact. Two other retrogression event can be seen in the metamorphic rocks of the Torres del Paine, first retrograde muscovite and lately chlorite + muscovite replacement of biotite and cordierite. They do not alter the Cl content in biotite due to the very low kinetics of Cl-OH exchange. Using the precise time scale of granite emplacement from previous work, I conclude that all three evidences of fluid flow are due to the nearly continuous exsolution of fluid from the different pulses of granite I.

## Résumé

Les fluides jouent un rôle important au cours du métamorphisme, ils sont bon agent de transport et ont donc un fort impact sur la cinétique de développement des réactions métamorphiques. La composition du fluide est également l'un des paramètres clés pour comprendre la stabilité de divers assemblages minéraux. Cette thèse porte sur la détermination in situ de la composition de certains isotopes et des éléments mineurs (OH-F-Cl) de la biotite et sur l'équilibre entre la phase fluide et la biotite au cours du métamorphisme.

Ceci a nécessité le développement d'un ensemble de matériau de référence de biotite de composition connu à la fois en isotopes de l'oxygène connu et en concentration de OH-F-Cl pour la mesure in situ en utilisant la spectrométrie de masse aux ions secondaires. Cette technique est connue pour être entravée par un fort effet de matrice à la fois pour la détermination élémentaire et isotopique. L'effet de matrice pour les isotopes de l'oxygène est une fonction de  $X_{Mg}$  et  $X_F$  et nécessite une analyse multivariée pour déterminer avec précision des valeurs de  $\delta^{18}O$  de biotites inconnues dans les échantillons naturels. Cela peut se faire avec une incertitude de 0,4 ‰ ( $2\sigma$ ) pour des biotites de même composition en éléments majeurs et 0,5 ‰ ( $2\sigma$ ) pour les biotites de compositions différentes. La teneur en eau, en fluor et en chlore est également entravée par un effet de matrice. Néanmoins, les deux premières peuvent être mesurées en utilisant seulement un fit polynomial de second ordre à partir des intensités d'ions mesurées ( $^{19}F/^{28}Si$  et  $^{35}Cl/^{30}Si$ , respectivement) et des valeurs de référence. La détermination de la teneur en eau présente un profil plus complexe puisque la détermination de la valeur absolue implique  $X_{Mg}$  comme variable supplémentaire aux intensités d'ions ( $^{16}O^1H/^{28}Si$ ). Cela nécessite une analyse multivariée pour modéliser correctement la valeur de référence de l'ensemble des matériaux de référence. Les isotopes de l'oxygène et les mesures OH-F-Cl ne présentent pas de variations dues à l'orientation des cristaux, ce qui permet de déterminer ces variables dans des biotites orientées aléatoirement à l'intérieur d'échantillons naturels.

La teneur en OH-F-Cl similaire dans la biotite de la biotite dans le minéral anhydre (andalousite) et dans la matrice permet de conclure que la composition du site hydroxylique de la biotite est maintenue après l'évolution du pic et n'est pas remise à zéro pendant le refroidissement. En particulier, Cl semble être très rétentive puisque la teneur en Cl représente la disponibilité initiale de Cl à la limite de grain de la biotite en croissance de la réaction de dégradation du chlorite. Dans le cas du contact d'Adamello occidental, les échantillons de faible teneur en auréole ont des variations plus élevées que les échantillons de haute qualité. Cette tendance à l'homogénéisation s'explique par la cinétique très faible pour l'échange de Cl-OH à

basse température. Cette faible cinétique est en bon accord avec l'observation de valeurs absolues très différentes pour la teneur en Cl des 5 échantillons sélectionnés. L'homogénéisation des échantillons de qualité supérieure est possible puisque les biotites se recristallisent. La teneur en fluorure montre le même comportement, avec l'absence de tendance liée à la température pour la valeur absolue. Néanmoins, il ne présente pas la même tendance d'homogénéisation que la teneur en Cl, ce qui est interprété avec une cinétique plus rapide, supportée par la taille relativement comparable des rayons des anions F et OH (1,33 et 1,53 Ångström, respectivement) (1,81 Ångström). Les variations de la teneur en eau de la biotite sont traditionnellement interprétées comme la conséquence de l'incorporation d'un cation hautement coordonné dans le site octaédrique ( $Ti^{4+}$ ,  $Fe^{3+}$  ou  $Al^{3+}$ ),  $O^{2-}$  étant substitué à  $OH^-$  pour maintenir la charge neutre. Les variations de la teneur en eau dans l'auréole de contact Adamello occidental ne montrent aucune tendance liée à ces cations, ici nous interprétons la teneur en eau dans la biotite en fonction de l'activité de l'eau pendant la recristallisation des biotites. Les biotites avec site hydroxylé rempli ont été équilibrées dans des conditions saturées en fluide alors que les biotites non stoechiométriques sont dans des échantillons qui ont été équilibrés dans des conditions sous-saturées ( $a_{H_2O} < 1$ ).

La connaissance de l'échange de Cl-OH a été utilisée pour suivre l'écoulement de fluide dans l'auréole de contact Torres del Paine. La teneur en chlore dans l'auréole de contact est constante à des valeurs faibles (environ 0,01% en poids) mais présente des valeurs significativement plus élevées pour certains échantillons proches de l'intrusion (0,1 à 0,2% en poids). Les isotopes d'hydrogène présentent également un changement proche de l'intrusion, avec des valeurs croissantes de la D à des signatures plus magmatiques (environ 80 ‰). La position du front d'infiltration pour les isotopes d'hydrogène permet de calculer un volume de fluide qui infiltre les roches environnantes de  $4m^3 / m^2$  de contact d'intrusion. Cette faible quantité de fluide est en bon accord avec l'absence de variations dans les isotopes de l'oxygène. Nous interprétons cette infiltration de fluide comme le résultat de la cristallisation du premier des trois granites. Les deux autres granites produisent une infiltration fluide, mais en quantité très limitée, qui ne sont responsables que de la stabilisation de muscovite rétrograde et du remplacement local de la biotite et de la cordiérite par une intercroissance de chlorite + muscovite. Ils ne modifient pas la teneur en Cl en biotite en raison de la très faible cinétique de l'échange de Cl-OH.

## Résumé grand public

Les grandes forces qui s'exercent à l'intérieur de la Terre sont responsables de la tectonique des plaques, c'est à dire du mouvement de grandes parties de la Terre qui parfois se rencontrent dans ce que l'on appelle des zones de convergences. Ces zones sont connues pour être le lieu principal de séismes mais aussi d'éruptions volcaniques. L'interaction entre des fluides mobiles et les roches environnantes est un des processus qui impact ces deux manifestations souvent meurtrières. Néanmoins, une roche est un agrégat de minéraux et ne comporte donc plus le fluide responsable de l'équilibration entre ces différents minéraux. L'étude de l'évolution des fluides à l'intérieur de la Terre nécessite donc de comprendre l'équilibre entre les minéraux accessibles à l'intérieur des roches échantillonnées à la surface de la terre et le fluide au moment de la formation de ceux-ci, souvent plusieurs millions d'années auparavant.

Cette thèse a pour but de comprendre l'équilibre entre un minéral hydraté, c'est-à-dire avec de l'eau sous forme  $\text{OH}^-$  dans sa structure atomique, et les fluides lors de réactions métamorphiques. Pour cela je me suis focalisé sur l'étude de la biotite car ce minéral est stable dans de nombreuses conditions et participe à beaucoup de réactions. Néanmoins les roches métamorphiques ont une structure particulière qui est la conséquence de l'action conjugué de la cristallisation de minéraux en équilibre lors de ces réactions et parfois de déformations. Il faut donc être capable d'analyser les minéraux dans leur contexte à l'intérieur des roches étudiées, pour ce faire de nombreuses méthodes in-situ ont été développées. La plupart de ces méthodes sont entravées par ce que l'on appelle des effets de matrice, c'est-à-dire que la composition du minéral analysé ne varie pas de manière linéaire par rapport aux résultats de mesures, ces résultats peuvent même varier en fonction de la composition d'autres éléments du minéral analysé. Cela est particulièrement vrai pour la méthode principale utilisée dans cette thèse qui est la microsonde ionique (SIMS). Connaître la vraie valeur de la variable que l'on souhaite analyser nécessite donc d'avoir des matériaux de référence où l'on connaît cette valeur de manière indépendante. Pour cela j'ai sélectionné des échantillons de biotites où nous avons accès à suffisamment de matériel (i.e. plusieurs centaines de grains voire milliers) pour faire une analyse d'un certain nombre de grains et connaître la vraie valeur à la fois en isotopes de l'oxygène et en teneur en chlore, fluor et eau. Les isotopes d'un élément sont des atomes avec un différent nombre de neutrons à l'intérieur du noyau, cela se traduit par une masse différente, ici les masses 16 et 18 de l'oxygène sont analysées. Lors d'une analyse in-situ en utilisant la SIMS, le rapport isotopique ( $^{16}\text{O}/^{18}\text{O}$ ) directement analysé est en réalité biaisé par la composition en fer et magnésium et en fluor du grain de biotite analysé. Il faut donc appliquer

une correction pour obtenir la vraie valeur des isotopes de l'oxygène. Il en va de même pour la teneur en eau, même si le nombre de variable biaisant les résultats est inférieur (seule la composition en fer et magnésium à un impact). La teneur en chlore et en fluor est encore plus simple à déterminer puisqu'elle n'est qu'une fonction polynomiale de second ordre du rapport isotopique mesuré à la SIMS (respectivement  $^{19}\text{F}/^{28}\text{Si}$  et  $^{35}\text{Cl}/^{30}\text{Si}$  pour le fluor et le chlore).

L'utilisation de la méthode de détermination des teneurs en OH-F-Cl avec la SIMS a permis de mieux comprendre la cinétique d'échange entre le fluide et la biotite lors du métamorphisme. En effet en analysant des biotites dans la matrice et en inclusion dans des minéraux anhydres, supposé gardé inchangé la composition de la biotite lors de l'exhumation des roches, le fait que les teneurs en OH-F-Cl soient les mêmes pour ces deux différents contextes texturaux indique que la biotite maintient sa composition lors de l'exhumation/refroidissement et que la teneur en OH-F-Cl mesurée représente la composition au moment de plus haute température, qui nous intéresse dans le cadre du métamorphisme. Le fait que la teneur en fluor et en chlore ne présente pas d'évolution liée à la température pour les différents échantillons équilibrés à différentes températures implique que le fluor et le chlore n'échangent que très difficilement lors du métamorphisme. Les teneurs représentent donc plutôt l'accessibilité de ces éléments au moment de la cristallisation de la biotite à moyenne température (environ  $500^\circ\text{C}$ ). Pour changer ces teneurs il est nécessaire de recristalliser un grain de biotite lors d'une réaction métamorphique à plus haute température, et cela en équilibre avec un fluide d'une composition complètement différente du fluide en équilibre avec la première cristallisation de ce grain de biotite. La signification de la teneur en eau de la biotite est un peu plus complexe car elle est en fait un marqueur de la présence ou non d'un fluide métamorphique aux joints de grains. En résumé, plus il y a d'eau aux joints de grains plus il y a d'eau qui peut rentrer à l'intérieur de la structure atomique de la biotite.

La compréhension de l'équilibre entre la teneur en chlore dans les biotites et le fluide métamorphique a permis de mettre en évidence l'infiltration d'un fluide provenant d'une chambre magmatique aujourd'hui à l'affleurement en Patagonie dans le massif du Torres del Paine. En effet les teneurs en chlore des biotites loin de l'intrusion sont assez faibles, mais pour quelques échantillons proches de l'intrusion elles augmentent de manière significative. Cela est cohérent avec les analyses de biotites provenant des roches magmatiques adjacentes qui ont une teneur en chlore très importante. Le fluide expulsé très tôt lors de la cristallisation du magma de composition granitique a percolé et s'est équilibré avec les biotites des roches juste au contact entre le magma encore chaud et les sédiments en train d'être chauffés. Cette augmentation de température des sédiments s'accompagne de réactions métamorphiques qui

cristallisent des biotites à moyennes température (environ 470°C) et d'autre minéraux à plus haute température (environ 520°C) lors d'une seconde réaction. Cette seconde réaction implique la recristallisation des biotites déjà présente suite à la première réaction, cela permet d'échanger le chlore du fluide avec ces biotites et donc de modifier la teneur en chlore de ces mêmes biotites. Puisque la teneur en chlore n'est pas modifié lors du refroidissement des roches, la teneur mesurée aujourd'hui représente bien la teneur au moment de l'infiltration du fluide magmatique.



# 1 Introduction

## 1.1 Fluid-rock interactions

Fluid-rock interactions play an important role during metamorphism, enhancing mass and heat transport, and is essential for mineral equilibration. Fluid has a strong influence on mineral assemblage stability (e.g. Ferry 1986, Baumgartner and Ferry 1991, Ague 1994, Ferry 2000), the rate and mechanism involved in reactions (e.g. Carlson 2010), and fluid will enhance partial melting (Goranson 1938, Tuttle and Bowen 1958, Luth et al. 1964). Fluid flow in contact aureole has been of particular interest, but most studies focused on metacarbonates due to the fact that recognizing fluid-rock interaction and its effect through index minerals (Ferry 1991, 2000) and the large stable isotope gradients (Roselle et al., 1999) is easy. Additionally, fluid-rock interactions have been recognized in metapelites using the O(4) site composition of hydrous minerals (Nijland et al. 1993, Higashino et al. 2013) or the channel composition of cordierite for example (Carrington and Harley 1996, 2012).

Many ore deposits are formed by intense water-rock interaction. For example, porphyry copper systems, which includes some of the world largest copper deposits, are formed by fluid-rock interaction associated with porphyritic intrusions in connections with large hydrothermal systems (e.g. Cooke et al. 2005, Sillito 2010). Hydrothermal systems are complex (e.g. (Nabelek and Labotka 1993; Roselle et al. 1999)), and often several individual fluid pulses are present.

This thesis consists of two methodological chapters on developing in-situ analysis of oxygen isotopes and chlorine-fluorine-hydrogen in biotite. The results are used to explore fluid-rock interaction and retention of hydrogen, fluorine, and chlorine in biotites in two contact aureoles, the Torres del Paine aureole in Patagonia, Southern Chile, and the Adamello aureole in the Alps, Northern Italy. These areas were selected because a lot of the phase petrology and the geology is well studied. The aureoles contain well exposed polytactic sequences, which had been

sampled previously (Floess, 2013; Bodner, 2013). The results of Bodner and Floess formed a solid basis for the current work.

Below is a short review of the methods and tools available to petrologists to track and identify fluid-rock interaction, with a focus on the methods used in this thesis. These paragraphs are complemented with a detailed description of the field areas studied.

### *1.1.1 Stable isotopes*

Stable isotopes are a powerful tool to track fluid-rock interactions. Infiltration of fluid disequilibrium fluids – originating typically from a completely different origin (e.g. magmatic fluid into the surrounding metamorphic rocks in contact aureole or in the lower crust) is readily tracked by the infiltration fronts (e.g. Baumgartner and Valley, 2001; Roselle et al., 1999; Nabelek et al., 1993). Stable isotopic studies on fluid flow have been conducted mainly in metacarbonates due to the large difference in isotopic signature between the sedimentary carbonate and magmatic fluid (Labotka et al. 1988, Bowman et al. 1994, Cook et al. 1997, Roselle et al. 1999), but rarely in metapellites. The position of the stable isotopes front can be used to infer the amount of fluid that flowed through the surrounding rocks (Baumgartner and Rumble, 1987; Baumgartner and Valley 2001). Accurate fluid amounts are quite often elusive, since sampled profiles are not necessarily in the flow direction. For example (Gerdes et al. 1995) showed that their sample profile was collected on a “side” of the reaction front, nearly perpendicular to the flow direction. Similarly, it has been shown that the sampling strategy will heavily influence the results of a study due to channelized fluid infiltration (Roselle et al. 1999). Hence care needs to be taken to correctly interpret the obtained isotopic profiles.

I use stable isotope geochemistry from the thesis of Robert Bodner (2013) to demonstrate that the fluid-rock interaction was spatially limited in the Torres del Paine contact aureole, and that only small amounts of fluids infiltrated the host rocks.

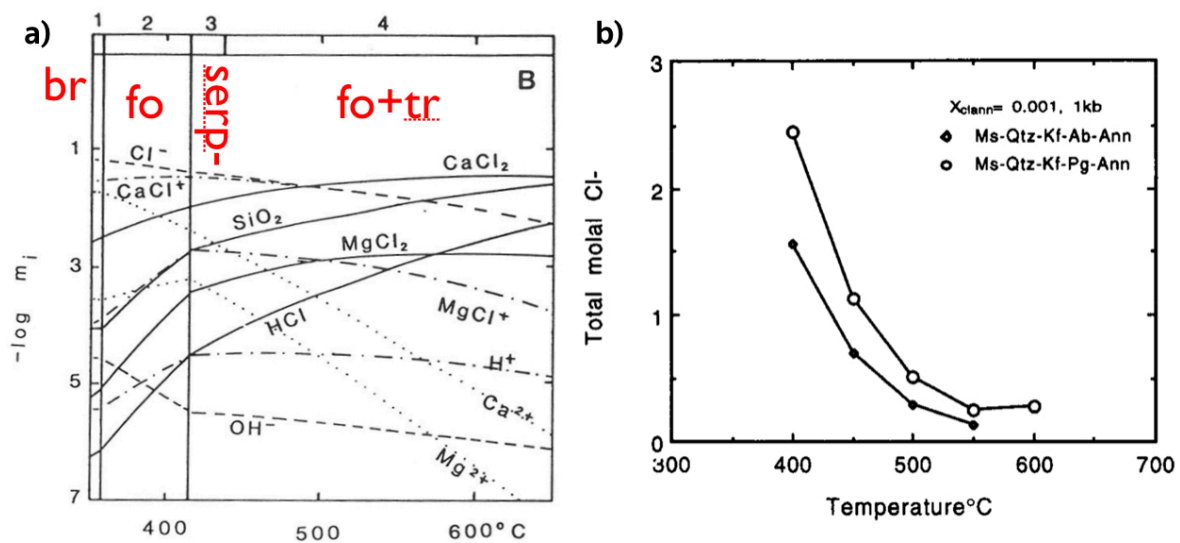


Figure 2: a) Evolution of molalities for major fluid species with increasing temperature and mineral assemblage change, mineral assemblages are in red, diopside in excess and antigorite in excess for zones 1 and 2, on the left of the –serp line. The concentration of the species in the fluid is a strong function of the mineral assemblage, and thus the pH of the fluid (modified from Eugster and Baumgartner 1987). b) Total chlorine dissolved in the fluid vs temperature in equilibrium with two different mineral assemblages (i.e. Na buffer change between albite, white diamonds, and paragonite, white dots), this shows the importance of the pH of the fluid on the chlorine concentration at constant chlorine content in biotite (from Zhu and Sverjensky 1991).

### 1.1.2 Fluorine and chlorine in metamorphism

Fluorine and chlorine are two of the most dominant anions in fluids in the earth's crust (Yardley 1985; Yardley and Graham 2002). Chlorine is of special interest since it complexes with cations that are either of economic importance (Pb, Cu, Ag, etc) or participate in mineral reactions during metamorphism (Fe, Mg, Ca, Na, K). Chlorine concentrations influence the pH of the fluid, which in turn has a huge effect on the solubilities of fluid species (Fig 1a). In addition, mineral assemblage variation will affect the pH of the fluid, which in turn changes the concentration of the dissolved species.

There are basically two ways to study the chlorinity or salinity of fluids during metamorphism: either through fluid inclusion studies (e.g. Crawford 1981, Roedder 1981)) or hydrous phase compositions (e.g. Munoz 1984, Yardley 1985, Zhu and Sverjenski 1991). This second way is strongly influenced by the speciation of the chlorine complexes, since chlorine content in hydrous phases is link directly to the concentration of the associated hydrogen chloride, not directly with chlorine in fluid phase. Indeed, this can be seen by equilibria involving HCl (such as reaction 1). On the other hand, the dissociation of HCl° is *pH* dependent, and hence changes in *pH* of the fluid will have a huge effect on chlorine content in hydrous phases (Fig 1b). Nevertheless, chlorine is strongly partitioned into the fluid phase at all natural P,T, and *pH* conditions. Since fluid is lost during prograde metamorphism, chlorine should also be removed sequentially, through the different dehydration reactions encountered by a pelitic rocks. Only a few studies have tried to determine the behavior of Cl during metamorphism: Yardley and Graham (2002) review the fluid inclusion literature, whereas Selverstone and Sharp (2015) used bulk rock chlorine geochemistry. They show that Cl does not get removed from most rocks. At the best, their data demonstrate that there is no easily interpretable trend. They suggest that chlorine content is more related to initial rock composition (figure 2). Nevertheless, the first study carried the potential pitfalls of fluid inclusions (leaking, recrystallization of the host mineral, preferential incorporation of elements due to different wetting angles). The second study lacked detailed petrologic constraints and many reactions studied were decarbonation reactions rather than dehydration reactions. The fact that samples were collected from distances of more than 50km makes it unlikely that all collected rocks had indeed similar initial halogen chemistry.

Here I present original data on the evolution of fluid composition in the contact aureoles of the Torres del Paine intrusive complex (Patagonia, Chile) and the Adamello batholith (Alps, Italy). In the first case I focused on the stable isotope geochemistry available to me in the literature

(Bodner, 2013) and combined them with original textural and chlorine concentration data on biotites formed during contact metamorphism in the graphite rich Cerro Torro and Punta Barossa Formations. These formations are both very proximal, unripe turbiditic sediments of Cretaceous age.

In the Adamello contact aureole the focus was on the biotite chlorine compositions in the Variscan Basement complex intruded by the Tertiary Western Adamello complex. Here minerals are larger, and SIMS analyses are possible on biotite inclusions and mica in the matrix. This permits to test the retention of halogens and hydrogen on the hydroxyl site.

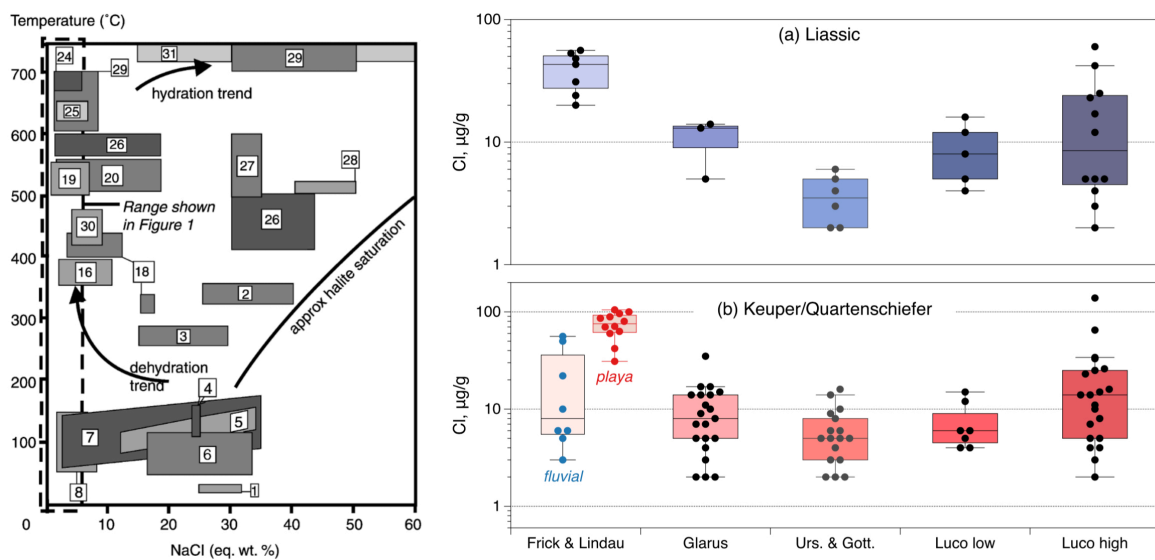


Figure 2: a) Evolution of salinity from fluid inclusions for formation waters and metamorphic fluids hosted by sequences deposited in shallow seas and at continental margins (from Yardley and Graham 2002). b) plot of the chlorine composition of bulk rocks from the Upper Triassic and Lower Jurassic from the Swiss Alps with increasing grade from the left to the right (from Selverstone and Sharp 2015). The trends visible in the left diagram were interpreted to show dehydration trends and fluid separation trends, depending on rock evolution and initial composition, while Selverstone and Sharp (2015) interpret that much of the chlorine is in the organic phase, which does not participate in reactions. No clear changes in concentration are apparent in either diagram as a function of prograde metamorphism.

Biotite exchanges chlorine with fluid through the reaction (e.g. Munoz, 1984):



Fluorine exchange is similar to the above reaction, using the neutral associated species  $\text{HF}^{\circ}$ . This fluid monitor has been used in ore petrology (e.g. Panigrahi et al. 2008, Rasmussen and Mortensen 2013) but rarely in metamorphic (e.g. Henry et al., 1988; Markl and Bucher, 1998, Sisson 1987).

## 1.2 Water content and the stoichiometry of the hydroxyl site

Since  $\text{H}_2\text{O}$  is not analyzable by common in-situ analytical techniques used in metamorphic and magmatic petrology (e.g. Electron Microprobe, LA ICP-MS), water content in hydrous minerals is usually not analyzed for. Nevertheless, the potential for non-stoichiometry of the O(4) site in biotite has been recognized for a long time (e.g. Wones and Eugster 1962), and this in turn could significantly influence the thermodynamic behavior of biotite.

Variations of water content in biotite that are not due to F-OH and Cl-OH substitutions have been explained by coupled substitutions (Dyar et al. 1993, Cesare et al. 2003, 2008), see figure 3. In these substitutions,  $\text{OH}^-$  is replaced by  $\text{O}^{2-}$  to maintain charge balance with the incorporation of tri- or quadrivalent cations ( $\text{Fe}^{3+}$ ,  $\text{Al}^{3+}$ ,  $\text{Ti}^{4+}$  mainly) in the octahedral site, which typically has only divalent cations, such as  $\text{Fe}^{2+}$  and  $\text{Mg}^{2+}$ . Such substitutions have been called deprotonation substitutions since they release  $\text{H}_2$  into the fluid. Alternatively, they have been called oxy-substitutions since they lead to a potentially significant oxy-component on the hydroxyl site. More complex schemes have been called upon to explain variations in biotites from Western Maine (Dyar et al. 1993, figure 3a), whereas only Ti-oxy substitution has been recently used to explain variations of water content in biotite of granulite facies rocks (Cesare et al. 2003, 2008, figure 3b).

In this thesis, I follow up on the hypothesis that  $O^{2-}$  content on the hydroxyl site can also be linked to the water activity in the system through the equilibrium:



This reaction implies that there are vacancies in the O(4) sites (here referred as  $\text{vac}^{\text{OH}}$ ); the lower the water activity with which the biotite equilibrates, the more hydrogen is lost in the form of water, and the more vacancies will be produced in the O(4) site. The challenge encountered is the non-equivocal prove that reaction 2 is indeed dominating in any given biotite.

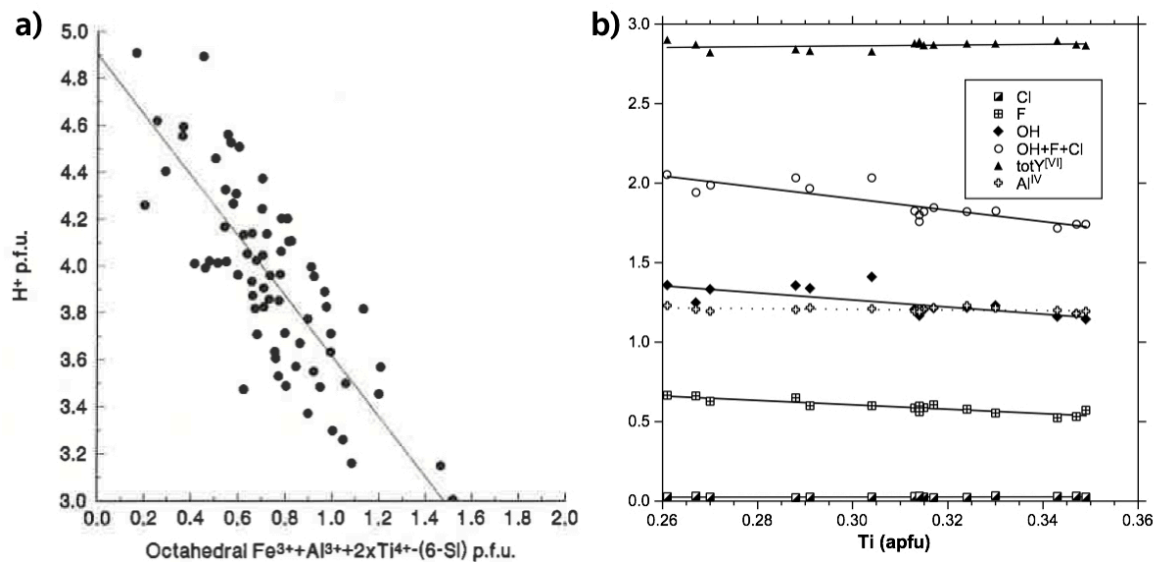


Figure 3: a) Correlation between H content and composition of the octahedral composition of biotite from metapelitic rocks from Western Maine (from Dyar et al. 1993). b) Correlation between OH, F, Cl, (OH + F + Cl), octahedral aluminum ( $\text{Al}^{\text{VI}}$ ), octahedral sum ( $\text{totY}^{\text{[VI]}}$ ) and titanium content from granulite facies rocks from South India. It shows the importance of the titanium oxy-substitution for OH content variations in fluid-undersaturated systems (from Cesare et al. 2008).

### 1.3 Geological settings

In order to study the equilibrium between biotite and fluid during metamorphism two contact aureoles were selected for this thesis: the Torres del Paine in Patagonia (Chile) and the aureole

of the Western Adamello Tonalite in the Italian Alps. Contact aureoles are an excellent place to study fluid-rock interactions during metamorphism since the thermal source is identified (i.e. the intrusive body) and continuous metamorphic gradients can be sampled over a small distance, allowing to track the evolution of biotite composition in rocks that encounter different dehydration reactions. These two contact aureoles have very different key features that potentially allows to understand the behavior of biotite OH-F-Cl content during metamorphism.

The Torres del Paine complex (TPC) is located in the southernmost part of the Andes of Chile in Patagonia. It consists of three major granite laccoliths, a mafic stock in the Western part of the granite intrusions, and a composite mafic laccolith at the bottom of the intrusive complex. They intruded the cretaceous turbidites of the Punta Barrosa and Cerro Torro Formations, between 12.60 and 12.43 Ma (Michel et al. 2008, Leuthold et al. 2012). It creates a small but well exposed contact aureole allowing the 3D study of the surrounding rocks, mainly composed of pelites, psammites, and sandstones, with minor carbonates. The pressure estimate of the intrusion is 750bar (Putlitz et al. 2001), from prehnite stability in carbonate and fayalite in the intrusion. The homogeneous bulk rock compositions of the pelites and the very low pressure for the intrusion is responsible for mappable isograds due to two major cordierite producing reactions: the chlorite breakdown far from the contact with the intrusive body and the muscovite breakdown reaction close to the contact (Figure re-drawn from Bodner 2013, figure 4a).

The Western Adamello contact aureole is part of the Adamello massif in the Northern Italian Alps (Callegari and Brack 2002). The Western Adamello Tonalite (WAT) intrude mainly into the Variscan basement and Liasic sediments (Floess and Baumgartner 2012). The rocks from the basement were metamorphosed during the Variscan at P-T conditions of 7-9 kbar and 570-610 °C at 330 Ma (Diella et al. 1992). They mainly consist of micaschists, phyllites and paragneisses that were strongly altered during the pre-Alpine sedimentary history and the Late-Cretaceous Orobic deformation phase (Floess and Baumgartner 2013, Diella et al. 1992). The

tertiary intrusion of the WAT created a typical low pressure contact aureole (with pressure around 2.5 kbar) with the chlorite breakdown reaction producing biotite and cordierite. Prograde metamorphism resulted in an andalusite-garnet zone and finally close to the contact the muscovite breakdown reaction formed K-feldspar and sillimanite, this last reaction enhanced partial melting in some rocks (Floess and Baumgartner 2012, Fig. 4b).

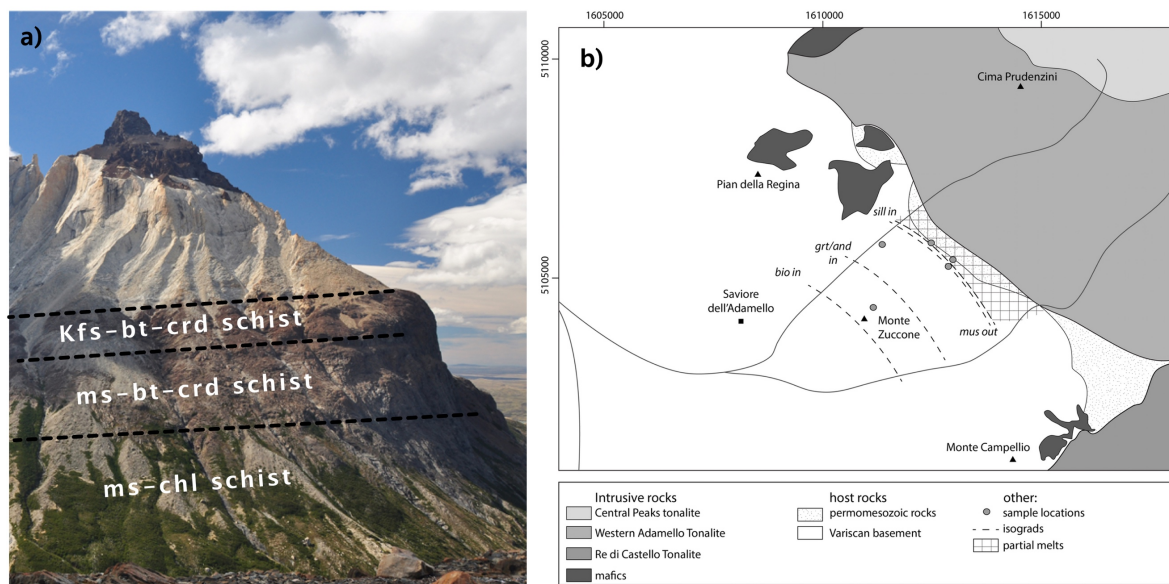


Figure 4: a) picture of the Torres del Paine laccolith with the extent of the contact aureole. The two different isograds are the black dashed lines, the evolution of the assemblages are in white (Bodner, 2013). b) map of the Western Adamello contact aureole with the different isograds and samples used in this study (from Floess 2013).

## 1.4 New in-situ methods

Mineral texture carry a tremendous amount of information in metamorphic rocks. These include for example the extent of equilibrium, permit to identify products reactants of reactions, and the chemical zoning can show the evolution of the reaction in a rock, and of course it is from textures that the relation between metamorphism and deformation in metamorphic environments is gained. To use the geochemical information stored in minerals it is essential to use in-situ methods for chemical analysis. Electron probe microanalysis

(EPMA), laser ablation inductively-coupled mass spectrometer (LA ICP-MS) or secondary ion mass spectrometry (SIMS)) are some of the tools that allow to determine geochemical informations without losing this crucial textural information. Nevertheless, these methods are hampered - to different degrees - by matrix effects, i.e. measured quantities are biased by the structure or chemical composition of the analyzed material. Theoretically advances in EPMA method has led to matrix correction programs that simplify the treatment of EPMA analyses and significantly reduced the need for standards of known composition (Armstrong 1989). The theoretical knowledge for the two other methods is still rather poorly constrained, especially for SIMS. This has led to the need for development of sets of reference materials (RMs) for the glasses and minerals of interest. LA ICP-MS requires less RMs than SIMS since major element composition for minerals has most of the time a minor effect. Development of reference material that are homogeneous and available in relatively large amounts (100 of mg or a few grams) has been the focus of many studies over the past two decades of SIMS measurements (Eiler et al. 1997). Matrix effects have been constrained for major, minor and trace element in minerals (Ottolini et al. 2002, 2006, Bulle and Layne 2014) as well as isotopic ratios (Riciputti et al. 1998, Ickert and Stern 2013, Sliwinskii et al. 2016), see figure 5.

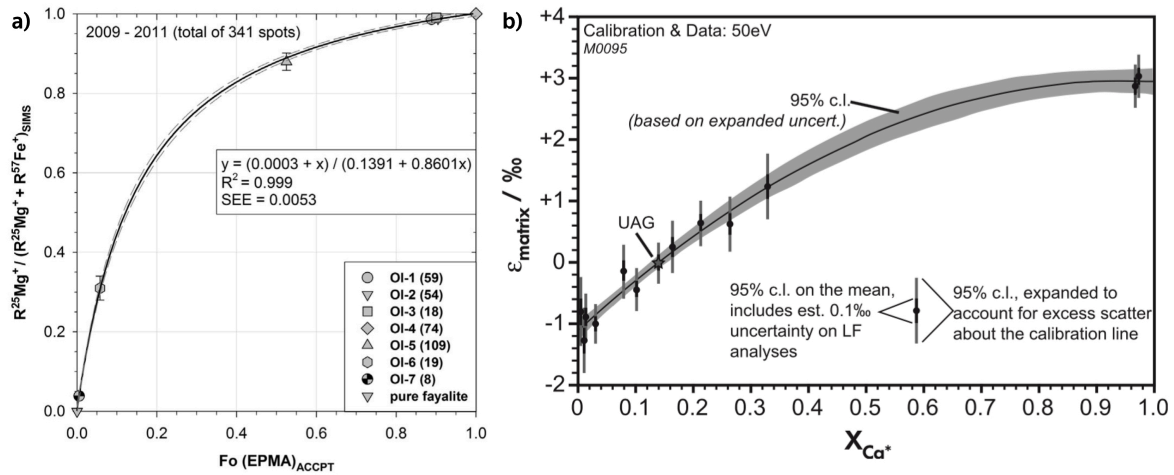


Figure 5: Working curve for the Fo content of olivine of reference material of known composition vs analyzed isotopic ratios of  $^{25}\text{Mg} / (^{25}\text{Mg} + ^{57}\text{Fe})$  with the SIMS (from Bulle and Layne 2014). b) Calibration of the instrumental bias (in permil) for oxygen isotopes of garnet reference materials plotted against the molar fraction of Ca (from Ickert and Stern 2013). Many other minerals have IMF values which can be fitted within error with linear working curves.

Before the power of SIMS analysis could be harnessed for chlorine, fluorine, and water content, as well as for oxygen isotopes, reference materials for their analysis had to be developed.

## 1.5 Outline of the thesis

The development of a set of new reference materials for SIMS analyses of biotite of different compositions is the topic of chapters 2 and 4. Chapter 2 focuses on the calibration of the matrix effect for  $\delta^{18}\text{O}$  SIMS analyses. Care was taken to evaluate the effect of crystal orientation.

Previous workers have found in some rare cases large effects on IMF, for example for baddeleyite or magnetite (Wingate and Compston 2000, Schmitt et al. 2010, Huberty et al. 2010). Chapter 4 looks at the homogeneity of these biotite crystals for OH-F-Cl concentration analysis. Several of the same reference materials turned out to be adequate for these analyses, and no orientation effect was found. Finally I propose in chapter 4 a working curve to

determine the water, fluorine and chlorine content of any biotite with a much better uncertainty for F and Cl than EPMA measurements.

In the chapter 3, hydrogen and oxygen isotopes for bulk rocks, with chlorine content in biotite, of both magmatic and metamorphic rocks of the Torres del Paine complex (TPC) are being used to study channelized fluid flow in metapelites. The PhD thesis of Robert Bodner (Bodner, 2013) reports a tremendous amount of sampling for the entire contact aureole of the TPC. These profiles from the roof, the side, and the base of the laccolith allowing the study of different gradients around the magmatic body to ensure the absence of sampling bias. Bodner reports stable isotope analysis for some of the profiles. The precise time scale and geochemical constraints of the individual intrusions (Michel et al. 2008, Leuthold et al. 2012, Leuthold et al. 2013) allow me to link the fluid flow to the intrusion of the different magmatic pulses.

The behavior of chlorine and fluorine during metamorphism is the focus of the chapter 5. The OH, F and Cl content in biotite of the Variscan basement rocks from the Western Adamello contact aureole have been determined using Secondary Ion Mass Spectrometry. This chapter compares the composition of biotite in the matrix with biotite inclusions in andalusite. The latter were shielded from any retrograde resetting. The high precision obtained with SIMS allowed me to look at variations with increasing grade and to study the kinetics of OH-F-Cl exchange between biotite and fluid during metamorphism. Finally, I show that the measurements of water content in biotite can be used to track water activity changes.

## 1.6 References

Ague, J. J. (1994). Mass transfer during Barrovian metamorphism of pelites, south-central Connecticut. II: Channelized fluid flow and the growth of staurolite and kyanite. *American Journal of Sciences*, 294, 1061–1134.

- Armstrong, J. T. (1989). CITZAF: Combined ZAF and Phi-Rho (Z) Electron Beam Correction Program, California Institute of Technology, Pasadena, CA.
- Baumgartner, L.P. and Rumble, D. (1988) Transport of stable isotopes: I: Development of a kinetic continuum theory for stable isotope transport. *Contributions to Mineralogy and Petrology*, 98, 417–430.
- Baumgartner, L.P., & Ferry, J.M. (1991) A model for coupled fluid-flow and mixed-volatile mineral reactions with applications to regional metamorphism. *Contributions to Mineralogy and Petrology*, 106, 273–285.
- Baumgartner, L.P. and Valley, J.W. (2001) Stable Isotope Transport and Contact Metamorphic Fluid Flow. *Reviews in Mineralogy and Geochemistry*, 43, 415–467.
- Bowman, J. R., Willett, S. D., & Cook, J. (1994). Oxygen isotopic transport and exchange during fluid flow: one-dimensional models and applications. *American Journal of Sciences*, 294, 1–55.
- Bodner, R. (2013) Metamorphism and Kinetics in the Torres del Paine Contact Aureole. PhD thesis, University of Lausanne.
- Bulle, F., & Layne, G. D. (2014). International Journal of Mass Spectrometry. *International Journal of Mass Spectrometry*, 361, 41–53.
- Callegari, E., & Brack, P. (2002). Geological Map of the Tertiary Adamello Batholith (Northern Italy) - Explanatory Notes and Legend. *Mem Sci Geol*, 54, 19–49.
- Carrington, D.P., & Harley, S. L. (1996). Cordierite as a monitor of fluid and melt H<sub>2</sub>O contents in the lower crust: An experimental calibration. *Geology*, 24, 647–650.
- Cooke, D. R., Hollings, P., & Walshe, J. L. (2005) Giant Porphyry Deposits: Characteristics, Distribution, and Tectonic Controls. *Economic Geology*. 100, 801–818.
- Cook, S.J., Bowman, J.R. and Forster, C.B. (1997) Contact metamorphism surrounding the Alta Stock; finite element model simulation of heat- and <sup>18</sup>O/<sup>16</sup>O mass-transport during prograde metamorphism. *American Journal of Science*, 297, 1–55.
- Crawford, M. L. (1981). Fluid inclusions in metamorphic rocks – low and medium grade. In: Short Course in Fluid Inclusions: Applications to Petrology (eds Hollister LS, Crawford ML), pp. 157–81. Mineralogical Association of Canada Short Course Handbook, 6.
- Dyar M. D., Guidotti C. V., Holdaway M. J., Colucci M. (1993) Nonstoichiometric hydrogen

- contents in common rock-forming hydroxyl silicates. *Geochimica et Cosmochimica Acta* 57, 2913–2918.
- Diella, V., Spalla, M. I., & Tunesi, A. (1992), Contrasting thermomechanical evolutions in the Southalpine metamorphic basement of the Orobic Alps (Central Alps, Italy). *Journal of Metamorphic Geology*, 10, 203–219.
- Eiler, J. M., Graham, C., and Valley, J. W. (1997). SIMS analysis of oxygen isotopes: matrix effects in complex minerals and glasses. *Chemical Geology*, 138, 221–244.
- Ferry, J. (1986) Reaction Progress: A Monitor of Fluid—Rock Interaction during Metamorphic and Hydrothermal Events. in Fluid—Rock Interactions during Metamorphism, ed. by J. Walther and B. Wood, Springer New York, vol. 5 of Advances in Physical Geochemistry, 60–88.
- Ferry, J. M. (1991). Dehydration and decarbonation reactions as a record of fluid infiltration. *Reviews in Mineralogy and Geochemistry*, 26, 351–391.
- Ferry, J. M. (2000). Patterns of mineral occurrence in metamorphic rocks. *American Mineralogist*, 85, 1573–1588.
- Floess, D. (2013) Contact metamorphism and emplacement of the Western Adamello Tonalite, PhD thesis, University of Lausanne.
- Floess, D., & Baumgartner, L. P. (2015). Constraining magmatic fluxes through thermal modelling of contact metamorphism. *Geological Society, London, Special Publications*, 422(1), 41–56.
- Gerdes, M. L., Baumgartner, L. P., Person, M., & Rumble, D. III (1995) One- and two-dimensional models of fluid flow and stable isotope exchange at an outcrop in the Adamello contact aureole, Southern Alps, Italy. *American Mineralogist*, 80, 1004–1019.
- Goranson, R. W. (1938) Silicate-H<sub>2</sub>O systems: Phase equilibria in the NaAlSi<sub>3</sub>O<sub>8</sub>-H<sub>2</sub>O and KAlSi<sub>3</sub>O<sub>8</sub>-H<sub>2</sub>O systems at high pressures and temperatures. *American Journal of Science*, 35, 71–91.
- Henry, D.J. (1988) Cl-rich minerals in Archean granulite facies ironstones from the Beartooth Mountains, Montana, USA: Implications for fluids involved in granulite metamorphism. Workshop on the Deep Continental Crust of South India -1, 67–69.

- Higashino, F., Kawakami, T., Satish-Kumar, M., Ishikawa, M., Maki, K., Tsuchiya, N., et al. (2013) Chlorine-rich fluid or melt activity during granulite facies metamorphism in the Late Proterozoic to Cambrian continental collision zone—An example from the Sør Rondane Mountains, East Antarctica. *Precambrian Research*, 234, 229–246.
- Huberty, J. M., Kita, N. T., Kozdon, R., Heck, P. R., Fournelle, J. H., Spicuzza, M. J., Huifang, X., & Valley, J.W. (2010). Crystal orientation effects in  $\delta^{18}\text{O}$  for magnetite and hematite by SIMS. *Chemical Geology*, 276, 269–283.
- Ickert, R. B., & Stern, R. A. (2013). Matrix Corrections and Error Analysis in High-Precision SIMS  $^{18}\text{O}/^{16}\text{O}$  Measurements of Ca-Mg-Fe Garnet. *Geostandards and Geoanalytical Research*, 37, 429–448.
- Labotka, T. C., Nabelek, P. I., & Papike, J. J. (1988) Fluid infiltration through the Big Horse Limestone Member in the Notch Peak contact-metamorphic aureole, Utah. *American Mineralogist*, 73, 1302–1324.
- Leuthold, J., Müntener, O., Baumgartner, L.P., Putlitz, B. and Chiaradia, M. (2013) A Detailed Geochemical Study of a Shallow Arc-related Laccolith; the Torres del Paine Mafic Complex (Patagonia). *Journal of Petrology*, 54, 273–303.
- Leuthold, J., Müntener, O., Baumgartner, L. P., Putlitz, B., Ovtcharova, M. and Schaltegger, U. (2012) Time resolved construction of a bimodal laccolith (Torres del Paine, Patagonia). *Earth and Planetary Science Letters*, 325-326, 85–92.
- Luth, W. C., Jahns, R. H., & Tuttle, O. F. (1964) The granite system at 4 to 10 kilobars. *Journal of the Geophysical Research*, 69, 759–773.
- Markl, G., & Bucher, K. (1998) Composition of fluids in the lower crust inferred from metamorphic salt in lower crustal rocks. *Nature*, 391, 781–783.
- Michel, J., Baumgartner, L.P., Putlitz, B., Schaltegger, U. and Ovtcharova, M. (2008) Incremental growth of the Patagonian Torres del Paine laccolith over 90 k.y. *Geology*, 36, 459–462.
- Munoz, J. L. (1984). F-OH and Cl-OH Exchange in Micas with Applications to Hydrothermal Ore Deposits. *Reviews in Mineralogy and Geochemistry*, 13, 469–493.
- Nabelek, P. I., & Labotka, T. C. (1993) Implications of geochemical fronts in the Notch Peak contact-metamorphic aureole, Utah, USA. *Earth and Planetary Science Letters*, 119, 539–559.

- Ottolini, L. P., Cámara, F., Hawthorne, F. C., & Stirling, J. (2002). SIMS matrix effects in the analysis of light elements in silicate minerals: Comparison with SREF and EMPA data. *American Mineralogist*, *87*, 1477–1485.
- Ottolini, L., Cámara, F., & Hawthorne, F. C. (2006). Strategies for Quantification of Light Elements in Minerals by SIMS: H, B and F. *Microchimica Acta*, *155*(1-2), 229–233.
- Rasmussen, K. L., & Mortensen, J. K. (2013). Magmatic petrogenesis and the evolution of (F:Cl:OH) fluid composition in barren and tungsten skarn-associated plutons using apatite and biotite compositions: Case studies from the northern Canadian Cordillera. *Ore Geology Reviews*, *50*(C), 118–142.
- Roedder, E. (1984) Fluid inclusions. *Reviews in Mineralogy*, *12*, 646 pages
- Roselle, G.T., Baumgartner, L.P., & Valley, J.W. (1999) Stable isotope evidence of heterogeneous fluid infiltration at the Ubehebe Peak contact aureole, Death Valley National Park, California. *American Journal of Science*, *299*, 93–138.
- Riciputti, L. R., Patterson, B. A., & Ripperdan, R. L. (1998). Measurement of light stable isotope ratios by SIMS: Matrix effects for oxygen, carbon, and sulfur isotopes in minerals. *International Journal of Mass Spectrometry*, 1–32.
- Panigrahi, M. K., Naik, R. K., Pandit, D., & Misra, K. C. (2008). Reconstructing physico-chemical parameters of hydrothermal mineralization of copper at the Malanjkhand deposit, India, from mineral chemistry of biotite, chlorite and epidote. *Geochemical Journal*, *42*, 443–460.
- Putlitz, B., Baumgartner, L. P., Oberhänsli, R., Diamond, L. and Altenberger, U. (2001) The Torres del Paine Laccolith (Chile); intrusion and metamorphism. LPI Contribution, abstract no. 3534.
- Schmitt, A. K., Chamberlain, K. R., Swapp, S. M. & Harrison, M. T. (2000). In situ U–Pb dating of micro-baddeleyite by secondary ion mass spectrometry. *Chemical Geology*, *269*, 386-395.
- Selverstone, J., & Sharp, Z. D. (2015). Chlorine isotope behavior during prograde metamorphism of sedimentary rocks. *Earth and Planetary Science Letters*, *417*(C), 120–131.
- Sillitoe, R. H. (2010) Porphyry Copper Systems. *Economic Geology*, *105*, 3–41.

- Sisson, V. B. (1987) Halogen chemistry as an indicator of metamorphic fluid interaction with the Ponder pluton, Coast Plutonic Complex, British Columbia, Canada. *Contribution to Mineralogy and Petrology*, 95, 123–131.
- Śliwiński, M. G., Kitajima, K., Kozdon, R., Spicuzza, M. J., Fournelle, J. H., Denny, A., & Valley, J. W. (2016). Secondary Ion Mass Spectrometry Bias on Isotope Ratios in Dolomite-Ankerite, Part I:  $\delta^{18}\text{O}$  Matrix Effects. *Geostandards and Geoanalytical Research*.
- Tuttle, O. F., & Bowen, N. L. (1958) Origin of granite in the light of experimental studies in the system  $\text{NaAlSi}_3\text{O}_8\text{-KAlSi}_3\text{O}_8\text{-SiO}_2\text{-H}_2\text{O}$ . *Geological Society of America Memoirs*, 74, 145p.
- Wingate, M. T. D., & Compston W. (2000). Crystal orientation effects during ion microprobe U–Pb analysis of baddeleyite. *Chemical Geology*, 168, 75-97.
- Yardley, B. W. D. (1985) Apatite composition and the fugacities of HF and HCl in metamorphic fluids. *Mineralogical Magazine*, 49, 77–79.
- Yardley, B. W. D., & Graham, J. T. (2002). The origins of salinity in metamorphic fluids. *Geofluids*, 249–256.

## 2 Biotite Reference Materials for SIMS oxygen isotopes analysis

Authors: Guillaume Siron, Lukas Baumgartner, Anne-Sophie Bouvier, Benita Putlitz, Torsten Vennemann

Published in Geostandards and Geoanalytical Research, doi:10.1111/ggr.12148

## 2.1 Introduction

Biotite minerals are an important hydrous mineral group in igneous and metamorphic rocks. Their general chemical formula can be written as  $K(Mg,Fe,Ti)_3[AlSi_3O_{10}](OH, Cl, F)_2$ . (Rieder *et al.* 1998).  $O^{2-}$  has been found to replace some of the elements on the hydroxyl site. Elemental compositions of biotite have been used in metamorphic petrology to estimate temperature or metamorphic grade (Ferry and Spear 1978, Hodges and Spear 1982, Spear 2014; Henry *et al.* 2005). Chlorine and fluorine concentrations on the hydroxyl site allows the study of fluid compositions (e.g., Muñoz 1984, Zhu and Sverjensky 1991, Volfinger *et al.* 1985). Finally, Ar-Ar geochronology (e.g., Villa 1990, Cosca *et al.* 1991) and Rb/Sr geochronology is possible because of the high K-content of biotite, and hence fluid flow can be dated using this mineral.

The advances in analytical stable isotope geochemistry over the last decade make it possible to use in-situ techniques to determine oxygen isotope compositions of biotite, provided adequate standard material is available. Oxygen isotopes are a powerful tool to trace the origin of fluids in metamorphic and igneous systems and to use them in combination with refractive minerals as an oxygen isotope thermometer (Baumgartner and Valley, 2001; Valley, 2001).

Biotite is a trioctahedral sheet silicate, which has a large crystallographic anisotropy. Tetrahedral-octahedral-tetrahedral sheets are stacked perpendicular to the c-axis of biotite crystals, resulting in excellent cleavage in the direction of the sheets, just one of the many parameters that are highly non-isotropic. For details on the crystal structure see Bailey, 1984. At present, there are two major analytical techniques for oxygen isotope measurements in silicates: laser-heating fluorination, allowing high precision ( $2\sigma \sim 0.2-0.3 \text{ ‰}$ ) and accurate measurements to be made on about 0.5 to 2 mg of material, and Secondary Ion Mass Spectroscopy (SIMS), which allows for in-situ analysis of small volumes corresponding to a

few nanograms. With modern SIMS instrumentation, rapid in-situ determination of oxygen isotopes is feasible (3-5 minutes/analysis), with a precision of about 0.3 ‰ (e.g., Kita *et al.* 2009, Valley and Kita 2009). Yet, SIMS analyses are hampered by an important instrumental mass fractionation (IMF), which can reach up to several tens of permil. This is due to instrumental configuration and analytical conditions used for SIMS (i.e. the optics and apertures) analysis, as well as the sputtering processes (Eiler *et al.* 1997). Several studies have shown that the IMF can vary systematically by several permil for oxygen isotope measurements (Eiler *et al.* 1997, Riciputti *et al.* 1998, Zeb Page *et al.* 2010, Ickert and Stern 2013, Śliwiński *et al.* 2016). In some minerals the crystal lattice orientation also influences the IMF for O, Fe, and S isotopes (Huberty *et al.* 2010, Kita *et al.* 2011). IMF can vary in a non-linear fashion with composition in a single solid solution, as has been demonstrated for example by Ickert and Stern (2013) and Śliwiński *et al.* (2016).

The Cameca IMS 1280HR of the SwissSIMS laboratory (Switzerland) was used to measure and calibrate the oxygen isotope composition of a set of new Reference Materials (RM) for biotite. The orientation dependence of IMF was investigated prior to the determination of the matrix effect for biotite.

## 2.2 Biotite reference material

To date, no RM has been established for *in-situ* oxygen isotope analyses of biotite. As part of this study, over 30 different biotites were screened for their homogeneity in major elements by electron microprobe analysis (EPMA). Chemically homogeneous samples were tested for isotopic homogeneity by laser heating fluorination analysis (LAF) and SIMS. Five biotite samples (named UNIL\_B1 to UNIL\_B5) were selected and studied in detail. They are homogeneous, down to the 10-20µm scale, covering the range of  $X_{Mg}$  from 0 to 0.86 (Table 1). A detailed description of the five biotites is given in the appendix (rock type, sample locality

or origin, grain size, and source). In addition, the homogeneity of the NBS30 biotite RM (Gonfiantini 1984) was examined for SIMS analyses. NBS30 is well-characterized for bulk  $\delta^{18}\text{O}$  values, but was to our knowledge never tested for in-situ analysis.

## 2.3 Analytical techniques

### 2.3.1 *Sample preparation*

Polishing of sheet silicates is notoriously difficult and represents a challenge for sample preparation. Five to ten biotite grains of 0.5-2 mm size were mounted in epoxy resin. NBS30, UNIL\_B3 and UNIL\_B4 have small grain sizes (100-300  $\mu\text{m}$ ), so that only the largest grains were used in order to facilitate sample preparation. The mounts were first ground and then polished using diamond paste, decreasing the diamond size from 10 to 0.5  $\mu\text{m}$ . This way a good polish with a minimum relief was obtained, which is essential for a good reproducibility and accuracy of SIMS analyses (Kita *et al.* 2009). All the grains were placed within 8 mm of the center of the mount (Kita *et al.* 2009, Peres *et al.* 2012). The mount used for the calibration of the matrix effect was scanned with a White Light interferometer Contour GTK-A (Brucker) in order to quantitatively determine the topography. The overall relief was found to be 10  $\mu\text{m}$  between border and center of the mount (over a distance of 1.3 cm). The relief between epoxy resin and individual grains was less than 5  $\mu\text{m}$ .

Table 1: Microprobe analyses of the reference materials in % m/m oxydes. 1SD variations for each Reference Material in brackets. Structural formulae are normalized to 22 oxygens.

	UNIL_B1	1SD	UNIL_B2	1SD	NBS30	1SD	UNIL_B3	1SD	UNIL_B4	1SD	UNIL_B5	1SD
SiO <sub>2</sub>	39.69	(0.26)	40.93	(0.43)	36.36	(0.16)	34.71	(0.37)	38.10	(0.33)	37.58	(0.33)
Al <sub>2</sub> O <sub>3</sub>	10.97	(0.1)	14.44	(0.23)	15.57	(0.23)	14.34	(0.27)	14.98	(0.14)	13.20	(0.26)
TiO <sub>2</sub>	2.12	(0.05)	0.50	(0.04)	3.18	(0.46)	5.54	(0.13)	1.73	(0.15)	0.04	(0.02)
FeO	17.99	(0.12)	6.68	(0.07)	19.99	(0.22)	23.96	(0.29)	10.63	(0.83)	32.04	(0.44)
MgO	13.78	(0.16)	22.08	(0.17)	9.89	(0.22)	6.70	(0.11)	18.55	(0.69)	0.01	(0.02)
MnO	0.63	(0.04)	0.02	(0.01)	0.21	(0.02)	0.16	(0.02)	0.10	(0.02)	1.21	(0.04)
CaO	b.d.l.		0.01	(0.01)	0.02	(0.02)	0.01	(0.01)	0.01	(0.01)	0.01	(0.01)
Na <sub>2</sub> O	0.53	(0.05)	0.38	(0.03)	0.14	(0.03)	0.06	(0.02)	0.09	(0.03)	0.27	(0.08)
K <sub>2</sub> O	9.21	(0.1)	9.38	(0.11)	9.17	(0.08)	8.97	(0.1)	9.95	(0.16)	7.97	(0.14)
F	2.96	(0.1)	0.19	(0.1)	0.13	(0.02)	n.m.		0.08	(0.05)	3.86	(0.11)
Cl	0.05	(0.03)	0.01	(0)	0.06	(0.01)	0.05	(0.01)	0.03	(0.01)	0.29	(0.04)
H <sub>2</sub> O <sup>a</sup>	2.11		4.28		3.58		2.68		3.84		2.05	
O=F	-1.23		-0.08		-0.05				-0.01		-1.61	
Total	98.81	(0.34)	98.88	(0.42)	98.25	(0.39)	97.17	(0.92)	98.02	(0.41)	96.93	(0.46)
Altot	1.969	(0.015)	2.448	(0.047)	2.829	(0.036)	2.666	(0.047)	2.618	(0.028)	2.598	(0.047)
Si	6.044	(0.015)	5.884	(0.036)	5.607	(0.013)	5.508	(0.05)	5.649	(0.027)	6.275	(0.05)
Al <sup>iv</sup> <sup>b</sup>	1.956	(0.015)	2.116	(0.036)	2.393	(0.013)	2.492	(0.05)	2.351	(0.027)	1.725	(0.05)
T site	8.000	(0)	8.000	(0)	8.000	(0)	8.000	(0)	8.000	(0)	8.000	(0)
Al <sup>vi</sup> <sup>c</sup>	0.013	(0.018)	0.332	(0.015)	0.436	(0.037)	0.173	(0.031)	0.267	(0.02)	0.873	(0.031)
Fe	2.291	(0.021)	0.804	(0.011)	2.578	(0.026)	3.162	(0.061)	1.319	(0.108)	4.474	(0.061)
Mg	3.128	(0.031)	4.732	(0.018)	2.273	(0.049)	1.576	(0.006)	4.101	(0.136)	0.003	(0.006)
Mn	0.081	(0.005)	0.002	(0.001)	0.027	(0.002)	0.021	(0.005)	0.012	(0.003)	0.171	(0.005)
Ti	0.242	(0.006)	0.054	(0.004)	0.368	(0.054)	0.657	(0.002)	0.193	(0.017)	0.005	(0.002)
O site	5.756	(0.015)	5.924	(0.013)	5.683	(0.038)	5.590	(0.036)	5.893	(0.017)	5.527	(0.036)
K	1.789	(0.022)	1.720	(0.022)	1.805	(0.016)	1.805	(0.032)	1.881	(0.028)	1.698	(0.032)
Na	0.155	(0.014)	0.106	(0.01)	0.043	(0.008)	0.018	(0.024)	0.026	(0.008)	0.089	(0.024)
Ca	0.001	(0.001)	0.001	(0.001)	0.003	(0.003)	0.001	(0.002)	0.002	(0.002)	0.001	(0.002)
A site	1.945	(0.022)	1.827	(0.024)	1.851	(0.015)	1.824	(0.022)	1.910	(0.024)	1.788	(0.022)
F	1.404	(0.047)	0.059	(0.7)	0.066	(0.008)	n.m.		0.039	(0.022)	2.035	(0.057)
Cl	0.020	(0.008)	0.003	(0.001)	0.016	(0.002)	0.015	(0.011)	0.007	(0.002)	0.082	(0.011)
OH												
XMg	0.59	(0.004)	0.86	(0.157)	0.48	(0.005)	0.34	(0.001)	0.76	(0.02)	0.00	(0.001)

<sup>a</sup> H<sub>2</sub>O are from TC/EA measurements, for details see Bauer and Vennemann 2015

<sup>b</sup> Al<sup>iv</sup> is calculate as follow: Altot if Altot + Si < 8 if not 8-Si

<sup>c</sup> Al<sup>vi</sup> is calculate as follow: Altot -Al<sup>iv</sup>

### 2.3.2 Electron Microprobe analysis (EPMA)

Major and minor element analyses of biotite were obtained at the Institute of Earth Sciences at the University of Lausanne with a JEOL 8200 Superprobe equipped with 5 wave dispersive spectrometers. The elemental concentrations of Si, Al, Ti, Fe, Mg, Mn, K, Na, Ca, F, and Cl were measured. The operating conditions were 15kV at 15nA, with a spot size of 10 μm.

Counting times were set to 15 seconds for background before and after peak and 30 seconds on the peak, except for Na and K where counting times were 10 seconds for background (each side) and 20 seconds on the peak. Natural minerals were used for the calibration. See supplemental data for details. The data were reduced with the CITZAF matrix correction routine (Armstrong 1989). Measurements of 20-30 points in 3 to 5 grains were made for each of the biotite RMs, using both profiles parallel to the crystallographic axis *c*, as well as perpendicular to *c* to investigate the homogeneity of each biotite. Data are given in Table 1. All the structural formulae were normalized to 22 oxygens, without Fe<sup>2+</sup>/Fe<sup>3+</sup> ratio corrections.

### 2.3.3 *Laser-heating fluorination*

The oxygen isotope composition of biotite was determined at the stable isotope laboratory of the University of Lausanne using a CO<sub>2</sub> laser-fluorination technique (see Sharp, 1990, Lacroix and Vennemann, 2015). Between 1 and 2 mg of each sample was loaded into a Pt-sample holder and dried in an oven for several hours at 110 °C. The holder in turn was loaded into the sample chamber, which was pumped using a turbo-molecular pump to achieve a vacuum better than 10<sup>-6</sup> mbars for a minimum of 1 hour. After two cycles of pre-fluorination, samples were heated with a CO<sub>2</sub>-laser in the presence of 50 mbars of pure F<sub>2</sub>. Excess fluorine was separated from oxygen by conversion using a KCl-trap held at 150 °C. Oxygen is further purified using cryogenic methods and a molecular sieve 13X and expanded into the inlet of a Thermo Finnigan MAT 253 gas source mass spectrometer. For each session only biotite sample(s) and a quartz reference were loaded to avoid potential contamination during analysis.

Oxygen isotope compositions are given in standard  $\delta$ -notation, expressed relative to VSMOW in permil (‰) (Coplen, 1988). Several quartz reference grains were measured during each analytical session. Biotite data were corrected to the average value of the quartz values analyzed

during the session. Either NBS-28 quartz was used with an accepted value of 9.64‰ (Coplen *et al.* 1983) or the in-house quartz Ls-1 with a value of 18.1 ‰, which had been calibrated against NBS-28. Replicate oxygen isotope analyses of the quartz references over the course of five analytical sessions (during 2013-2015) have an average precision of 0.14 ‰ (1 $\sigma$ ) and an accuracy of 0.11 ‰ (1 $\sigma$ ).

Table 2: Laser fluorination data: oxygen isotope composition of biotite reference materials and quartz standards

Sample	$\delta D$ corrected ‰	water content wt%	no. analyses
<b>UNIL_B2</b> 01-Feb-16	<b>-64 ± 0.22 (1sd)</b>	<b>4.28 ± 0.11 (1sd)</b>	(n=2)
<b>UNIL_B1</b> 01-Feb-14	<b>-88 ± 0.57 (1sd)</b>	<b>2.11 ± 0.01 (1sd)</b>	(n=2)
<b>UNIL_B3</b> 01-May-15	<b>-47 ± 0.49 (1sd)</b>	<b>2.68 ± 0.03 (1sd)</b>	(n=2)
<b>UNIL_B4</b> 01-May-15	<b>-64 ± 0.49 (1sd)</b>	<b>3.84 ± 0.01 (1sd)</b>	(n=2)
<b>UNIL_B5</b> 01-May-15	<b>-166 ± 0.69 (1sd)</b>	<b>2.05 ± 0.07 (1sd)</b>	(n=2)
<b>Lausanne_1 qtz</b>			
01-Feb-14	-60 ± 4.17 (1sd)	3.53 ± 0.17 (1sd)	(n=6)
01-May-15	-62 ± 1.87 (1sd)	3.48 ± 0.10 (1sd)	(n=4)
01-Feb-16	-63 ± 0.78 (1sd)	3.50 ± 0.03 (1sd)	(n=2)
Uncertainties refer to 1 standard deviation (1sd) Data are normalized to quartz reference materials LS-1 and NBS-28 qtz Accepted $\delta^{18}O$ values for these are 18.1 ‰ and 9.64 ‰ relative to VSMOW Precision and accuracy are routinely $\leq 0.2$ ‰ or better (1 sd) - for details see above Accepted $\delta^{18}O$ value for NBS30 is 5.1 ± 0.12‰ relative to VSMOW Bold values are the final values for each RM			

### 2.3.4 Secondary Ions Mass Spectrometry (SIMS)

Oxygen isotopes measurements were conducted with the IMS 1280HR of the SwissSIMS facility with a 1.5nA Cs<sup>+</sup> primary beam at 20kV. A focused high-density primary beam in Gaussian mode was used, with a 10 μm spot size and a 10 μm raster. <sup>16</sup>O and <sup>18</sup>O were simultaneously collected on faraday cups with a mass resolution of ~2200. The electron gun was used for charge compensation and carefully tuned at the beginning of each week.

An analysis of ca. 4 minutes is made up of 60 seconds pre-sputtering to remove the gold coating and surface contaminations, followed by an automated secondary beam centering (≈ 60 s) and 20 cycles of 5 seconds data acquisition. An internal error of ~0.2 % (2σ) was typically obtained. A typical 12-24 hours session was started by a calibration of the background of the two faraday cups and a mass calibration. The magnetic field was stabilized using the Nuclear Magnetic Resonance probe of the 1280HR.

## 2.4 Results and discussion

### 2.4.1 Test for orientation dependent fractionation effects

Lattice orientation effects of ca. 5 ‰ have been described for oxygen isotope analyses by SIMS in magnetite and hematite (e.g., Huberty *et al.* 2010). These effects were attributed to ion channeling effects in highly symmetric minerals. Similarly, an orientation-dependence for U/Pb ages has been suggested for baddeleyite (Wingate and Compston, 2000; Schmitt *et al.*, 2010), which is monoclinic. Hence, orientation effects needed to be evaluated in the highly non-isotropic biotite.

The biotite lattice is composed of sheets of silica and aluminum tetrahedra (T) interlayered with an octahedral sheet (O) containing mainly iron, magnesium, and aluminum. They are assembled to form a tetrahedral-octahedral-tetrahedral (TOT) coordination atomic layering (“sandwich”). TOT packages are stacked along the c-axis and bound together by interlayer cations of K and H, Cl, or F. Because biotite has this strong crystalline anisotropy, the reproducibility of SIMS oxygen isotopes analyses was tested for different lattice orientations of the grains. Grains were mounted with the c-axis parallel and perpendicular to the surface of the mount resulting in different orientations with the primary ion beam, which has an incidence of  $\approx 30^\circ$  from the normal of the sample). The data are shown in Fig. 1. There are no variations between grains of different orientations: the overall reproducibility for all grains during the session is the same as that for any individual grain (see Figure 1), between 0.3 and 0.4 ‰. The oxygen yield (i.e.  $^{16}\text{O}$  cps normalized to primary current in nA) does not show any variations related to orientation of the grains neither (see EXCEL supplementary data sheet). Hence no orientation effect is discernable at the level of the homogeneity of the biotite grains and the precision of the measurement.

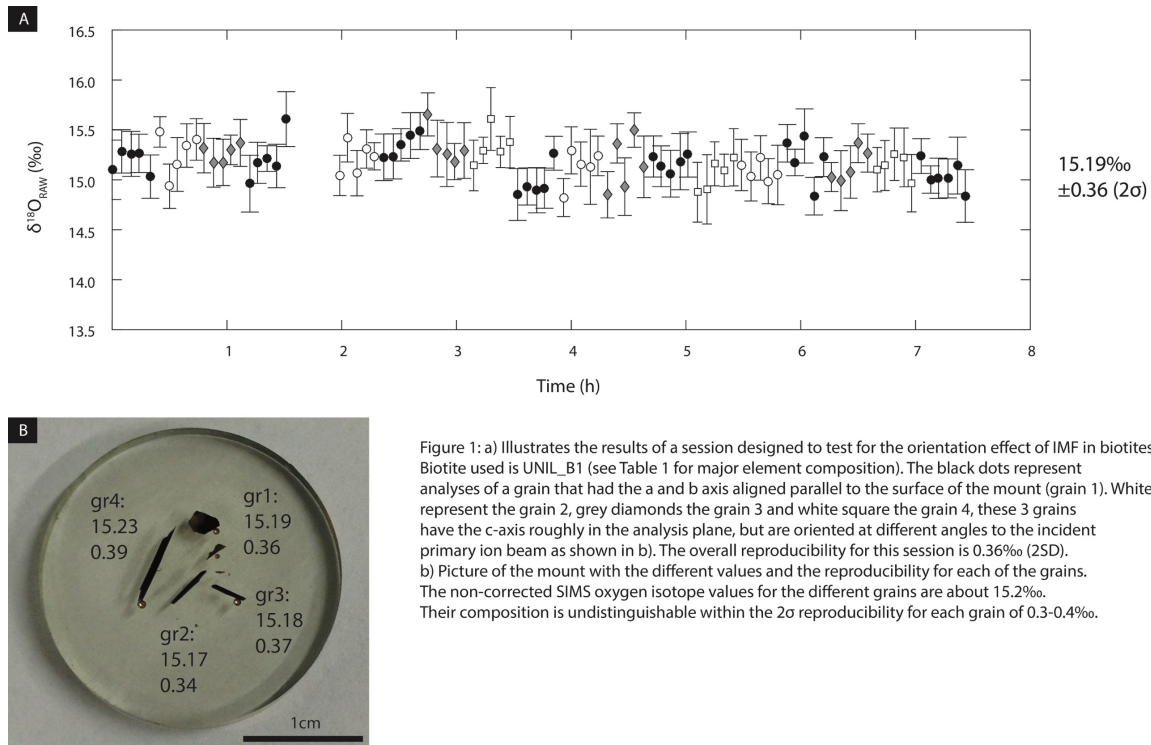


Figure 1: a) Illustrates the results of a session designed to test for the orientation effect of IMF in biotites. Biotite used is UNIL\_B1 (see Table 1 for major element composition). The black dots represent analyses of a grain that had the a and b axis aligned parallel to the surface of the mount (grain 1). White dots represent the grain 2, grey diamonds the grain 3 and white square the grain 4, these 3 grains have the c-axis roughly in the analysis plane, but are oriented at different angles to the incident primary ion beam as shown in b). The overall reproducibility for this session is 0.36‰ (2SD). b) Picture of the mount with the different values and the reproducibility for each of the grains. The non-corrected SIMS oxygen isotope values for the different grains are about 15.2‰. Their composition is undistinguishable within the  $2\sigma$  reproducibility for each grain of 0.3-0.4‰.

#### 2.4.2 $\delta^{18}O$ homogeneity tests for the 6 biotite RMs for in-situ analyses

Useful biotite RMs for SIMS analyses require that (a) they are homogeneous in major element composition to obtain a reproducible IMF; (b) the range of compositions of the RMs need to cover that of the biotite to be analyzed; and (c) a homogeneous oxygen isotope composition is required for each RM, within the reproducibility obtainable for oxygen isotope analyses (0.3 ‰). Finally, a quite large amount of material (ideally 10 to 100 grains) are needed for at least one of the RMs, since we mount at least one biotite RM with every unknown biotite (along with a reference quartz grain). The oxygen isotope value of the biotite RMs were obtained by multiple laser fluorination analyses (see Table 2), here referred to as reference values.

Homogeneity of the potential RMs was evaluated by analyzing 3-7 randomly selected grains from the mineral separates of each biotite RM. A total of 15 to 25 analyses were made on each grain, from at least 3 different locations within each grain, provided they were big enough. Otherwise the maximum number of analyses were for grains which were too small. A

reproducibility of 0.25 to 0.35 ‰ ( $2\sigma$ ) on 5 points on a restricted area of the grain was typically measured. The overall reproducibility for a biotite RM during a session is better than 0.4 ‰ ( $2\sigma$ , see Figure 2). UNIL\_B1 and UNIL\_B2 have the best reproducibility. It is less than 0.3 ‰. NBS-30 is also homogeneous at a level of 0.3 ‰, but the grains are very small and thus hard to polish. This increases the risk that the variations observed are due to topographic effects. UNIL\_B3 is the finest-grained RM and polishing is very difficult. Hence, despite its excellent homogeneity in major elements it is difficult to achieve a reproducibility of 0.3 ‰. It requires an extremely good and careful polishing protocol. UNIL\_B4 is clearly the least reproducible of all the RMs. The heterogeneity is partly due to subtle variations in major element compositions (see Figure 3). Nevertheless, the  $\delta^{18}\text{O}$  reproducibility is better than 0.4 ‰. UNIL\_B5 can have a rim of slightly different composition visible with BSE images, but its reproducibility is close to 0.3 ‰, with some points (1 out of 10) having either lower or higher values (by 1 to 3 ‰) when compared to the majority of the analyses. Including these points will decrease the reproducibility to 0.4-0.5 ‰, but does not affect the calibration of the matrix effect. We recommend to use UNIL\_B1 or UNIL\_B2 as RMs to mount with each 1-inch plug because of their good reproducibility and ease of preparation. They have big grains of typically 1 to 3 mm size, with flat cleavage planes.

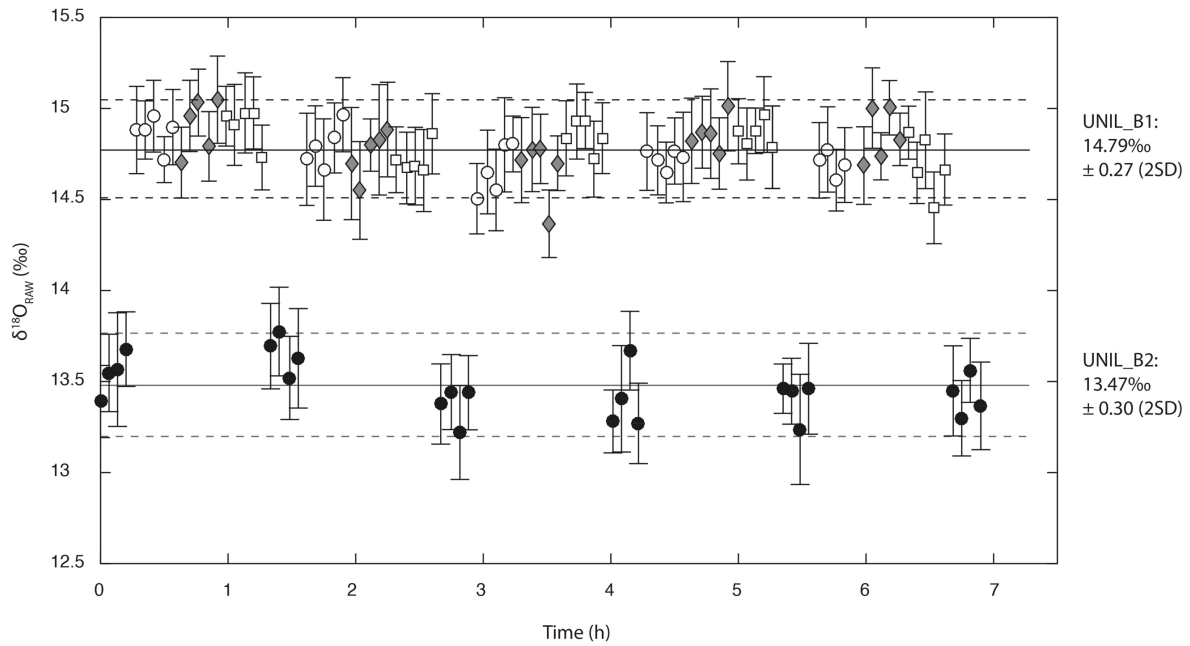


Figure 2. A typical analysis session of three grains of the UNIL\_B1 biotite with a measurement repeatability of 0.27‰ (2s) for the entire session. The filled diamonds represent grain 1, open squares are analyses of grain 2 and open circles those of grain 3. UNIL\_B2 was used as internal reference crystal (black dots), which had a measurement repeatability of 0.30‰ (2s). No drift was observed in this session, which lasted ca. 7 h.

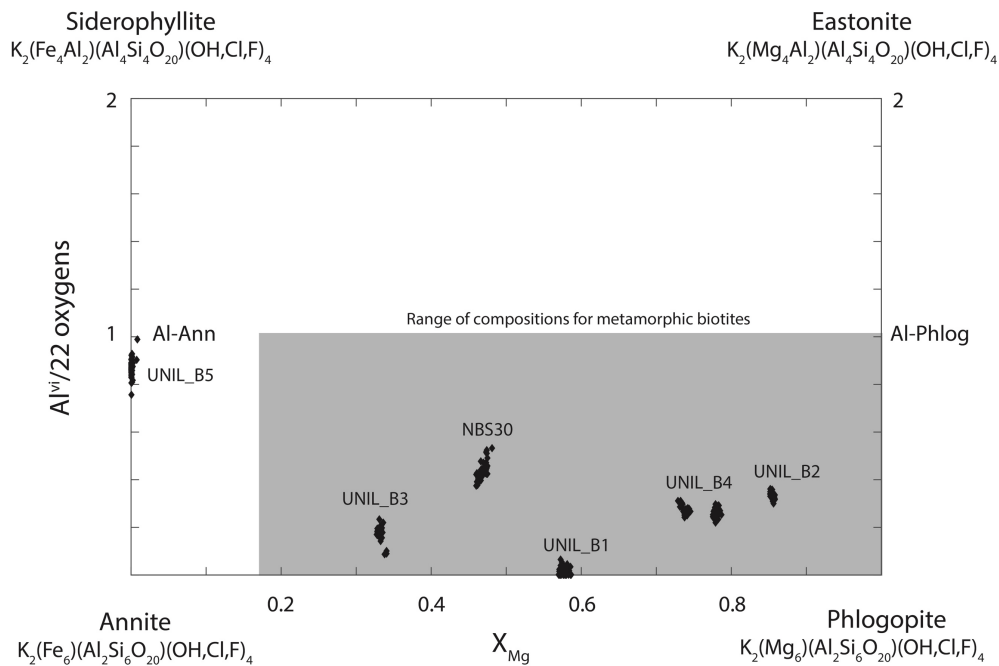


Figure 3. Outline of the composition space of the biotite group minerals.  $Al^{VI}$  represents the  $Si_{-1}R^{2+}_{-1}Al^{IV}Al^{VI}$  exchange vector,  $X_{Mg}$  the  $Fe_{-1}Mg$  vector. The grey area represents the range of composition of most metamorphic biotite from lower amphibolite facies to granulite facies (from Guidotti 1984).

### 2.4.3 Investigation of the matrix effect on IMF

The data presented in this section have been collected during two sessions on the 12th and 19th of April, 2015. During these sessions all 6 biotite RMs were analyzed on the same mount, using one or more grains of each RM, with at least 10 points for each biotite. UNIL\_B3, is the exception: only 5 points were obtained, since only one small grain was left after polishing. Since all biotite RMs were analyzed on the same mount, in the same session, and assuming constant analytical conditions, all variations in IMF should reflect the differences in sputtering and secondary ionization behavior. Empirical procedures have been used in Earth Sciences to account for these effects, although a generally accepted theoretical framework is still missing (Eiler *et al.* 1997). The matrix effect can be computed as follows:

$$\alpha_{\text{SIMS}} = \frac{(^{18}\text{O}/^{16}\text{O})_{\text{SIMS}}}{(^{18}\text{O}/^{16}\text{O})_{\text{LAF}}}$$
$$\alpha_{\text{SIMS}} = \frac{(1 + \delta^{18}\text{O}_{\text{SIMS}}/1000)}{(1 + \delta^{18}\text{O}_{\text{LAF}}/1000)} = 1 + \text{IMF}/1000$$

Rearranging this equation leads to:

$$\text{IMF} = \delta^{18}\text{O}_{\text{SIMS}} - \delta^{18}\text{O}_{\text{LAF}} - (\text{IMF} \times \delta^{18}\text{O}_{\text{LAF}}/1000)$$

Then if IMF is small (<20‰), the relation can be simplified to:

$$\text{IMF} (\text{‰}) = \delta^{18}\text{O}_{\text{SIMS}} - \delta^{18}\text{O}_{\text{LAF}}$$

The  $(^{18}\text{O}/^{16}\text{O})_{\text{SIMS}}$  and  $\delta^{18}\text{O}_{\text{SIMS}}$  are the drift corrected (if needed) average oxygen isotope ratio and delta notation respectively of a biotite RM during a session of SIMS measurements,

$(^{18}\text{O}/^{16}\text{O})_{\text{LAF}}$  and  $\delta^{18}\text{O}_{\text{LAF}}$  are the reference value of the same RM as determined by the laser-heating fluorination method.

The uncertainty on the IMF for each RM reported in this study corresponds to the propagated reproducibility of SIMS analyses and laser fluorination analyses, using  $2\sigma$  values.

$$\sigma = \sqrt{(\sigma_{\text{SIMS}})^2 + (\sigma_{\text{LAF}})^2}$$

$\sigma_{\text{SIMS}}$  represents the 2 standard deviation of the mean (2SE) of all the measurements during a SIMS session on each RM,  $\sigma_{\text{LAF}}$  is the 2 standard deviation of the mean (2SE) for the reference value of all the corrected laser fluorination measurements for the same RM.

Only uncertainties in the dependent variable (IMF) were considered, since variations and uncertainties in major element compositions of each RM are very small (e.g. Table 1). In the absence of a basic functional theory for IMF, graphs of IMF versus major element composition were used to identify potential correlations.

Assuming a linear relationship, we can write:

$$\text{IMF} = a + \sum_{i=1}^n b_i \cdot X_i$$

where  $a$  and  $b_i$  are the constants to be determined by least squares regression and  $X_i$  represents the mole fraction of different elements,  $i$ . A weighted least square fit procedure was used (Bevington and Robinson 2002), since uncertainties on the individual RM are not the same (see discussions above). A measure of the quality of the fit is given by the  $\chi^2$  per point (MSWD).

$$\chi^2 = \sum_{i=1}^n \left( \frac{y_i - y_{calc}}{\sigma_i} \right)^2$$

$y_i$  and  $\sigma_i$  are respectively the measured IMF average and the uncertainty on the  $i_{th}$  RM,  $y_{calc}$  is the calculated IMF value.

Table 3: IMF and uncertainties of the reference materials for the two sessions discussed in the text.

RM	Session 12th of April				Session 19th of April			
	IMF	2SE	2SD	n	IMF	2SE	2SD	n
UNIL_B1	2.85	0.15	0.46	25	1.79	0.14	0.38	25
UNIL_B4	3.75	0.11	0.43	25	2.82	0.12	0.41	19
UNIL_B2	4.25	0.16	0.44	25	3.46	0.16	0.38	19
NBS30	3.35	0.12	0.35	25	2.25	0.14	0.47	19
UNIL_B5	1.29	0.10	0.39	23	0.03	0.14	0.45	19
UNIL_B3	2.96	0.18	0.35	5	2.18	0.38	0.77	5

The choice of chemical variables is restricted by two structural factors. First by the exchange vectors, which can be expressed using end-members (phlogopite-annite and Al-annite-Al-phlogopite for biotites, see Figure 3), and secondly by compositional dependencies, which will result in elemental correlations, such as Fe-Mg, which occupy the octahedral site and the empirically observed Fe-F avoidance rule for biotite (Rosenberg and Foit, 1977). This suggests that the fluorine composition will largely correlate with  $X_{Mg}$ , and thus might not have to be considered as an independent variable.

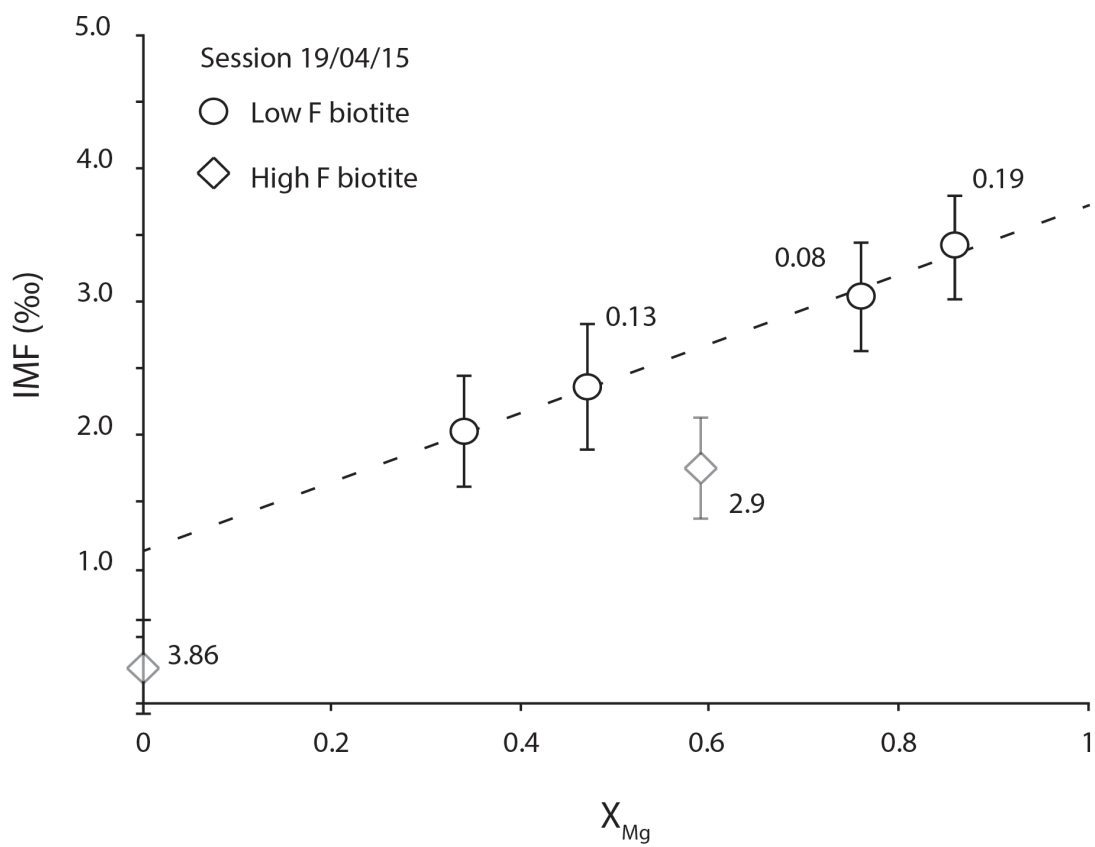
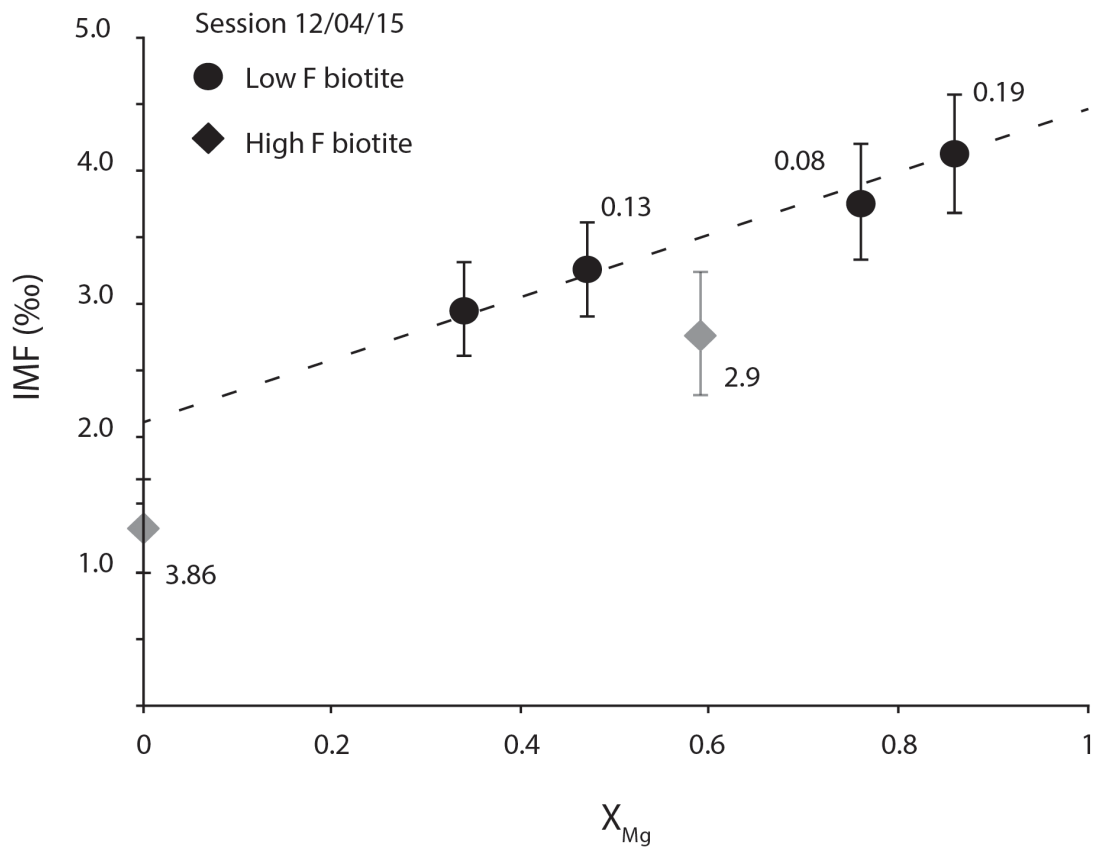


Figure 4. Plots of IMF versus  $X_{Mg}$  from two sessions. The dashed line is the fit taking into account only low F biotites (round dots). Transparent diamonds are for biotite samples with higher F content, not used for the fit. The value next to each point is the F content in % m/m.

At a first glance we expected that biotite should have the same behavior as other minerals e.g., olivine or low Ca-pyroxene (Valley and Kita 2009), which show a strong Mg-Fe exchange-related IMF. This is partly true, because taking all biotite RMs into account gives us a  $\chi^2$  per point of 0.797 and 1.235 respectively for the two sessions, demonstrating that  $X_{Mg}$  is probably the most important factor controlling IMF. We obtained a  $\chi^2$  per point lower than 1 for the first session, but the values for both UNIL\_B1 and UNIL\_B5 are outside the uncertainty. The second session is even less linear for these two biotites. Nevertheless, if only F poor biotite are used,  $X_{Mg}$  can produce a successful fit.

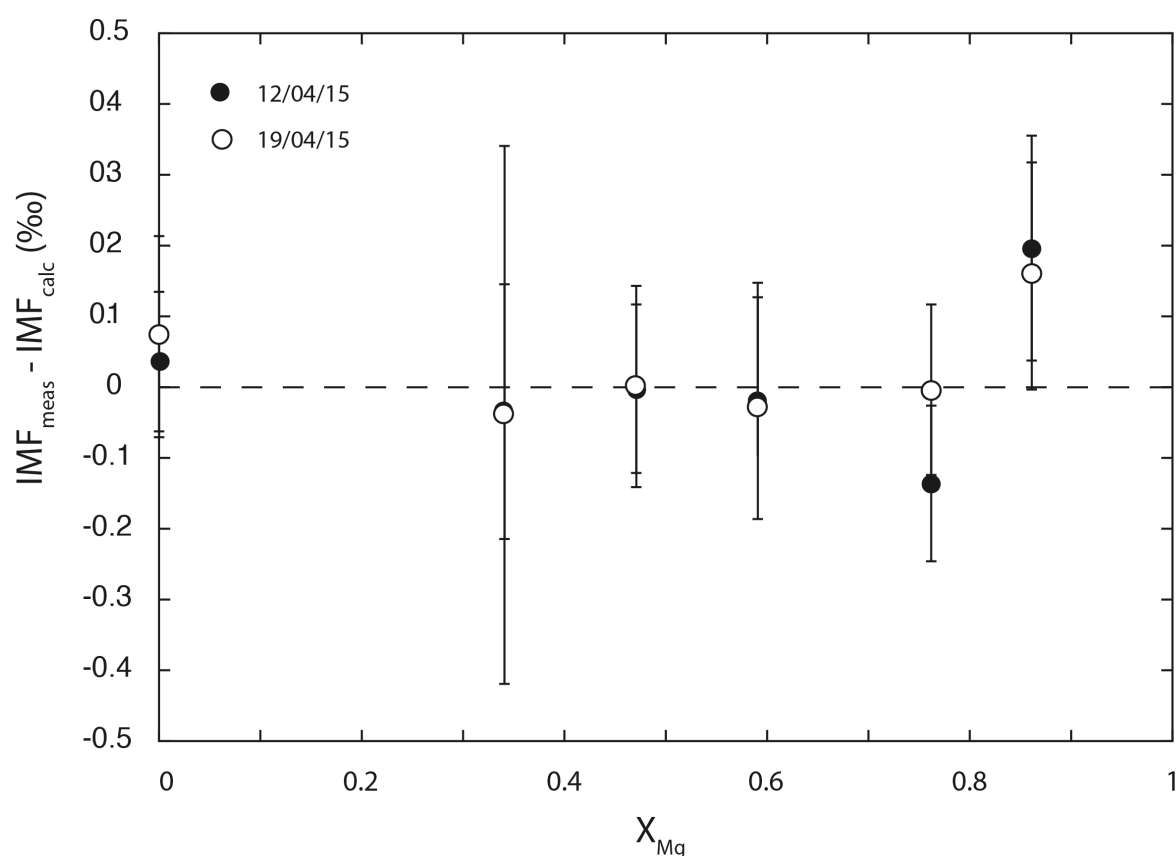


Figure 5. Difference between measured and modelled IMF value, using  $X_{Mg}$  and  $X_F$  as variables. The measured IMF values for most RMs deviated from the calculated IMF values by less than the calculated measurement uncertainty except the UNIL\_B2. The values of  $\chi^2$  per point for each session were 0.897 (12/04/15) and 0.843 (19/04/15), respectively. See text for further explanation.

To constrain the IMF for all biotite RMs a multivariate analysis is required. The following fit combinations for the multivariate analysis were considered:  $X_{Mg}$  and  $Al^{vi}$ ,  $X_{Mg}$  and Ti,  $X_{Mg}$  and Si,  $X_{Mg}$  and finally  $X_{Si}$ ,  $X_{Mg}$ ,  $Al^{vi}$  and Ti and finally  $X_{Mg}$  and  $X_F$ . The best correction scheme is obtained for a combination of  $X_{Mg}$  and  $X_F$ . With these two most RMs can be fitted within uncertainty, with the exception of UNIL\_B2, which is 0.2‰ off the fit (Figure 5). The  $\chi^2$  per point for these two sessions are 0.897 and 0.843 respectively.

#### 2.4.4 Uncertainties

The within-spot uncertainty of an unknown analysis (sample) can be computed as the standard deviation of the mean of 20 cycles during an *individual* analysis. This value is typically between 0.15 and 0.3 ‰ for the oxygen isotopes analyses on biotite, as presented here. It is always lower than the reproducibility of a few analyses of the same sample grain even if homogeneous, indicating additional factors contributing to the uncertainty of a small number of analyses. Hence we propose to determine the reproducibility for an *individual* analysis from the reproducibility of the RMs analyses before and after each block of 10-15 unknown. This 2SD value is typically  $\pm 0.3$ ‰ for biotite. Of course this requires homogeneous RM.

Since SIMS measurements need to be corrected for IMF, the accuracy (i.e. how well the reference value will be obtained) of a SIMS analysis depends on the quality of the IMF calibration. The uncertainties on the reference value of the RMs (as given by LAF) are important in the case of biotite. It has been demonstrated that they typically are in the order of 0.1-0.3 ‰ ( $2\sigma$ ). This uncertainty given by the LAF measurements needs to be propagated along with the uncertainty of SIMS analysis to obtain the total uncertainty on the IMF. The goodness of the fit will have a minor effect on the final uncertainty in the cases shown here, but this will

depend on the quality of any given individual SIMS session. Considering the arguments outlined above we suggest an uncertainty of 0.4-0.5 ‰, depending on the individual sessions.

## 2.5 Conclusion

Here we show that SIMS analyses of biotite are not hampered by orientation effects within the limits of the analytical precision. Hence, the oxygen isotope composition of biotite can be measured with confidence in natural samples, on individual grains and even in thin section. The uncertainty on multiple analyses is typically better than 0.3 ‰ ( $2\sigma$ ) when comparing biotites with similar major element compositions. A slightly higher uncertainty of  $<0.5$  ‰ ( $2\sigma$ ) is possible if comparing biotite grains of different compositions or if analyses from different sessions are used.

The IMF of biotite is a function of the  $X_{Mg}$  and  $X_F$  in biotite. These two variables need to be calibrated at the beginning of each session in order to analyse biotites, and a multivariate analysis of the RMs needs to be completed, if fluorine contents are significant. The current set of reference materials allows us to determine the oxygen isotopes composition of biotite with low F content, i.e. below 0.2wt%. More reference material with higher F content would be needed to extend the range of composition analyzable. We recommend to mount two RMs together with the unknown (UNIL\_B1 or UNIL\_B2) and to analyze them regularly during each session. In this way one RM can be used to correct for a potential drift and the second to check the accuracy of the calibration. This will decrease the final uncertainty of the measurements. Reference materials UNIL\_B1 and UNIL\_B2 are available on request; please contact the SwissSIMS laboratory for further information.

## 2.6 Acknowledgements

The authors thank Nicolas Meisser (Natural History Museum of Lausanne) for providing UNIL\_B1, Johannes Vrijmoed for UNIL\_B2, Sakiko Olsen for UNIL\_B4 and UNIL\_B5, and Johannes Hunziker for UNIL\_B3 (KAW1202 sample). We thank the two reviewers for proposing significant improvements in presentation and interpretations of the results.

Research was supported by SNF grant 200021-153094 and the KIP-6 PCI grant CASA to LPB.

## 2.7 References

- Armstrong, J. T. (1989). CITZAF: Combined ZAF and Phi-Rho (Z) Electron Beam Correction Program, California Institute of Technology, Pasadena, CA.
- Bailey, S. W. (1984). Crystal chemistry of the true micas. *Reviews in Mineralogy and Geochemistry*, 13, 13–60.
- Bauer, K. K., & Vennemann, T. W. (2014). Analytical methods for the measurement of hydrogen isotope composition and water content in clay minerals by TC/EA. *Chemical Geology*, 363, 229–240.
- Baumgartner, L.P., & Valley, J.W. (2001). Stable isotope transport and contact metamorphic fluid flow. *Reviews in Mineralogy and Geochemistry*, 43, 415-467.
- Bevington, P. R., & Robinson, D. K. (2002). Data reduction and error analysis for the Physical Sciences, 3th Edition. *McGraw-Hill Education*, 336p.
- Coplen, T. B., Kendall, C., & Hopple, J. (1983). Comparison of stable isotope reference samples. *Nature*, 302, 23-238.
- Coplen, T. B. (1988). Normalization of oxygen and hydrogen isotopes data. *Chemical Geology: Isotope Geosciences section*, 72, 293-297.
- Cosca, M. A., Sutter, J. F., & Essene, J. E. (1991). Cooling and inferred uplift erosion history of the Grenville orogen, Ontario - constraints from Ar-40/Ar-39 thermochronology. *Tectonics*, 10, 959-977.

- Eiler, J. M., Graham, C., and Valley, J. W. (1997). SIMS analysis of oxygen isotopes: matrix effects in complex minerals and glasses. *Chemical Geology*, 138, 221–244.
- Ferry, J. M., & Spear, F. S. (1978). Experimental calibration of the partitioning of Fe and Mg between biotite and garnet. *Contributions to Mineralogy and Petrology*, 66, 113–117.
- Guidotti, C.V. (1984). Micas in Metamorphic rocks, *Reviews in Mineralogy*, 13, 257–468.
- Gonfiantini, R. (1984). Advisory group meeting on stable isotope reference samples for geochemical and hydrochemical investigations, IAEA, Vienna, 19–21 September 1983. Report to the Director General. International Atomic Energy Agency, Vienna, Austria.
- Henry, D. J., Guidotti, C. V., & Thomson, J. A. (2005). The Ti-saturation surface for low-to-medium pressure metapelitic biotites: Implications for geothermometry and Ti-substitution mechanisms. *American Mineralogist*, 90, 316–328.
- Hodges, K. V., & Spear, F. S. (1982). Geothermometry, geobarometry and the Al<sub>2</sub>SiO<sub>5</sub> triple point at Mt. Moosilauke, New Hampshire. *American Mineralogist*, 67, 1118–1134.
- Huberty, J. M., Kita, N. T., Kozdon, R., Heck, P. R., Fournelle, J. H., Spicuzza, M. J., Huifang, X., & Valley, J.W. (2010). Crystal orientation effects in  $\delta^{18}\text{O}$  for magnetite and hematite by SIMS. *Chemical Geology*, 276, 269–283.
- Ickert, R. B., & Stern, R. A. (2013). Matrix Corrections and Error Analysis in High-Precision SIMS 18O/ 16O Measurements of Ca-Mg-Fe Garnet. *Geostandards and Geoanalytical Research*, 37, 429–448.
- Ingamells, C.O., & Engels, J.C. (1976). Preparation, analysis and sampling constants for a biotite. *U.S. National Bureau of Standards, Special Publications*. 422, 403–419.
- Kita, N. T., Ushikubo, T., Bin Fu & Valley, J. W. (2009). High precision SIMS oxygen isotope analysis and the effect of sample topography. *Chemical Geology*, 264, 43–57.
- Kita, N. T., Huberty, J. M., Kozdon, R., Beard, B. L., & Valley, J. W. (2011). High-precision SIMS oxygen, sulfur and iron stable isotope analyses of geological materials: accuracy, surface topography and crystal orientation. *Surface and Interface Analysis*, 43, 427–431.
- Lacroix, B., & Vennemann, T. (2015). Empirical calibration of the oxygen isotope fractionation between quartz and Fe–Mg-chlorite. *Geochimica et Cosmochimica, Acta* 149, 21–31
- Li, Q.L., Chen, F., Li, X., Wang, F., & He, H. (2008). Single grain Rb–Sr isotopic analysis of

- GA-1550 biotite, LP-6 biotite and Bern-4M muscovite  $^{40}\text{Ar}$ – $^{39}\text{Ar}$  dating standards. *Geochemical Journal*, 42, 263-271.
- Munoz, J. L. (1984). F-OH and Cl-OH Exchange in Micas with Applications to Hydrothermal Ore Deposits. *Reviews in Mineralogy and Geochemistry*, 13, 469–493.
- Peres, P., Kita, N. T., Valley, J. W., Fernandes, F., & Schuhmacher, M. (2012). New sample holder geometry for high precision isotope analyses. *Surface and Interface Analysis*, 45, 553–556.
- Riciputti, L. R., Patterson, B. A., & Ripperdan, R. L. (1998). Measurement of light stable isotope ratios by SIMS: Matrix effects for oxygen, carbon, and sulfur isotopes in minerals. *International Journal of Mass Spectrometry*, 1–32.
- Rieder, M., Cavazzini, G., DYakonov, Y. S., Frank-Kamenetskii, V. A., Gottardi, G., Guggenheim S., et al. (1998). Nomenclature of the micas. *The Canadian Mineralogist*, 36, 41–48.
- Rosenberg, P. E., & Foit, F. F. (1977). Fe<sup>2+</sup>-F avoidance in silicates. *Geochimica et Cosmochimica Acta*, 41, 345-346.
- Schmitt, A. K., Chamberlain, K. R., Swapp, S. M. & Harrison, M. T. (2000). In situ U–Pb dating of micro-baddeleyite by secondary ion mass spectrometry. *Chemical Geology*, 269, 386-395.
- Sharp, Z. D. (1990). A laser-based microanalytical method for the in-situ determination of oxygen isotope ratios of silicates and oxides. *Geochimica et Cosmochimica Acta*, 54, 1353-1357.
- Śliwiński, M. G., Kitajima, K., Kozdon, R., Spicuzza, M. J., Fournelle, J. H., Denny, A., & Valley, J. W. (2016). Secondary Ion Mass Spectrometry Bias on Isotope Ratios in Dolomite-Ankerite, Part I:  $\delta^{18}\text{O}$  Matrix Effects. *Geostandards and Geoanalytical Research*.
- Spear, F. S. (2014). The duration of near-peak metamorphism from diffusion modelling of garnet zoning. *Journal of Metamorphic Geology*, 32, 903–914.
- Valley, J. W. (2001). Stable isotope thermometry at high temperatures. *Reviews in Mineralogy and Geochemistry*, 43, 365-413.
- Valley, J. W., Kitchen, N., Kohn, M. J., Niendorf, C. R., & Spicuzza, M. J. (1995). UWG-2, a

- garnet standard for oxygen isotope ratios: Strategies for high precision and accuracy with laser heating. *Geochimica et Cosmochimica Acta*, 59, 5223–5231.
- Valley, J.W., & Kita, N. (2009). In situ oxygen isotope geochemistry by ion microprobe. Mineralogical Association of Canada Short Course 41.
- Villa, I. M. (1990). Geochronology and excess Ar geochemistry of the Lhotse Nup leucogranite, Nepal Himalaya. *Journal of Volcanology and Geothermal Research*, 44, 89-103.
- Volfinger, M., Robert, J-L., Vielzeuf, D. & Neiva, A. M. R. (1985). Structural control of the chlorine content of OH-bearing silicates (micas and amphiboles). *Geochimica et Cosmochimica Acta*, 49, 37-48.
- Wingate, M.T.D., & Compston W. (2000). Crystal orientation effects during ion microprobe U–Pb analysis of baddeleyite. *Chemical Geology*, 168, 75-97.
- Page, F. Z., Essene, E. J., Mukasa, S. B., & Valley, J. W. (2010). A Garnet-Zircon Oxygen Isotope Record of Subduction and Exhumation Fluids from the Franciscan Complex, California. *Journal of Petrology*, 55, 103–131.
- Zhu, C. & Sverjensky, D. A. (1991). Partitioning of F-Cl-OH between minerals and hydrothermal fluids. *Geochimica et Cosmochimica Acta*, 55, 1837-1858.

### 3 Channelized igneous fluid infiltration documented in the Torres del Paine contact aureole

Authors: Guillaume Siron, Robert Bodner, Lukas Baumgartner, Benita Putlitz, Othmar Muntener, Torsten Vennemann

Proposed journal: American Mineralogist

### 3.1 Introduction

Fluid circulation is common in contact aureoles, and evidences of fluid-rock interactions have been well documented (Ferry 1986, Nabelek and Labotka 1993, Gerdes et al. 1995, Roselle et al. 1999, Ferry 2000, Nabelek and Labotka 1993). It plays an important role in mass and heat transport during metamorphism (Ferry 1986, Baumgartner and Rumble 1988, Baumgartner and Valley 2001, Cui et al. 2001, Gerdes et al. 1998), influences mineral assemblage stability (Ferry 1986, Baumgartner and Ferry 1991, Cartwright and Buick 1996, Ferry 2000), reaction kinetics (Carlson 2010) and can enhance partial melting at low temperatures (Goranson 1983, Tuttle and Bowen 1958, Luth et al. 1964, Holness and Clemens 1999, Wohlers and Baumgartner 2012).

Stable isotopes are a powerful tool to track fluid infiltration and origin of this fluid. In contact aureoles, evidences of magmatic fluid infiltration has been well described in metacarbonates and marls (Labotka et al. 1988, Cook et al. 1997, Baumgartner et al. 1989, Holness 1997, Roselle et al. 1999), but rarely in metapelites. The position of stable isotopes fronts yield constraints on the amount of fluid that infiltrated a rock using transport theory (Baumgartner and Rumble 1988, Baumgartner and Valley 2001, Bickle and Naker 1990).

Flow can be driven by the thermal gradients (Norton and Knight 1977, Furlong et al. 1991, Gerdes et al. 1995, Cook et al. 1997, Dutrow et al. 1999), successive dehydration reactions in the aureole and the fluid expelled from the intrusion (Furlong et al., 1991, Hanson 1995). The permeability structure of host rocks can be complicated, leading to complex 2D and 3D exchange fronts (e.g. Gerdes et al., 1995; Roselle et al., 1999) and the flow itself will influence the permeability structure (Norton and Knight, 1977, Furlong et al. 1991, Hanson 1995, Eldursi et al. 2009). It has been shown that the sampling strategy will influence the results of fluid flux

calculations in an environment controlled by channelized fluid flow significantly; e.g. the flow can easily be overestimated if petrologic sampling criteria are used (Roselle et al. 1999).

Here we present field evidences of fluid flow, bulk rock stable isotope ( $\delta^{18}\text{O}$ ,  $\delta\text{D}$ ) and chlorine concentrations in biotite to document scale of water rock interaction, source and relative timing of fluid-rock interaction in the Torres del Paine contact aureole, Patagonia. These different approaches were chosen since they have different sensitivity for monitoring fluid flow, or give complementary insight into the sources of the fluid and its water-rock interaction. The Torres del Paine represents one of the best natural laboratory to study fluid flow due to its 3D outcrops exposure (Baumgartner et al. 2007), precise time scale and geochemical constraints on magmatic history (Michel et al. 2008, Leuthold et al. 2012, Leuthold et al. 2013) permits to link pulses of fluid flow to detailed igneous history of the granitic complex. Hydrogen isotope can trace even small amount of water infiltration, while oxygen isotopes require larger amounts to document fluid flow (e.g. Baumgartner and Valley, 2001). Finally, chlorine concentrations should permit to trace water-rock interaction during fluid loss (see chapter 4) as well as identify potential infiltration of igneous fluids from crystallizing plutons, since the residual igneous fluids are typically chlorine rich (Candela 1997).

### 3.2 Geological setting

The Torres del Paine intrusive complex (TPIC) is located in the southernmost Andes of Chile in Patagonia. It consists of three major granite laccoliths, a mafic stock and a composite mafic laccolith. They intruded the Cretaceous turbidites between 12.60 and 12.43 Ma (Michel et al. 2008; Leuthold et al., 2012). The intrusion is elongated in west-east direction with a total length of 12km and a north-south extension of 8km (Fig. 1a). The major feeder zone of the TPIC is situated at the western end of the laccolith (Baumgartner et al. 2007; Leuthold et al., 2013, 2014). A small, well defined contact aureole was formed in the Cretaceous Punta Barrosa and

Cerro Torro Formation. These formations are mainly composed of pelites, psammites and sandstone, with minor thick (>10m) conglomerate layers in the Cerro Torro formation (Wilson, 1991; Hubbard and Schultz, 2008; Fildani, 2005). They also contain some minor carbonate layers with a thickness of a few centimeters to a few decimeters. This cretaceous sequence represents a thick sequence of turbidites, shed from the west into the foreland trench of the Andes (Fildani et al. 2008b; Hubbard and Schultz, 2008; Hubbard et al. 2008). The intrusion was emplaced at ca. 750 bars (Putlitz et al., 2001), based on the stability of prehnite in metacarbonate, fayalite in the granites, as well as some fluid inclusions in the myriolitic cavities of the granites.

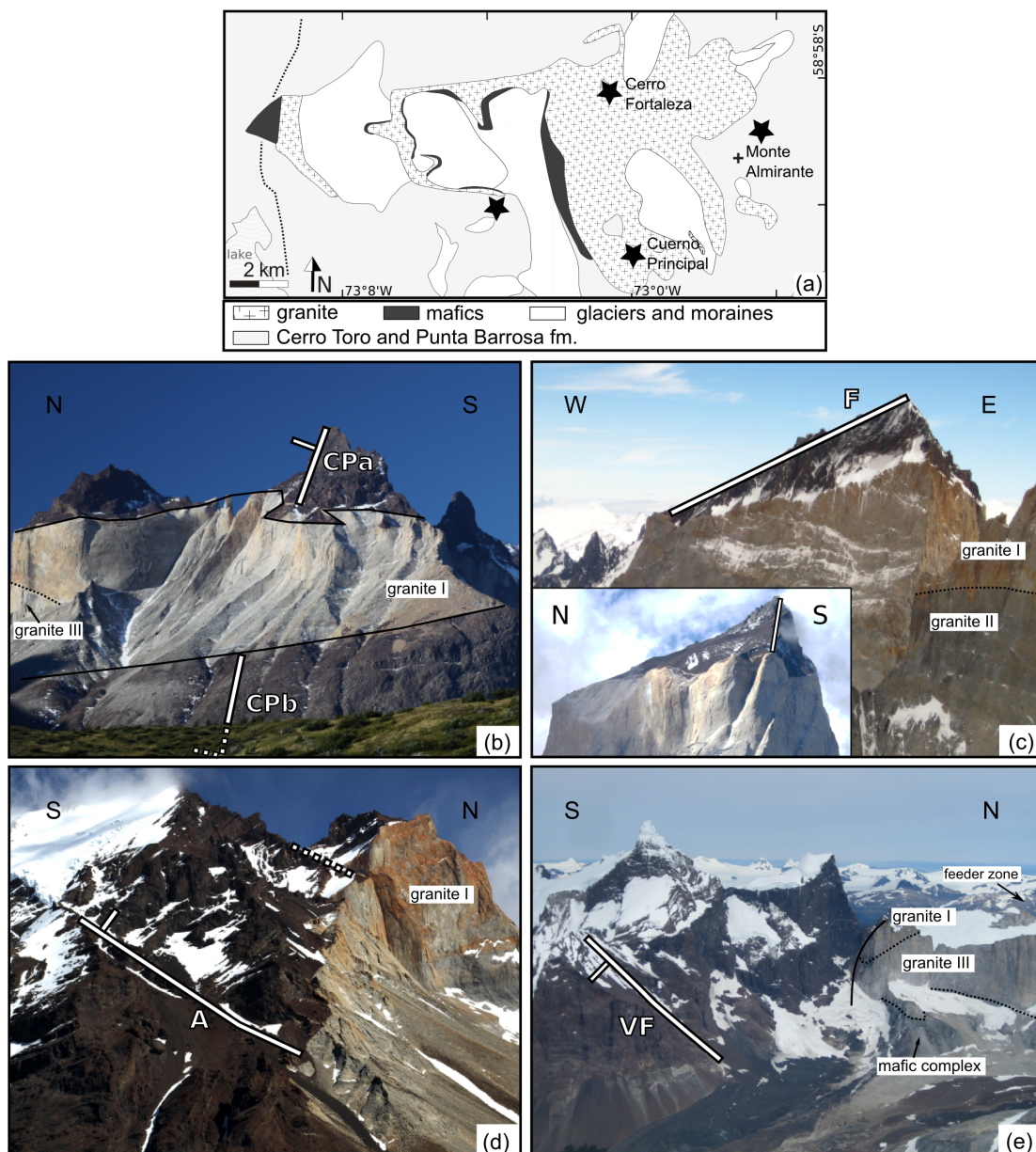


Figure 1 : (a) Geological map of the Torres del Paine Intrusion (TPI); it has a west-east and a north-south extension of about 12 and 8 km, respectively. The TPI is a bimodal laccolith which consists of three older granitic (12.59-12.50 Ma, Michel et al. 2008) and three younger mafic (12.5-12.43 Ma, Leuthold et al. 2012) pulses. It intruded into the sediments of the Punta Barrosa and Cerro Toro formations. The investigated localities are situated in the Cerro Toro formation (black stars). (b) A profile above and below the intrusion was investigated at the Cuerno Principal, at the south end of the TPI. The thickness of the contact aureole is indicated by the perpendicular white line. It is 400 and 150 m below and above the intrusion, respectively. (c) The thickness of the contact aureole at the investigated profile on the Cerro Fortaleza is unknown, because the summit still contains cordierite. The thickness from the upper contact to the summit is 260 m. At the Fortaleza the intrusion is thicker than at the other profile localities. It is at least 1.5 km, but the bottom of the intrusion is not exposed. (d) The Monte Almirante is situated at the east end of the laccolith. This represents the front end of the magma flow (Baumgartner et al., 2007). One profile above the intrusion was investigated. The contact aureole thickness is 200 m. (e) The profile in the Valle Frances is situated at the side of the intrusion. The thickness of the contact aureole is approximately 200m, measured perpendicular to the subvertical contact. (b)-(e) Abbreviations: CPa (Cuerno Principal above), CPb (Cuerno Principal below), F (Fortaleza), A (Almirante) and VF (Valle Frances).

### 3.3 Methods

The oxygen isotope composition of bulk rocks was determined using the CO<sub>2</sub> laser-fluorination technique (see Sharp, 1990, Lacroix and Vennemann, 2015) at the stable isotope laboratory of the University of Lausanne. Between 1 and 2 mg of powder of each sample was loaded into a Pt-sample holder and dried in an oven for several hours at 110 °C. The holder was then loaded into the sample chamber, which was pumped using a turbo-molecular pump to achieve a vacuum better than 10<sup>-6</sup> mbars for a minimum of 1 hour. After two cycles of pre-fluorination, samples were heated with a CO<sub>2</sub>-laser in the presence of 50 mbars of pure F<sub>2</sub>. Excess fluorine was separated from oxygen by conversion using a KCl-trap held at 150 °C. Oxygen is further purified using cryogenic methods and a molecular sieve 13X and expanded into the inlet of a Thermo Finnigan MAT 253 gas source mass spectrometer. Oxygen isotope ratios are given in standard δ-notation, expressed relative to VSMOW in permil (‰) (Coplen, 1988). Several aliquots of quartz standard were measured during each analytical session.

Hydrogen isotope composition was analyzed using the Thermal Conversion Elemental Analyzer (TC/EA), see Bauer and Vennemann (2014). 1 to 2 mg of sample powder were weighted into silver cups and crimped. They were placed into an auto-sampler, mounted on top of the TC/EA. The auto-sampler is connected to a ceramic tube that contains a smaller glassy carbon tube, glassy carbon chips, and a graphite cup for the reduction of the sample at 1450°C to form H<sub>2</sub> and CO from H<sub>2</sub>O and C. The gases were transferred using a He gas carrier via a gas chromatographic column into the mass spectrometer. Both <sup>1</sup>H and D isotopes, as long as water content, are then measured using a Finnigan Thermo Delta Plus XL. In-house standards (kaolinite K17 and biotite G1) are analyzed repeatedly during the session for normalization and possible corrections. Reproducibility for δD analyses of the standards is typically ± 2‰, 1 sigma.

Major and minor element analyses of biotite were obtained with a JEOL 8200 Superprobe equipped with 5 wavelength dispersive spectrometers. The concentration of the elements Si, Al, Ti, Fe, Mg, Mn, K, Na, Ca, F and Cl were measured. The operating conditions were 15kV, a beam current of 15nA, with a spot size of 10  $\mu\text{m}$ . Counting times were set for most elements to 15 seconds for background before and after peak and 30 seconds on the peak. Counting times were reduced for Na and K to 10 seconds on the background and 20 seconds on the peak. Scapolite (Cl), albite (Na), wollastonite (Ca), orthose (Si, K), andalusite (Al), fayalite (Fe), forsterite (Mg) and MnTi oxide (Mn, Ti) were used as reference standards. The data were reduced with the CITZAF matrix correction routine of Armstrong 1989. Structural formulae for biotite were normalized to 22 oxygens. All iron was assumed as  $\text{Fe}^{2+}$ , no  $\text{Fe}^{3+}$  corrections was attempted.

### 3.4 Sampling strategy

A total of 5 sampled profiles were collected in the host rocks around the intrusion to reflect the different parts of the intrusion accessible. All sample were collected within the metapelites of the Cerro Toro Formation. They are dark grey to black, oxide and graphite rich samples. Biotite, white mica, and cordierite can be identified in a few of the samples macroscopically. Three profiles are located above the intrusion, one at the side and one below. The different positions are illustrated on the map in figure 1a with black stars. The profiles in the roof of the pluton were collected at the Cuerno Principal (CPa, Fig. 1b), another at the Cerro Fortaleza (F, Fig. 1c), and the third profile on Monte Almirante Nieto (A, Fig. 1d). Three samples from the Monte Almirante Nieto (Fig. 1d) were taken on a ridge which is located about 500m further to the east than the rest of this profile (dotted line in Fig. 1d, A\* in table 3). They are treated together with the rest of the Mte. Almirante Nieto profile because of the similar position relative to the intrusion. All these samples were collected in 2010 during a climbing expedition for geologic

sampling. The profile below the intrusion is from the Cuerno Principale (CPb, Fig. 1b), and the final profile, located at the side of the intrusion, and slightly above it, is from the Eastern ridge of the Co. Paine Principal, in Valle Frances (VF, Fig. 1e). The TPIC granites were emplaced from the West, from the Olguin range, east of Lago Grey towards the East (Michel et al., 2007; Leuthold et al., 2012, 2013). The Cuerno Principal is located at the southern side of the pluton, while the Co. Fortaleza profile is at the northern side of the TPIC, at its maximal N-S extension. Hence the Co. Fortaleza and Cuerno Principale profiles are located in the roof of the side of the intrusion. The Mte Almirante Nieto profile is located at the Eastern end of the intrusion, which represent the front end of the magma flow direction (Leuthold et al., 2013, Baumgartner et al. 2007). The Valle Frances profile is located at the west of the intrusion center, where the incoming magma fanned out and turned towards the south. Finally, a profile below the intrusion was also sampled at the Cuerno Principal location. Hence both a profile on top and below the TPIC intrusion, at the same location with respect to the intrusion, is available for study.

The width of the contact aureole is a function of the thickness of the laccolith, the location above or below the intrusion, and the detailed intrusion geometry (e.g. Furlong et al. 1991). The sequence of metamorphic reactions is the same in all profiles, since the chemistry of the Cerro Toro Formation is very similar at all of these locations. A detailed mineralogic and phase petrology study is given below. The granite thickness is 800m at Cuerno Principale (Fig. 1b), which produces a contact aureole above of 150m and an aureole below the granite of 400m width. The distances quoted for the aureole width are the position of the biotite- and cordierite-in isograd. At the Fortaleza (Fig. 1c) the intrusion is a composite intrusion, composed of 3 different batches of granite. The cumulative thickness is not precisely known since the lower contact with the surrounding rocks is not exposed. Current exposure is ca. 1.5km of granitic rocks. The thickness of the aureole is over 260m, since the sample from the summit (Fig. 1c) still contains cordierite. At Monte Almirante (Fig. 1d) the granite has a thickness of at least

800m, and the contact aureole a thickness of 200m. The thickness of the contact aureole at the Valle Frances profile is approximately 200m. Sample distances were projected on a horizontal line, perpendicular to the sub-vertical contact (Fig. 1e).

## 3.5 Results

### 3.5.1 *Metamorphism*

The Anchimetamorphic metapelites of the Cerro Toro Formation are characterized by abundant clastic minerals. Minerals preserved are plagioclase, k-feldspar, quartz, biotites, and muscovite. Some clay minerals, chlorite, kaolinite and pyrite crystallized during the Anchizone metamorphism, and these minerals form the matrix (Süssenberger et al., submitted). The detrital grains originated from the erosion of the Patagonian Batholith and its contact metamorphic series. The sediments were deposited on the shelf and deltas on the eastern side of the Andean orogeny. Material was transported into the deep-sea trench by turbidites (Fildani et al. 2008b; Hubbard et al. 2008). The outermost parts of the contact aureole are characterized by formation of hydrated minerals from these clastic precursors.

The first well defined reaction is the breakdown of chlorite (chl), reacting with muscovite and quartz, to produce biotite (bt) and cordierite (crd). Cordierite is poikiloblastic and usually contains biotite and quartz inclusions. Biotite grain size is usually on the order of 10 $\mu$ m, often in clusters and randomly distributed in the rocks. Metamorphic muscovite has the same textures than biotite. Any remaining muscovite breaks down at higher metamorphic grade, reacting with biotite, to form k-feldspar and additional cordierite. No aluminosilicates have been found anywhere in the aureole of the TPIC. Hence the TPIC contact aureole is typical for a very low pressure environment. It corresponds to the 1a bathozone of Pattison and Tracy (1991).

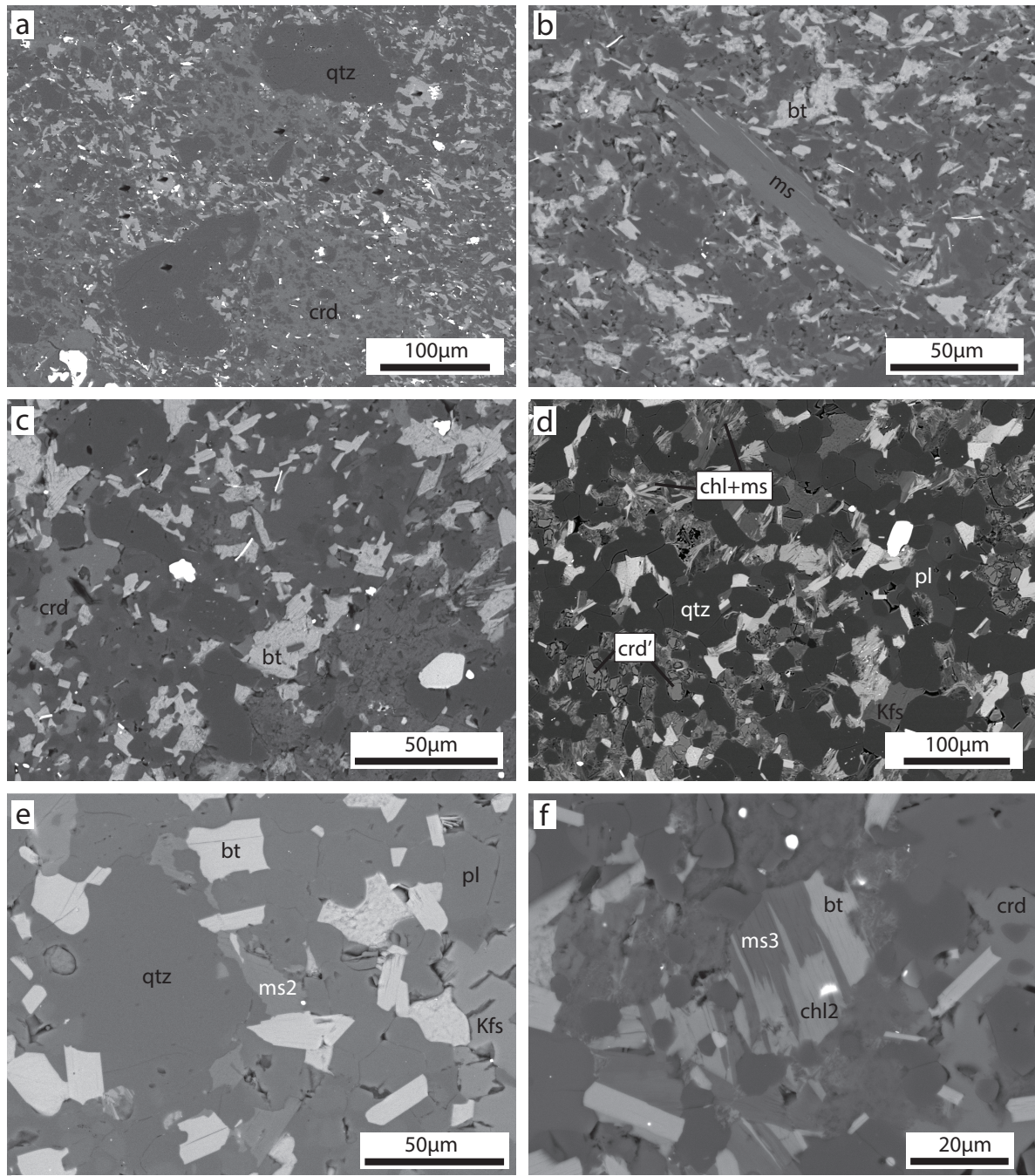


Figure 2 : BSE images of different samples of the Torres del Paine contact aureole showing textural change during metamorphism and fluid infiltration; a) big grains of detritic quartz (qtz) and metamorphic cordierite (crd) in the sample 07TP56 at 300m from the contact; b) detritic muscovite in the sample 07TP55 at 400m from the contact; c) decrease in grain size of cordierite and quartz in the 07TP58 at 150m from the contact; d) altered cordierite at the grain boundary (crd') in the sample 12P22 at 0m from the contact, abundant retrogression of cordierite and biotite to chlorite + muscovite (chl+ms), plagioclase (pl) and quartz (qtz) are equigranular and homogeneously distributed in the rock; e) retrograde muscovite in the high Cl content in biotite sample 10TP57 at 0m from the contact, biotites have grain boundaries well defined and is more homogeneously distributed at the thin section scale; f) chlorite + muscovite intergrowth in the low chlorine content 10TP54 at 1m from the contact. See text for more details.

The Torres del Paine contact aureole shows a decrease in grain size for most of the reactant minerals. Big detrital quartz can be found in the outer aureole (Fig. 2a), even within the cordierite zone where it is consumed by the chlorite breakdown reaction. Quartz and plagioclase exhibit a more homogeneous grain size distribution at the thin section scale for rocks that experienced muscovite breakdown. Detritic muscovite can be found in the outer aureole as big grains, coexisting with small, newly grown, metamorphic muscovite (Fig. 2b). These variations in mineral texture with increasing grade indicates a recrystallization of the rock matrix including the reactants when muscovite reacts out at high temperature to form K-feldspar.

Rocks far from the contact with the intrusive have bigger cordierite grains (Fig. 2a) than rocks close to the contact (Fig. 2f), which have already experienced the muscovite breakdown reactions, and have typically a larger modal amount of cordierite. This indicates that the textures reflect mostly reaction textures, with minor recrystallization of the product mineral cordierite.

In contrast, biotite grain size has an opposite trend. In the outer part, biotites are very small, e.g. less than 10 $\mu\text{m}$ , often in clusters (Fig. 2b and 2c). In the inner part, biotites are bigger (10-25 $\mu\text{m}$ ) and distributed in the rock much more homogeneously (Fig. 2d and 2e). The Torres del Paine contact aureole rocks also exhibit different stage of retrogression. Newly grown muscovite after K-feldspar are present in several samples (Fig. 2e), they are distinct from prograde metamorphic muscovite since they are bigger. Even if cordierite is usually well preserved in the Torres del Paine contact aureole, many samples show evidences of destabilization of cordierite, sometimes it is locally altered at the grain boundary (Fig. 2d), but more often cordierite is completely replaced by muscovite and chlorite intergrowth. Biotite can also be replaced by muscovite and chlorite (Fig 2f).

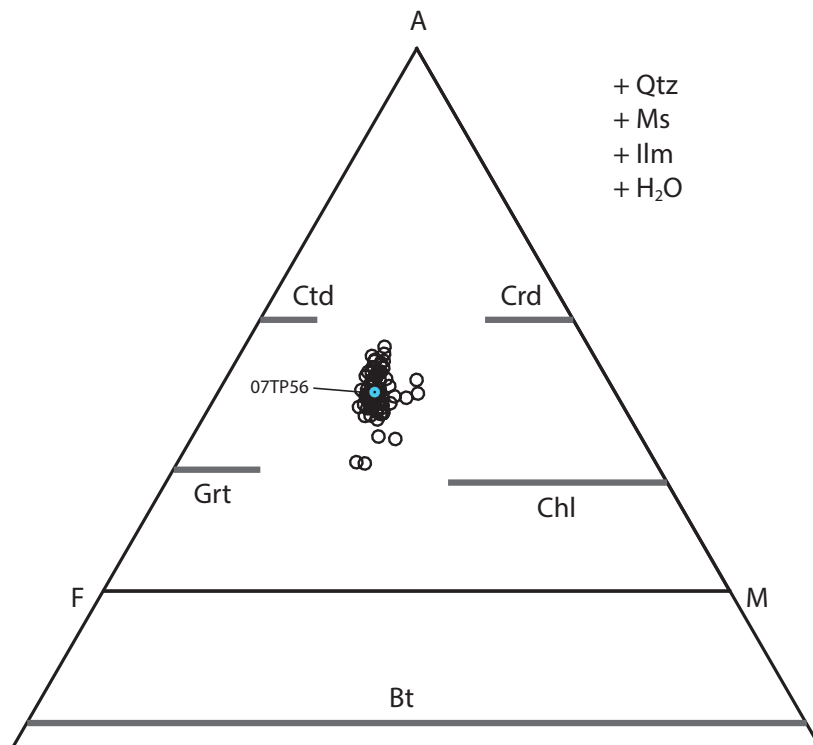


Figure 3: Thompson like AFM triangular plot of all the bulk rock composition of the Torres del Paine contact aureole, projected through muscovite and FeO corrected for ilmenite. Blue symbol represents the bulk rock composition (sample 07TP56) chosen for thermodynamic modeling.

Pseudosections were computed using the *Perple\_X* software (Connolly 2009), version 6.6.6. Due to the small variations in bulk rock chemistry of the Torres del Paine samples (see Fig. 3), sample 07-TP-56 was chosen for pseudosections calculations, since its composition is typical for most metapelites of the TPIC contact aureole. Ti has been excluded from the composition by projection through ilmenite (i.e. associated Fe moles were subtracted from the bulk rock composition), no correction for Ti in biotite was attempted since it is usually low (below 0.5 p.f.u. for 22 oxygen formulae). Graphite, present in most samples, was set as a saturated component and fluid compositions were calculated using the equation of state by Connolly and Cesare 1993 (EoS 10 in *Perple\_X*). An  $X_{O_2}$  of 1/3 was set to impose a H<sub>2</sub>O rich fluid (see Connolly and Cesare, 1993 for a discussion of this variable). This choice was made, since the fluid produced is mostly H<sub>2</sub>O, and hence, water-rich conditions most likely prevail during

contact metamorphism of metapelites in the Torres del Paine contact aureole. The choice of this fluid equation of state instead of the CORK from Holland and Powell (1991) results in a small shift of the reactions towards lower temperatures (less than 20°C compare to equation of state from Holland and Powell (1991)) for the dehydration reactions leading to biotite, cordierite, and k-feldspar isograds.

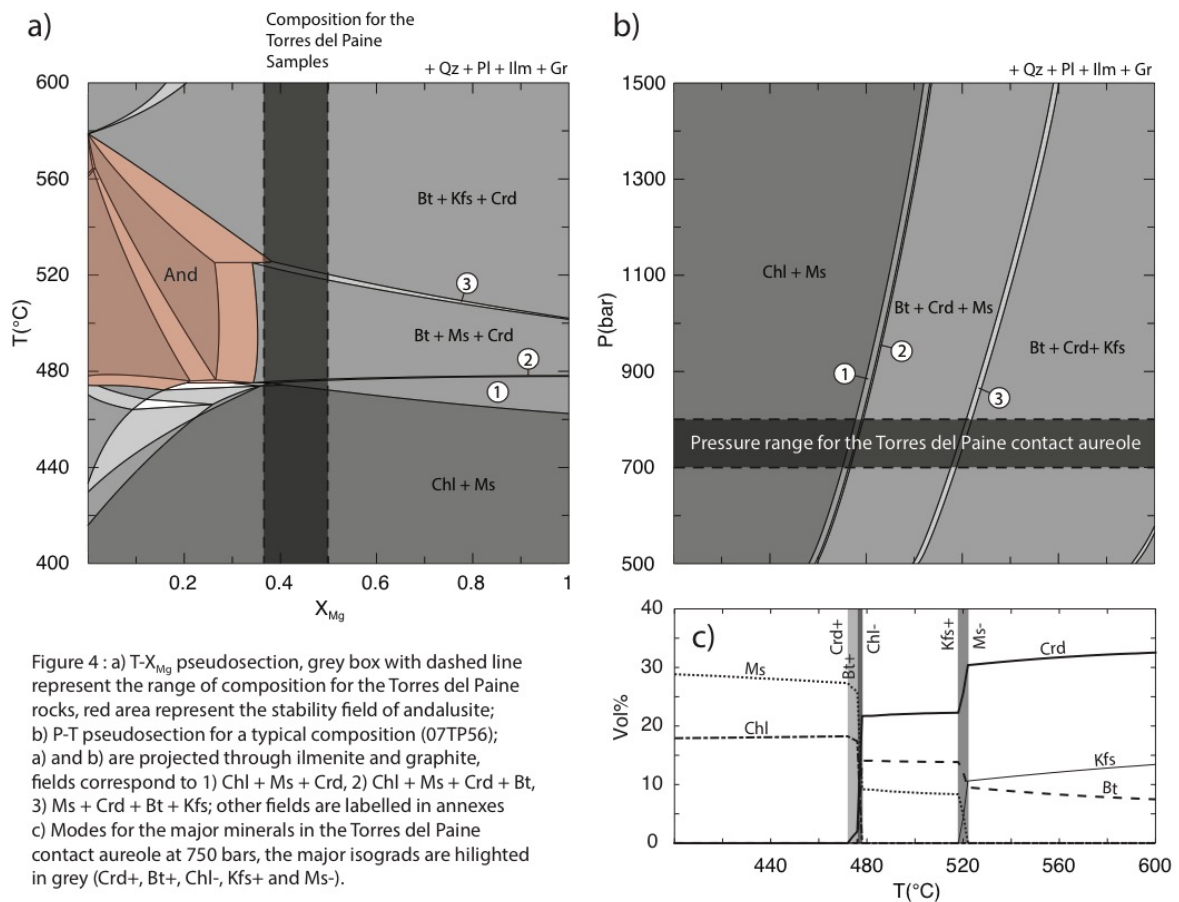


Figure 4 : a) T- $X_{Mg}$  pseudosection, grey box with dashed line represent the range of composition for the Torres del Paine rocks, red area represent the stability field of andalusite; b) P-T pseudosection for a typical composition (07TP56); a) and b) are projected through ilmenite and graphite, fields correspond to 1) Chl + Ms + Crd, 2) Chl + Ms + Crd + Bt, 3) Ms + Crd + Bt + Kfs; other fields are labelled in annexes c) Modes for the major minerals in the Torres del Paine contact aureole at 750 bars, the major isograds are highlighted in grey (Crd+, Bt+, Chl-, Kfs+ and Ms-).

Pressure can be estimated based on assemblages in meta-marls, fluid inclusions, and the presence of fayalite in k-feldspar and quartz bearing miralotic cavities in the granite to be 75MPa (Putlitz et al., 2001; Baumgartner et al., 2007). This is consistent with the absence of aluminosilicate, which also indicates very low-pressure metamorphism. Figure 4 shows a phase diagrams calculated for the composition of the selected pelite sample (07TP56). The

metamorphic reactions observed correspond well to the calculated phase diagram for this pelite sample. Interestingly, temperatures do not change much for the  $X_{Mg}$  range of 0.4 and 0.6 observed in these rocks. Both isograds, the crd-in (field 1) and kfs-in (field 3), are only slightly ( $<10^{\circ}C$ ) displaced in temperature with changes in  $X_{Mg}$ . The temperature for the isograd bt-in (field 2) is not affected by changes in bulk rock composition (Fig. 4a). This agrees well with the observation that all pelitic compositions show the appearance of cordierite at the same distance from the intrusion, allowing to mapping the isograd easily (Fig. 4a). The temperatures are  $470^{\circ}C$  for crd-in isograd and  $520^{\circ}C$  for kfs-in isograd (Fig. 4b). Figure 4c shows calculated volume percent of the major phases in the rock, in good agreement with the observed mineralogical evolution in the aureole. Even if cordierite is stable at slightly lower temperature than biotite the major episode of cordierite growth is related to the chlorite breakdown reaction, with cordierite and biotite as products of this reaction (Fig. 4c). The second episode of growth for cordierite happens during the muscovite breakdown reaction, where also K-feldspar is produced. Fe/Mg is obtained from biotites, resulting in a minor consumption of biotite (Fig. 4c).

Table 1: Assemblages of the samples from the two profiles Cuerno Principale below and Valle Frances

Samples	crd	bt	pl	ms	Kfs	chl + ms	ilm	Py
07TP55	+	+	+	+		+	+	+
07TP56	+	+	+	+		+	+	+
07TP58	+	+	+	+			+	+
07TP63	(+)	+	+		+		+	+
10TP54	+	+	+	R	+	+	+	+
10TP57	+	+	+	R	+	+	+	+
12P26	+	+	+		+		+	+
12P25	+	+	+		+	+	+	+
12P24	+	+	+		+	+	+	+
12P23	+	+	+	R	+	+	+	+
12P22	+	+	+	R	+	+	+	+

Abbreviations: crd = cordierite; bt = biotite; pl = plagioclase; ms = muscovite; Kfs = K-feldspar; Chl + ms = chlorite + muscovite intergrowth; ilm = ilmenite; py = pyrite-pyrrhotite; (+) = minor amount

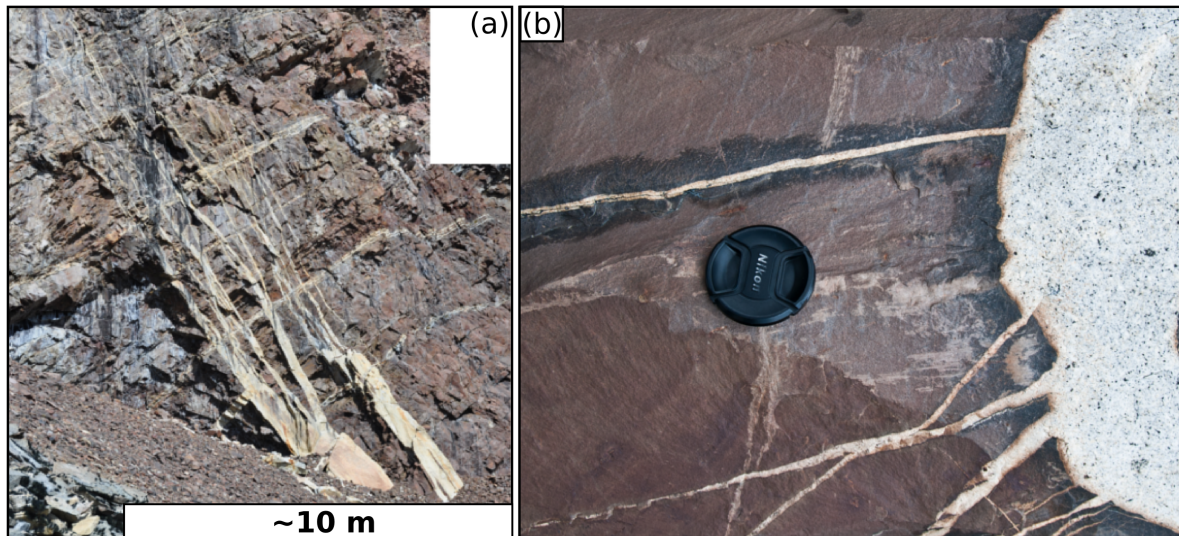


Figure 5 : Field observations of dykes in the first 50m around the main body of the laccolith; a) horse tail dykelets; b) dykelets and the bleaching zone around them. See text for more details.

### 3.5.2 *Field observations of fluid flow*

The Torres del Paine intrusion has abundant miarolitic cavities in all granitic and most mafic intrusive rocks. Cavities are more abundant towards the rim of the intrusion and modal abundances can reach up to 20-30% in the most external parts of the oldest granite, the Almirante granite (Michel et al., 2007; Baumgartner et al., 2012; Leuthold et al., 2013). These rocks are fined-grained and have graphic quartz-feldspar intergrowths. The cavities are typically isolated, but they can form in some rare cases interconnected tube-like structures surrounded by r granite gress. These cavities mark igneous fluid exsolution upon cooling and solidification of the granite. The cavities are filled mainly with euhedral quartz and feldspars, with fayalite, tourmaline, chlorite, pyrite, zeolites and carbonates (Bodner 2013). Some miaroles are completely filled with coarse quartz, forming pods up to one meter in size. These textures indicate a granite melt with near-eutectic composition, which was highly water saturated. At a pressure of 75MPa – the likely emplacement pressure (see below) water saturation of a granitic magma is reached at ca 3 wt% of water (Holtz et al., 1995).

Fluid infiltration textures – veins, or bleaching zone, skarns, etc – are rarely visible, despite the fact that the contact is extremely well exposed (see Fig. 1). The only obvious features are veins which continue on strike from dykes emanating from the intrusion into the host rocks. Numerous dykes emanate from the intrusion into the host rock on the Eastern end of the intrusion, as well as on north and south side of the intrusion. Similar dykes are observed in the distal roof parts. These dykes are similar to ring dykes in that they emanate from the rim of the intrusion about vertically from the contact, dipping towards the center of the intrusion (Fig. 5a). Their spacing is a few hundred meters in the roof. They start from within the intrusion, and can be followed for 10's to a couple of hundred meters into the host rock. They explode into a myriad of dyklets about halfway along their length. The end of each dyklet is continued by a fissure-like vein, which produces hornblende veins surrounded by bleached zones in the metacarbonates and metapelites. The veins are maximum couple millimeter wide, surrounded by a bleaching zone of a few centimeter width (Fig. 5b). The bleaching zone is due to the oxydation of the organic matter present in the sedimentary rocks. Fluid infiltration is localized along these veins. Similar bleaching zones can be found in the metasediments close to the contact. The zone is typically less than 1 meter wide, and only locally visible.

Table 2: Isotopic compositions for whole rock granites, quartz and biotites from granite and quartz from miaroles

		$\delta^{18}\text{O}$	$\delta\text{D}$
Granites	Whole rock	7.1 - 9.1 ‰	
	Quartz	9.1 - 9.9 ‰	
	Biotite	5.1 - 6.0 ‰	-97 to -95 ‰ -88 to -83 ‰
Quartz from cavities		8.8 - 11.1 ‰	

### 3.5.3 *Stable isotopes*

#### **Oxygen and hydrogen isotope composition of the Torres del Paine igneous complex.**

Whole rock oxygen isotope compositions range for mafic rocks from 5.5‰ to 7.8‰ for gabbro-norites, gabbros, and diorites, with the diorites having the lowest  $\delta^{18}\text{O}$  values (Leuthold, 2011). Granite whole rock oxygen isotope ratios vary between 7.1‰ to 9.1‰. Oxygen isotopes range from 9.1-9.9‰ for quartz and 5.1-6.0‰ for biotite (Table 2). The values fall into the field characteristic for A-type granitic plutons (Sheppard 1986). Quartz in miarolitic cavities show a slightly wider range for quartz (table 2) of 8.8-11.1‰. They overlap with those of the granites. Oxygen isotopes thermometry on fayalite-quartz pairs from miarolitic cavities give a temperature of  $750 \pm 30^\circ\text{C}$  (Putlitz et al., 2001; Putlitz et al., in prep). Quartz-biotite pairs from the granites give  $600\text{-}640^\circ\text{C}$ . Biotite is a fast diffuser for oxygen, so that these are most likely closure temperatures and not crystallization temperatures. Temperatures as high as these are rare for granitic rocks, and indicative for fast cooling (Eiler et al., 1993; Putlitz et al. 2001). Magmatic biotites hydrogen isotopes from the different granites of the Torres del Paine complex span a very narrow range of -97 to -83‰ (table 2), with the exception of one sample (-126‰), that most likely was altered. Granite I has biotites with values slightly lower from -97 and -95‰ than granite III between -88 and -83‰. The granite III has typical values for granitic biotites, while the granite I values lie in the lighter part of the common  $\delta\text{D}$  signature (Sheppard 1986).

**Chlorine content in igneous biotites.** The chlorine content of biotite from four samples from the granitic complex varies between 0.3 and 0.8 wt%. These high chlorine concentrations are consistent with a progressive enrichment of the Magmatic Volatile Phase (MVP) due to the incompatibility of Cl with the crystallizing minerals. The biotite has a higher iron content in these granites, with  $X_{\text{Fe}}$  between 0.15 and 0.32.

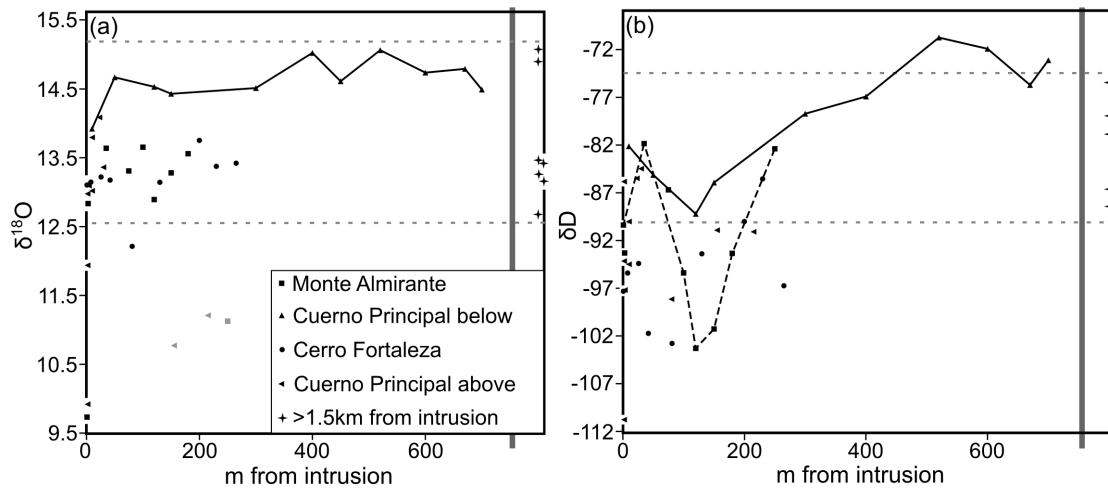


Figure 5 : Bulk rock isotopic measurements in the contact aureole; a) oxygen isotopes do not show any trend indicating small amount of fluid infiltration; b) hydrogen isotopes do show a clear trend with a decrease due to Rayleigh fractionation until 150m, and an infiltration front marked by a slight increase close to the contact. See text for more details.

Table 3: bulk rock isotopic measurements in the Torres del Paine aureole

Sample	Profile	distance	grain size	$\delta D$ (‰)	$\delta^{18}O$ (‰)
09TP6	A	1	< 200 $\mu m$	-90.38	9.73
09TP9	A	3	< 200 $\mu m$	-93.31	12.83
09TP11	A	35	< 200 $\mu m$	-81.84	13.63
09TP13	A	75	< 200 $\mu m$	-86.69	13.31
09TP14	A	100	< 200 $\mu m$	-95.39	13.65
09TP15	A	120	< 200 $\mu m$	-103.29	12.89
09TP18	A	150	< 200 $\mu m$	-101.26	13.28
09TP19	A	180	< 200 $\mu m$	-93.34	13.56
09TP22	A	250	< 1 mm	-82.39	11.13
10P55	A*	40	< 200 $\mu m$	-95.24	-
07TP63	CPb	10	< 200 $\mu m$	-82.13	13.92
07TP60	CPb	50	< 200 $\mu m$	-85.13	14.67
07TP59	CPb	120	< 200 $\mu m$	-89.21	14.53
07TP58	CPb	150	< 200 $\mu m$	-85.93	14.43
07TP56	CPb	300	< 200 $\mu m$	-78.72	14.51
07TP55	CPb	400	< 200 $\mu m$	-76.92	15.02
07TP54	CPb	520	< 200 $\mu m$	-	14.61
07TP45	CPb	520	< 200 $\mu m$	-79.74	15.06
07TP53	CPb	600	< 200 $\mu m$	-71.92	14.74
07TP48	CPb	670	< 200 $\mu m$	-75.71	14.79
07TP52	CPb	700	< 200 $\mu m$	-73.11	14.49
10P103	CPa	2	< 200 $\mu m$	-85.83	11.94
10P105	CPa	2	< 200 $\mu m$	-94.15	12.98
10P111	CPa	2	< 200 $\mu m$	-110.76	9.92
10P84	CPa	2	< 200 $\mu m$	-97.24	13.11
10P72	CPa	10	< 200 $\mu m$	-94.49	13.02
10P78	CPa	10	< 200 $\mu m$	-90.01	13.8
10P91	CPa	23	< 200 $\mu m$	-85.49	14.09
10P95	CPa	30	< 200 $\mu m$	-84.47	13.36
10P86	CPa	80	< 200 $\mu m$	-98.14	-
10P99	CPa	155	< 1 mm	-90.92	10.77
10P101	CPa	215	< 1 mm	-91.08	11.21
10P144	F	1	< 200 $\mu m$	-97.32	23.11
10P142	F	8	< 200 $\mu m$	-95.41	13.15
10P140	F	26	< 200 $\mu m$	-94.4	13.22
10P138	F	40	< 200 $\mu m$	-101.72	13.18
10P134	F	80	< 200 $\mu m$	-102.78	12.21
10P130	F	130	< 200 $\mu m$	-93.39	13.14
10P120	F	200	< 200 $\mu m$	-90.01	13.75
10P118	F	230	< 200 $\mu m$	-85.54	13.38
10P114	F	265	< 200 $\mu m$	-96.73	13.42
L5	S	>1500	< 200 $\mu m$	-80.77	15.08
L2A	S	>1500	< 200 $\mu m$	-86.64	14.86
L17	S	>1500	< 200 $\mu m$	-75.41	12.68
L12	S	>1500	< 200 $\mu m$	-88.33	13.27
L20	S	>1500	< 200 $\mu m$	-78.94	13.47
L23	S	>1500	< 200 $\mu m$	-89.32	13.44
L31	S	>1500	< 200 $\mu m$	-78.03	13.15
L40	S	>1500	< 200 $\mu m$	-75.08	-

Profiles: A = Almirante; A\* = Almirante samples with a small offset from regular profile; CPb = Cuerno Principale below; CPa = Cuerno Principale above; F = Fortaleza

### **Host rock isotope data**

Bulk rock oxygen and hydrogen isotopes ratios have been determined for the profiles above and below the Cuerno Principale, as well as for the profiles at Co. Fortaleza and at the Mte. Almirante Nieto. Several samples far from the contact aureole have also been analyzed in order to evaluate the initial heterogeneity of the isotopic values. They are plotted schematically on the right-hand side of the diagrams of figure 6.

**Host rocks oxygen isotopes.** Within each profiles oxygen isotopic signature were found to be homogeneous. However, comparison of the different profiles show differences: especially the isotope ratios profile below the intrusion at Cuerno Principale has values which are approximately 1‰ higher than for the other profiles. But taking into account all profiles, the  $\delta^{18}\text{O}$  signatures still lies into the initial heterogeneity (dashed lines in Fig. 6a). Only three samples (two from the Cuerno Principale above and one from the Monte Almirante profile) show very distinct oxygen isotopes values at distances of 155, 215 and 250m from the intrusion. In fact, these are samples which are texturally different, containing coarse clasts (>1mm) of quartz and feldspar. Their texture and mineralogy identify them as aluminium rich, immature sandstones, while the other samples had very fine grained protholiths with only small clats (<200 $\mu\text{m}$ ) if any remained after contact metamorphism. Hence, we suggest that their protholith isotopic composition might have been different.

Two additional samples have low  $\delta^{18}\text{O}$  values between 9.8-10.0‰. They were collected very close to the intrusion (<1m away from the contact) and are bleached (see fig. 2b). In addition, these samples contain a few millimeter-thick veinlets of granitic material. Hence these samples reflect intense interaction with fluids and melts emanating from the intrusion.

**Host rocks hydrogen isotopes.** The hydrogen isotopes show a clear pattern in the contact aureole in contrast to the oxygen isotopes. This is especially evident for the two profile below the intrusion at the Cuerno Principale below and above the granite at Monte Almirante Nieto

(Fig. 6b). In these two profiles the  $\delta D$  values decreases when approaching the intrusion up to about 100m away from the contact. The lowest values were measured at the Monte Almirante with -104.0‰. Hydrogen isotopes increase again closer to the intrusion, to reach a maximum at the contact, with a value of -82.0‰. Since the hydrogen signature is mainly carried by biotites in the samples close to the intrusion it can be directly compared to values of the granites, which are also dominated by hydrogen in biotite. They are very similar to the values of the granites, which vary between -97 and -83‰ (see above).

Table 4: Average compositions for biotites from samples of the different profiles

	Valle Frances						Cuerno Principale below						Co Fortaleza		
	12P22	12P23	12P24	12P25	12P26	12P27	10TP57	10TP54	07TP63	07TP58	07TP56	07TP55	10P144	10P138	10P134
SiO <sub>2</sub>	35.25	35.61	35.58	35.73	35.16	35.47	35.53	34.99	35.12	34.68	34.97	35.82	35.98	35.29	34.47
Al <sub>2</sub> O <sub>3</sub>	18.03	19.77	17.84	18.10	18.68	19.03	18.91	17.55	19.04	19.29	19.52	20.28	17.99	17.20	17.40
TiO <sub>2</sub>	3.96	1.24	4.40	4.39	4.14	3.29	3.73	3.97	2.66	2.80	2.33	1.38	4.25	4.38	4.24
FeO	21.66	20.65	20.64	22.27	21.08	20.56	20.81	21.69	22.17	21.26	23.21	21.87	20.67	20.75	22.11
MgO	6.72	7.91	7.50	6.95	7.55	7.66	7.63	7.36	7.17	7.11	7.60	8.06	8.40	7.74	7.31
MnO	0.12	0.09	0.08	0.12	0.09	0.06	0.20	0.10	0.28	0.05	0.07	0.06	0.12	0.03	0.07
CaO	0.00	0.00	0.01	0.05	0.00	0.00	0.00	0.02	0.01	0.01	0.01	0.00	0.01	0.08	0.24
Na <sub>2</sub> O	0.10	0.19	0.00	0.12	0.16	0.10	0.10	0.12	0.14	0.13	0.10	0.18	0.04	0.09	0.05
K <sub>2</sub> O	9.12	8.96	9.04	8.93	9.03	9.21	9.46	8.93	9.07	8.50	8.15	8.22	9.30	9.02	9.12
F	0.00	0.00	0.00	0.00	0.00	0.00	0.00	0.00	0.00	0.00	0.00	0.00	0.00	0.00	0.00
Cl	0.12	0.01	0.01	0.03	0.01	0.04	0.17	0.02	0.10	0.01	0.01	0.01	0.02	0.03	0.02
Total	95.08	94.43	95.10	96.69	95.90	95.42	96.54	94.75	95.76	93.84	95.97	95.88	96.78	94.61	95.03
Al <sup>tot</sup>	3.281	3.583	3.221	3.236	3.353	3.423	3.377	3.204	3.445	3.531	3.513	3.618	3.194	3.131	3.185
Si	5.443	5.476	5.451	5.420	5.355	5.413	5.384	5.421	5.392	5.386	5.340	5.422	5.420	5.451	5.354
Al <sup>iv</sup> <sup>a</sup>	2.557	2.524	2.549	2.580	2.645	2.587	2.616	2.579	2.608	2.614	2.660	2.578	2.580	2.549	2.646
T site	8.000	8.000	8.000	8.000	8.000	8.000	8.000	8.000	8.000	8.000	8.000	8.000	8.000	8.000	8.000
Al <sup>vi</sup> <sup>b</sup>	0.724	1.058	0.672	0.657	0.708	0.835	0.761	0.625	0.837	0.917	0.854	1.040	0.614	0.583	0.539
Fe	2.797	2.656	2.644	2.825	2.685	2.624	2.637	2.810	2.846	2.761	2.964	2.769	2.604	2.681	2.872
Mg	1.547	1.813	1.713	1.572	1.714	1.743	1.724	1.700	1.641	1.646	1.730	1.819	1.886	1.782	1.693
Mn	0.016	0.012	0.010	0.015	0.012	0.008	0.026	0.013	0.036	0.007	0.009	0.008	0.015	0.004	0.009
Ti	0.460	0.143	0.507	0.501	0.474	0.378	0.425	0.463	0.307	0.327	0.268	0.157	0.482	0.509	0.495
O site	5.543	5.682	5.547	5.570	5.593	5.587	5.573	5.611	5.668	5.658	5.825	5.792	5.601	5.559	5.608
K	1.796	1.758	1.767	1.728	1.755	1.793	1.829	1.765	1.776	1.684	1.588	1.587	1.787	1.778	1.807
Na	0.030	0.057	0.000	0.035	0.047	0.030	0.029	0.036	0.042	0.039	0.030	0.053	0.012	0.027	0.015
Ca	0.000	0.000	0.002	0.008	0.000	0.000	0.000	0.003	0.002	0.002	0.002	0.000	0.002	0.013	0.040
A site	1.826	1.814	1.768	1.772	1.802	1.823	1.858	1.804	1.820	1.725	1.619	1.640	1.800	1.818	1.862
F	0.000	0.000	0.000	0.000	0.000	0.000	0.000	0.000	0.000	0.000	0.000	0.000	0.000	0.000	0.000
Cl	0.031	0.002	0.002	0.006	0.002	0.009	0.043	0.004	0.027	0.002	0.002	0.003	0.006	0.007	0.006
XMg	0.356	0.406	0.393	0.357	0.390	0.399	0.395	0.377	0.366	0.373	0.369	0.396	0.420	0.399	0.371

<sup>a</sup> Al<sup>iv</sup> is calculate as follow: Al<sup>tot</sup> if Al<sup>tot</sup> + Si < 8 if not 8-Si

<sup>b</sup> Al<sup>vi</sup> is calculate as follow: Al<sup>tot</sup> - Al<sup>iv</sup>

Table 4: Average compositions for biotites from samples of the different profiles (suite)

	Cuerno Principale above					Mte Almirante							
	10P72	10P93	10P92	10P91	10P95	10P6	09TP10	10P54	09TP11	09TP13	09TP14	09TP15	09TP18
SiO <sub>2</sub>	35.15	34.77	34.85	35.00	34.91	35.31	35.59	35.52	35.69	35.14	34.58	34.33	34.73
Al <sub>2</sub> O <sub>3</sub>	19.35	17.38	17.88	18.95	18.27	16.90	17.75	17.20	17.85	17.97	17.98	17.60	19.00
TiO <sub>2</sub>	3.55	4.57	4.58	3.79	3.66	4.59	3.81	4.22	3.93	3.74	4.50	4.11	3.71
FeO	22.90	23.49	22.74	22.34	21.61	20.77	21.93	20.83	21.15	21.33	22.86	22.88	21.90
MgO	6.31	6.76	6.55	6.68	7.59	8.87	7.39	8.67	8.13	8.28	7.05	7.36	7.81
MnO	0.07	0.06	0.09	0.05	0.22	0.18	0.08	0.09	0.06	0.10	0.09	0.09	0.08
CaO	0.05	0.00	0.01	0.00	0.08	0.03	0.00	0.00	0.00	0.01	0.02	0.03	0.01
Na <sub>2</sub> O	0.08	0.08	0.06	0.07	0.03	0.17	0.15	0.08	0.18	0.13	0.05	0.09	0.07
K <sub>2</sub> O	8.92	8.95	9.13	9.14	9.38	8.73	9.32	9.13	9.09	9.22	9.17	9.14	9.24
F	0.00	0.00	0.00	0.00	0.00	0.00	0.00	0.00	0.00	0.00	0.00	0.00	0.00
Cl	0.05	0.01	0.02	0.02	0.05	0.04	0.01	0.13	0.01	0.04	0.01	0.03	0.01
Total	96.43	96.07	95.91	96.04	95.80	95.59	96.03	95.87	96.09	95.96	96.31	95.66	96.56
Al <sup>tot</sup>	3.477	3.158	3.243	3.417	3.306	3.045	3.200	3.094	3.199	3.237	3.252	3.212	3.406
Si	5.359	5.360	5.363	5.355	5.360	5.398	5.445	5.422	5.427	5.370	5.307	5.315	5.283
Al <sup>iv</sup> <sup>a</sup>	2.641	2.640	2.637	2.645	2.640	2.602	2.555	2.578	2.573	2.630	2.693	2.685	2.717
T site	8.000	8.000	8.000	8.000	8.000	8.000	8.000	8.000	8.000	8.000	8.000	8.000	8.000
Al <sup>vi</sup> <sup>b</sup>	0.837	0.518	0.606	0.772	0.665	0.443	0.645	0.517	0.626	0.607	0.560	0.527	0.689
Fe	2.920	3.029	2.927	2.859	2.775	2.655	2.806	2.659	2.690	2.726	2.934	2.963	2.786
Mg	1.434	1.554	1.503	1.524	1.737	2.021	1.685	1.973	1.843	1.886	1.613	1.699	1.771
Mn	0.009	0.008	0.012	0.006	0.029	0.023	0.010	0.012	0.008	0.013	0.012	0.012	0.010
Ti	0.407	0.530	0.530	0.436	0.423	0.528	0.438	0.485	0.450	0.430	0.520	0.479	0.425
O site	5.607	5.638	5.578	5.597	5.629	5.671	5.585	5.645	5.616	5.662	5.638	5.679	5.681
K	1.735	1.760	1.793	1.784	1.837	1.703	1.819	1.778	1.763	1.798	1.795	1.805	1.793
Na	0.024	0.024	0.018	0.021	0.009	0.050	0.044	0.024	0.053	0.039	0.015	0.027	0.021
Ca	0.008	0.000	0.002	0.000	0.013	0.005	0.000	0.000	0.000	0.002	0.003	0.005	0.002
A site	1.767	1.784	1.812	1.805	1.859	1.758	1.863	1.802	1.816	1.838	1.814	1.837	1.815
F	0.000	0.000	0.000	0.000	0.000	0.000	0.000	0.000	0.000	0.000	0.000	0.000	0.000
Cl	0.012	0.003	0.004	0.005	0.013	0.010	0.003	0.034	0.004	0.010	0.003	0.008	0.003
XMg	0.329	0.339	0.339	0.348	0.385	0.432	0.375	0.426	0.407	0.409	0.355	0.364	0.389

<sup>a</sup> Al<sup>iv</sup> is calculate as follow: Al<sup>tot</sup> if Al<sup>tot</sup> + Si < 8 if not 8-Si

<sup>b</sup> Al<sup>vi</sup> is calculate as follow: Al<sup>tot</sup> - Al<sup>iv</sup>

**Chlorine content in metamorphic biotite.** Figure 7a shows the average chlorine content of samples from the different profiles from the contact aureole. Chlorine concentrations vary within each sample, but show no systematics with the distance from the intrusion, with the exception of four samples collected just next to the intrusion contact. They are samples from 3 different profiles: these are 2 samples from the profile below the granite at Cuerno Principal, one sample from the Valle Frances side profile, and one sample from the profile above the granite at Mte. Almirante Nieto. They all are from the immediate proximity of the granite (i.e. less than 20m).

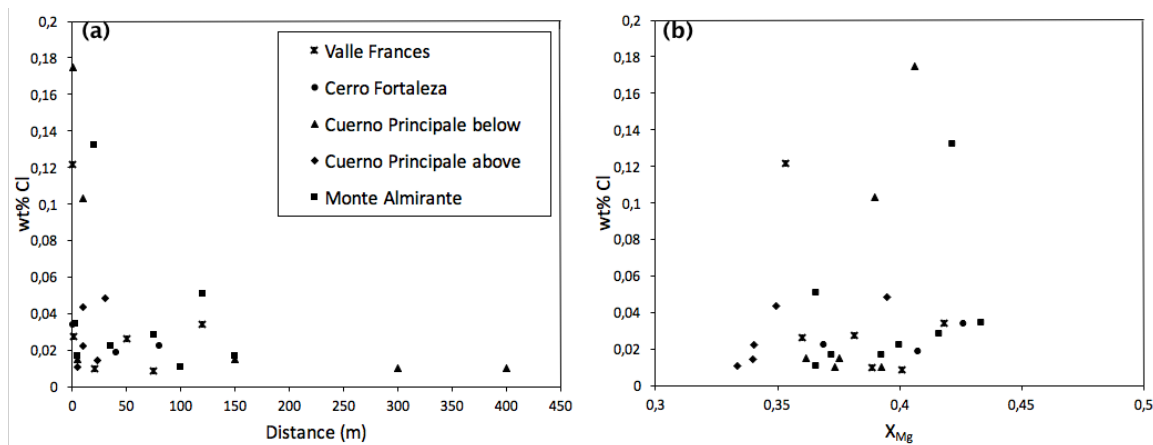


Figure 7 : Average composition of metamorphic biotite in the contact aureole; a) Cl content distribution in the contact aureole for the 5 profiles studied, with high Cl content close to the intrusion demonstrating the magmatic fluid infiltration; b) Cl content vs  $X_{Fe}$ , variations in biotite. Note that the Mg-Cl avoidance rule (Munoz 1984) would suggest that there should be a positive correlation with iron content if the changes were only due to an increase in iron content. The lack of correlations confirms that biotite exchanged chlorine with different fluids.

Chlorine concentrations in biotite in the distal aureole varies between 0.01-0.06 wt%. Chlorine concentrations in biotite close to the contact can reach a value of up to 0.18 wt%. The later values are 3 to 10 times larger than that observed in distal host rocks. It is well established that chlorine content can be higher in iron-rich biotite, this so-called « Mg-Cl avoidance rule » (Rosenberg and Foit 1977, Munoz 1984). This is important since  $X_{Fe}$  of biotite will increase with temperature, and hence similar chlorine activities could result in an increase of chlorine in biotite due to the Mg-Cl avoidance rule. Figure 7b) is exploring this possibility. It is apparent that there is no correlation between these variables. Additionally, no correlation between  $Al^{IV}$  or Ti content has been found, excluding a crystallographic control as potential explanation for the Cl content variations. This confirms that it is not the crystal chemistry which determined the changes in chlorine concentration in biotite, but that these changes are due to exchange with fluids of different composition.

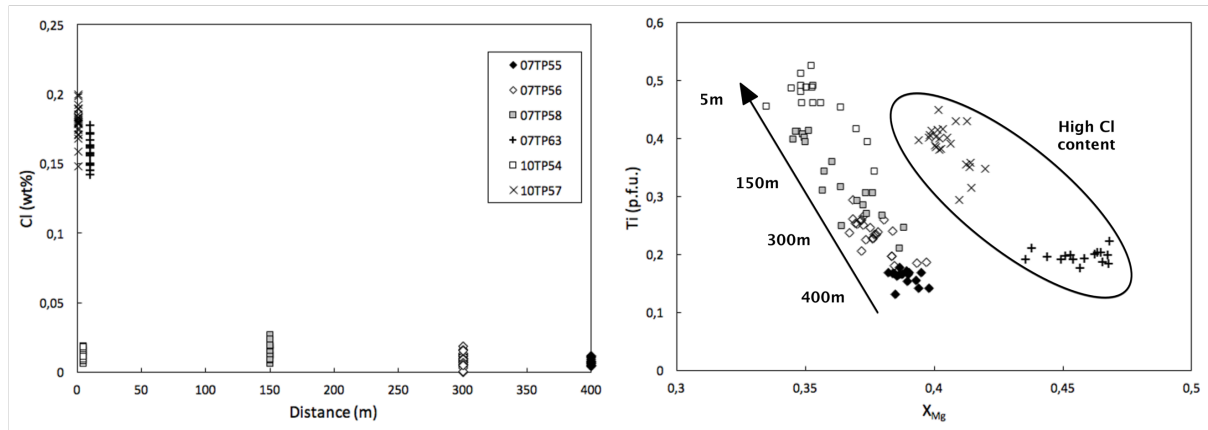


Figure 8 : Biotite compositions from the Cuernos Principale below profile; a) Cl content in biotite evolution in the profile; b) Ti vs  $X_{Mg}$ , two different trends, the low Cl content with a normal evolution, decrease in  $X_{Mg}$  and increase in Ti with increasing temperature, and the high Cl content at higher  $X_{Mg}$ , this demonstrate that these two populations have been equilibrated with two different fluids. See text for more details.

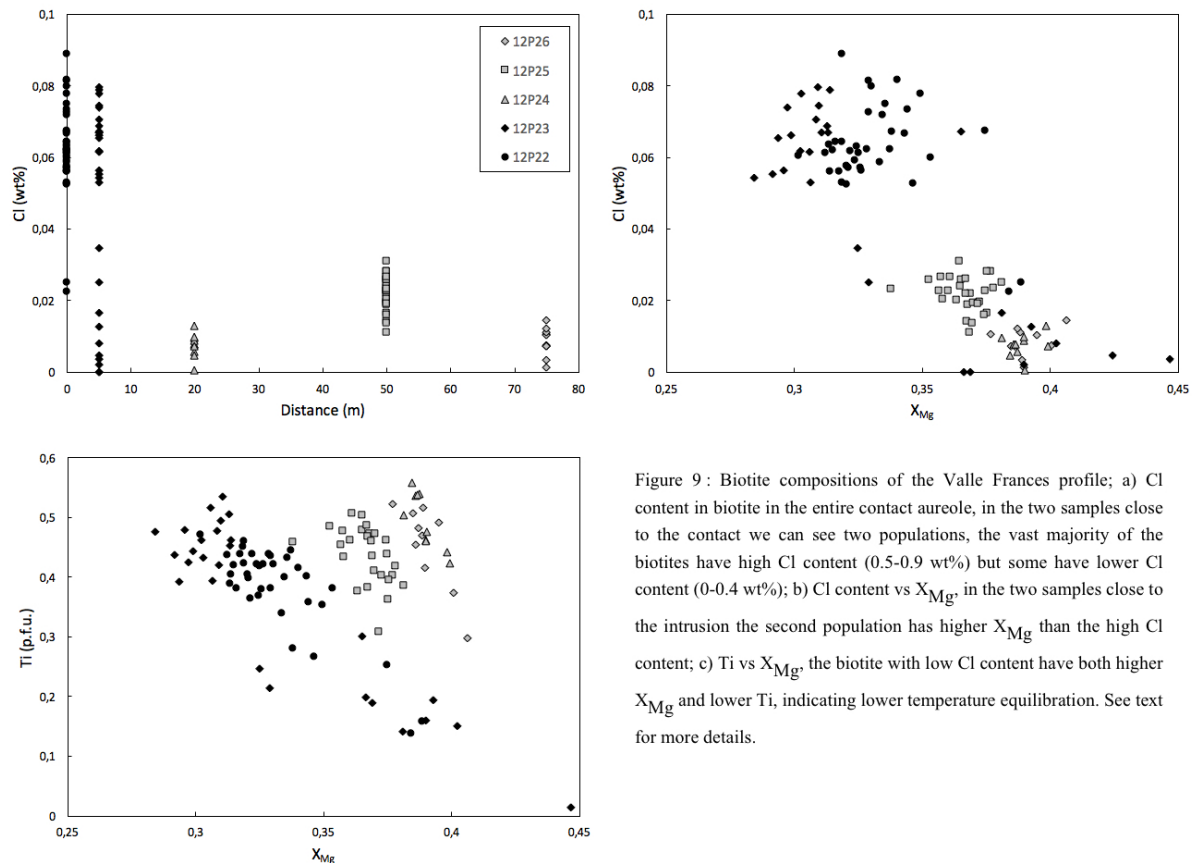


Figure 9 : Biotite compositions of the Valle Frances profile; a) Cl content in biotite in the entire contact aureole, in the two samples close to the contact we can see two populations, the vast majority of the biotites have high Cl content (0.5-0.9 wt%) but some have lower Cl content (0-0.4 wt%); b) Cl content vs  $X_{Mg}$ , in the two samples close to the intrusion the second population has higher  $X_{Mg}$  than the high Cl content; c) Ti vs  $X_{Mg}$ , the biotite with low Cl content have both higher  $X_{Mg}$  and lower Ti, indicating lower temperature equilibration. See text for more details.

## 3.6 Discussion

### 3.6.1 *Fluid flow evidences*

Oxygen isotopes composition document that rocks adjacent to the contact did have some magma and fluid infiltration, notably in the oxidized, bleached zones (Fig. 2b). Otherwise, the profiles do not show trends that could be interpreted as the result of fluid infiltration. The absence of a significant oxygen isotope infiltration front (Baumgartner and Valley, 2001) suggests that there was a limited amount which infiltrated the host rocks. A potential explanation for that is that oxygen is the dominant element of minerals, about half of the atoms of a rock is usually oxygen which makes it difficult to record exchange. Unless new minerals are formed or recrystallized, oxygen is only accessible by diffusion, which is very slow in general (Roselle et al. 1999, Müller et al. 2009). In the Torres del Paine only three different discontinuous reactions occur during contact metamorphism and the number of newly crystallized or recrystallized minerals is relatively small. Some of them do not even enter into reactions, like plagioclase or quartz. A significant amount of oxygen is then only accessible by diffusion, which makes the oxygen stable isotopes a less sensitive marker of fluid flow. Nevertheless, the absence of a marked oxygen isotope trends in the contact aureole is a good argument for a limited amount of fluid flow.

Hydrogen isotopes is a more suitable proxy for fluid flow for three reasons: 1) hydrogen diffusion is much faster than oxygen diffusion; 2) all metamorphic isograds are the result of dehydration reactions and 3) hydrogen content in rocks is smaller than oxygen which require less fluid to significantly change hydrogen isotope signatures. Hydrogen is mainly present in hydrous minerals in the contact aureole, biotite in the inner part and biotite and muscovite in the outer part. But hydrogen can also be store in the channels of cordierite in the entire aureole. At lower temperature, most of the hydrogen is bound in chlorite. Minor amount of apatite is

stable in the Torres del Paine contact aureole, but its fraction is too small to have a significant effect on hydrogen isotopes and do not participate in dehydration reactions. Since kinetics of isotopic exchange by recrystallization is orders of magnitude faster than by diffusion (Baumgartner and Valley 2001), hydrogen isotopes in the Torres del Paine should monitor more efficiently fluid flow.

Indeed, the different hydrogen isotopes profile of the Torres del Paine do show a significant trend in the contact aureole (Fig. 6b).

The decrease in the outer part is interpreted to reflect Rayleigh fractionation. Here Rayleigh fractionation is an endmember process for calculating the effect of instantaneous fluid loss, as soon as it is produced by the dehydration reactions. Since water is enriched in D with respect to hydrous silicates, as water is removed from the rocks it takes a disproportionate amount of deuterium with itself, producing a lighter isotopic solid residue. The amount of fluid needed can be estimated by a back of the envelope type estimation. Here we assume that water loss can be modelled to be in isotopic equilibrium with biotite. Assuming 480°C, the temperature of chlorite breakdown calculated from phase petrology as an approximate temperature of water loss, about 40% of the water contained initially in the hydrous silicates needs to be lost to produce the ca. 20‰ lower  $\delta D$  values observed ( $\alpha_{bt-H_2O} = 0.95453$ , Suzuoki and Epstein, 1976). At a temperature of 520° a little over 45% of the water loss is required using the fractionation factors of Suzuoki and Epstein, 1976. The overall amounts of fluids lost are in agreement with the actual water loss estimated from phase petrology calculations above. Given the sharpness of the isograds, one would expect from these models a step-like decrease in  $\delta D$ . The relative smooth decrease on the other hand is expected if reaction kinetics is somewhat sluggish, so that the individual reactions occur over a temperature range of ca. 50°C. Crystal size analysis and thermal modelling by Bodner (2013) suggest that indeed this is the case. A sluggish reaction

kinetics has also been proposed by Waters and Lovegrove (2002) and Pattison and Tinkham (2009).

Close to the contact (at about 100m) the  $\delta D$  values are showing a trend from lighter to heavier values. This increase in the innermost part of the aureole is interpreted as the signature of magmatic fluid infiltration. A rough estimate of fluid flux can be obtained using the distance of the  $\delta D$  isotope front from the contact with the intrusion, which is assumed to be the source of the fluids. Additional details to the following treatment can be found in Baumgartner and Rumble (1988) and Baumgartner and Valley (2001). A full equilibration between the rock and the fluid is assumed. This assumption is reasonable since a high fraction of hydrous phases are newly crystallized during metamorphism and because hydrogen diffusion is relatively fast.

Here we intend to get a maximum estimate of the amount of fluid flow, in order to determine the potential effect of fluid flow on contact metamorphism in the Torres del Paine. In stable isotope transport theory, the isotopic front always lags behind the actual fluid front. This retardation factor can be described by the relation:

$$\frac{v_f \cdot t}{v_\delta \cdot t} = \kappa \quad (2)$$

where  $\kappa$  represents the retardation factor,  $v_f$  is the velocity of the fluid front, and  $v_\delta$  the velocity of the isotope front,  $t$  stands for time and then the combination  $v_i \cdot t$  represents the distance of front  $i$  ( $i =$  isotope ( $\delta$ ) or fluid ( $f$ )) from the intrusion. The retardation factor  $\kappa$  can be approximated by the equilibrium constant  $K_D$  between fluid and rock,

$$\kappa \approx K_D = \alpha \frac{\beta_s \bar{V}_f}{\beta_f \bar{V}_s} \quad (3)$$

Here,  $\beta$  is the stoichiometry of hydrogen in the solid ( $s$ ) and the fluid ( $f$ ),  $\alpha$  the fractionation factor from Suzuoki and Epstein (1976), and  $\bar{V}$  the molar volume of the respective phases, i.e.  $41 \text{ cm}^3 \cdot \text{mol}^{-1}$  for a fluid composed of pure water and  $150 \text{ cm}^3 \cdot \text{mol}^{-1}$  for biotite. Equation (3)

is valid for very small porosities (Baumgartner and Rumble, 1988), which are assumed to be the case in the extremely fine grained metapelites of the Cerro Toro formation. We use a contact temperature of 500 °C (Tobler 2012) for this estimate, for only 10% of volume of biotite in the rock, this results in a  $K_D$  of 2.9. According to equation (2) the distance of the isotope front from the intrusion has to be known, in order to be able to calculate the fluid front. The greatest distance where magmatic fluid infiltration can be clearly seen is 150 m (fig. 4b), because there the lowest  $\delta D$  values are found. Further away the trend has been interpreted as Rayleigh fractionation earlier in this paper. Combining equations (2) and (3), and using an isotope equilibration front of 150 m, a time integrated flux of roughly  $4\text{m}^3 / \text{m}^2$  is needed.

In comparison with other contact aureoles in the literature this is a small amount of fluid. Bowman et al. (1994) calculated  $\sim 500 \text{ m}^3/\text{m}^2$  using oxygen isotope depletion in siliceous dolomite around the Alta stock. Similarly, Nabelek and Labotka (1993) obtained  $720 \text{ m}^3/\text{m}^2$  to produce the oxygen isotope signal in the Notch Peak contact aureole. The low value calculated in the Torres del Paine is in good agreement with the absence of a marked oxygen isotope record of fluid infiltration. Using the above values to compute the position of the oxygen isotopes infiltration front results in a distance of less than 1m. The actual sampling was not adequate to fully characterize a 1m oxygen isotope front. Even if as mentioned earlier some samples have very low  $\delta^{18}\text{O}$  signatures at the contact. This together with the high variability of sedimentary  $\delta^{18}\text{O}$  signatures, explains why no well-defined, pronounced oxygen isotopic depletion zone is observed in the Torres del Paine contact aureole.

The final tracer used in this study to investigate fluid flow is the chlorine content of biotite. Chlorine content is link to the total dissolved Cl in the fluid (Zhu & Sverjensky 1991), and using experimentally calibrated  $K_D$  for a comparable assemblage allow us to look at the fluid composition in the contact aureole. Figure 8a show the evolution of the Cl content for the Cuerno Principale profile, a good setting since the geometry of the country rocks compare to

the intrusion allowed us to sample rocks from approximately the same layer. In this profile we can clearly see the absence of trend for the Cl content in biotite in the contact aureole. The Cl content is between 0.01-0.03 wt% (Fig. 8a). Close to the contact with the granite two of three samples exhibit a clear different signature, with 0.15-0.20 wt% in Cl content (samples 07TP63 and 10TP57, at 10 m and 0 m respectively), compare to the 0.01-0.03 wt% of the low Cl content sample (10TP54). These three samples are very close to the contact and attained a peak temperature of about 600°C. At this temperature, the  $K_D$  between biotite and fluid is about 0.1 (Zhu and Sverjensky 1991). This means that the high Cl content have been equilibrated with a fluid with approximately 1 mole of chlorine per kg of water and the sample with low Cl content biotites with a fluid with a concentration 10 times lower.

The major element composition of the low chlorine content samples shows a normal trend for low pressure metamorphism with decrease in  $X_{Mg}$  and increase in the Ti content with increasing temperature (Henry et al. 2005), see figure 8b. The two samples with high Cl content have very different  $X_{Mg}$  and Ti content, this could be the results of the equilibration with a completely different fluid. The sample 07TP63 has been sampled close to a carbonate layer and have very minor cordierite amount, that would explain the low Ti content for the biotites in this sample. The other high Cl content sample do not show any evidences of a different bulk rock composition than the low Cl content sample next to it. See table 1 for the assemblages of the samples.

The Valle Frances profile shows a slight different history, it also exhibits the high chlorine content in biotite close to the intrusion, with Cl content reaching 0.09wt% close to the contact for two samples. The samples far from the contact have the same low Cl content than the Cuerno Principale profile, e.g. 0.1-0.3 wt% (Fig. 9a). The rocks from the Valle Frances profile have much more variations in bulk rock chemistry since the geometry does not allow us to sample the same layer, then the  $X_{Mg}$  of biotites from these rocks are more variable, even if the thickness

of the profile sampled was more restricted. But an interesting feature in the two high Cl content samples close to the contact is the coexistence of two distinct populations. The high Cl content biotites have high Ti content (above 0.25 p.f.u.) and lower  $X_{Mg}$  (below 0.3) and the low Cl content biotites have lower Ti content (below 0.25 p.f.u.) and higher  $X_{Mg}$  (above 0.3), see figure 9b. Since the normal evolution for biotite involve increasing Ti content and decreasing  $X_{Mg}$ , we interpret the first population to be representative of the peak conditions and the second to have not been equilibrated during muscovite breakdown reaction. The different Cl content of these two populations show that they have been equilibrated with two completely different fluids.

### *3.6.2 Timing of fluid infiltration*

The timing of fluid infiltration is a very important feature in contact aureole experiencing fluid flow since it can potentially have a huge effect on heat and mass transport, especially if it happens early. In this paragraph, we will attempt to identify the relative timing of fluid infiltration in the Torres del Paine contact aureole.

The granites of the Torres del Paine laccolith are typical A-type granite (Michel et al. 2008), which, in general, are very dry and hot (Clemens et al. 1986). Therefore, the granites become water saturated at the very end of cooling, after subsequent degree of crystallization. This is supported by the paired quartz-fayalite temperatures of 750°C measured in the miaroles of the granite I. This would imply that fluid expulsion was acting at late stage of granite crystallization. Nevertheless, granite I shows internal layering corresponding to different pulses with a thickness of a few meter, these layers are clearly visible on the field. The consequence of this incremental emplacement would be a nearly continuous fluid flow starting at early stage in the metamorphic history of the surrounding rocks, even for this A-type granite.

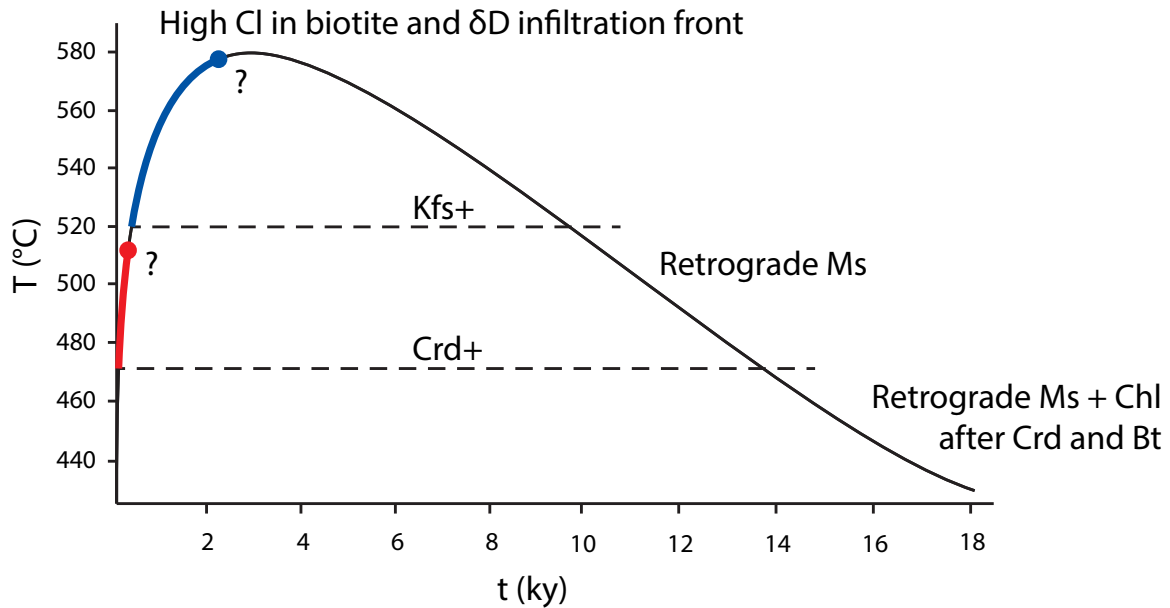


Figure 10: temperature-time evolution for a metapelite from the Cuernos Below profile at the contact with the intrusion. Red and blue lines represent the interval of development for the two main dehydration reactions responsible of the cordierite and K-feldspar isograds, i.e. the chlorite and muscovite breakdown respectively. The three main evidences of fluid flow are represented close to the T-t curve.

The fact that chlorine content in biotite is retentive and thus hard to exchange unless biotite recrystallizes (Siron et al., in prep) imply that high chlorine content close to the intrusion need to reflect highly saline fluid infiltration during muscovite breakdown reaction, when biotite recrystallizes and then is open to change its chlorine content. This textural argument fits well with the fact that hydrogen and chlorine will be much more accessible during recrystallization of the hydrous phase. We interpret this to be the result of an early fluid infiltration episode during prograde evolution. The retrograde muscovite after K-feldspar are evidence of fluid infiltration during cooling, but at still high temperature, i.e. between the K-feldspar-in isograd (520°C) and the biotite and cordierite isograd (470°C). Chlorite-muscovite intergrowth after cordierite or biotite represent later alteration since it must happen below 470°C.

The textural interpretations are supported by the incremental growth mechanism of granite emplacement for the Torres del Paine intrusive complex. Michel et al. (2008) pointed that each pulse for this granite has enough time to crystallize before next pulse emplaces, thus allowing

saturation for the Magmatic Volatile Phase (MVP) and exsolution from the crystallized magma. This would be consistent with an early source of magmatic fluid for the surrounding rocks. Additionally, the high Cl content of the magmatic biotites is in good agreement with the high Cl content of the biotites that we interpret as being equilibrated with this fluid.

Figure 10 represents the temperature-time evolution for a metapelites at the contact between the intrusion and the surrounding rocks for the Cuernos Principale below profile. It has been computed taking into account the enthalpies of endothermic dehydration reactions, heat produced due to hydration far from the contact as long as the influence of several pulses of granite emplacement (Bodner 2013). Since the three different evidences of fluid infiltration, i.e. high chlorine content and  $\delta D$  infiltration front, retrograde muscovite and finally chlorite + muscovite intergrowth after cordierite and biotite, are spaced in a 15 ky window, it is very unlikely that they represent 3 distinct fluid infiltration event but rather the nearly continuous emplacement/crystallization of pulses of granite I.

### 3.7 Conclusion

The Torres del Paine laccolith intruded into a very shallow level of the crust, at a depth of about 2-3 km. It created a small, but well exposed contact aureole that experience three distinct episodes of igneous fluid infiltration.

The metamorphic rocks are infiltrated by a nearly continuous flow of igneous fluid, this is recorded in the metapelites by three episodes of geochemical and textural evidences. The first episode of fluid flow is recorded both by hydrogen isotope ratios and the chlorine content in biotite in the proximity of the intrusive contact. This episode of fluid infiltration happened close to peak metamorphic temperatures. Since the fluid flux of ca.  $4\text{m}^3/\text{m}^2$  is small, a corresponding oxygen front would only be located about 1m from the contact. Some samples close to the contact do indeed show a decrease in  $\delta^{18}\text{O}$ . These localized changes in oxygen isotope

composition go hand in hand with an oxidation of graphitic material in the vicinity of the contact.

A second episode of fluid flow is marked by retrograde muscovite after K-feldspar. Only a few retrograde muscovite crystals were found in these rocks and hence the amount of fluid was very small. A third episode of fluid flow is shown by late replacement of cordierite and biotite by muscovite and chlorine intergrowth. This episode of pinitization is quite pervasive, since some retrogradation is found in nearly all samples. Nevertheless, pinitization is typically limited to a few spots in every thin section, and hence it also represents a minor amount of fluids. Based on thermal modelling, the short interval between these three different geochemical and textural evidences allow us to conclude that the source of fluid for these three episodes is most likely the successive exsolution of fluid at the end of the fast crystallization of the different batches for the granite I.

### 3.8 References

- Aoya, M., Kouketsu, Y., Endo, S., Shimizu, H., Mizukami, T., Nakamura, D. and Wallis S. (2010) Extending the applicability of the Raman carbonaceous-material geothermometer using data from contact metamorphic rocks. *Journal of Metamorphic Geology*, 28, 895–914.
- Baumgartner, L. P. and Rumble, D. (1988) Transport of stable isotopes: I: Development of a kinetic continuum theory for stable isotope transport. *Contributions to Mineralogy and Petrology*, 98, 417–430.
- Baumgartner, L. P., Gieré, R., Trommsdorff, V., and Ulmer, P. (1989) Field guide for the Southern Adamello. in *Guidebook for the excursion to the Central Alps, Bergell and Adamello*, Consiglio Nazionale delle Ricerche, Sienna, Italy, 91–115.
- Baumgartner, L. P., and Ferry, J. M. (1991). A model for coupled fluid-flow and mixed-volatile mineral reactions with applications to regional metamorphism. *Contributions to Mineralogy and Petrology*, 106, 273–285.
- Baumgartner, L. P., Michel, J., Putlitz, B., Leuthold, J., Müntener, O., Robyr, M. and

- Darbellay, B. (2007) Field guide to the Torres del Paine Igneous Complex and its contact aureole. in Field guide book GEOSUR 2007, vol. 185.
- Baumgartner, L. P. and Valley, J. W. (2001) Stable Isotope Transport and Contact Metamorphic Fluid Flow. *Reviews in Mineralogy and Geochemistry*, 43, 415–467.
- Beyssac, O., Goffé, B., Chopin, C. and Rouzaud, J. N. (2002) Raman spectra of carbonaceous material in metasediments: a new geothermometer. *Journal of Metamorphic Geology*, 20, 859–871.
- Bickle, M. and J. Baker (1990) Migration of reaction and isotopic fronts in infiltration zones: assessments of fluid flux in metamorphic terrains. *Earth and Planetary Science Letters*, 98, 1–13.
- Bodner, R., Baumgartner, L. P., and Foster, C. T., Jr. (2013). Cordierite nucleation and growth rates in the Torres del Paine contact aureole. *Goldschmidt 2013 Conference Abstracts*, 724.
- Bowman, J. R., Willett, S. D. and Cook, S. J. (1994) Oxygen isotopic transport and exchange during fluid flow: one-dimensional models and applications. *American Journal of Sciences*, 294, 1-55.
- Candela, P. A. (1997). A review of shallow, ore-related granites: Textures, volatiles, and ore metals. *Journal of Petrology*, 38, 1619–1633.
- Cartwright, I., and Buick, I. S. (1996) Determining the direction of contact metamorphic fluid flow: an assessment of mineralogical and stable isotope criteria. *Journal of Metamorphic Geology*, 14, 289–305.
- Clemens, J. D., Holloway, J. R. and White, A. J. R. (1986) Origin of an A-type granite: Experimental constraints. *American Mineralogist*, 71, 317–324.
- Cook, S. J., Bowman, J. R. and Forster, C. B. (1997) Contact metamorphism surrounding the Alta Stock; finite element model simulation of heat- and  $^{18}\text{O}/^{16}\text{O}$  mass-transport during prograde metamorphism. *American Journal of Science*, 297, 1–55.
- Cui, X. J., Nabelek, P. I., and Liu, M. (2001). Heat and fluid flow in contact metamorphic aureoles with layered and transient permeability, with application to the Notch Peak aureole, Utah. *Journal of Geophysical Research*, 106, 6477–6491.
- Cui, X. J., Nabelek, P. I., and Liu, M. A. (2002). Numerical modeling of fluid flow and

- oxygen isotope exchange in the Notch Peak contact-metamorphic aureole, Utah. *Geological Society of America Bulletin*, 114, 869–882.
- Eiler, J. M., Valley, J. W., and Baumgartner, L. P. (1993). A new look at stable isotope thermometry. *Geochimica Et Cosmochimica Acta Supplement*, 57(11), 2571–2583.
- Eldursi, K., Branquet, Y., and Guillou-Frottier, L. (2009). Numerical investigation of transient hydrothermal processes around intrusions: Heat-transfer and fluid-circulation controlled mineralization patterns. *Earth and Planetary Sciences Letters*, 288, 70–83.
- Ferry, J. (1986) Reaction Progress: A Monitor of Fluid—Rock Interaction during Metamorphic and Hydrothermal Events. in *Fluid—Rock Interactions during Metamorphism*, ed. by J. Walther and B. Wood, Springer New York, vol. 5 of *Advances in Physical Geochemistry*, 60–88.
- Fildani, A. (2005). Stratigraphic record across a retroarc basin inversion: Rocas Verdes–Magallanes Basin, Patagonian Andes, Chile. *Geological Society of America Bulletin*, 117(11), 1596.
- Fildani, A., Romans, B. W., Fosdick, J. C., Crane, W. H., and Hubbard, S. M. (2008a). Orogenesis of the Patagonian Andes as reflected by basin evolution in southernmost South America. *Ores and Orogenesis: Circum-Pacific Tectonics, Geologic Evolution, and Ore Deposits: Arizona Geological Society, Digest*, 22, 259–268.
- Fildani, A., Schultz, M. R., Graham, S. A., and Leier, A. (2008b). A deep-water amalgamated sheet system, Punta Barrosa Formation, Marina's cliff, Chile. Poster, xx, 1–3.
- Forester, R. W. and Taylor, H. P. J. (1976)  $^{18}\text{O}$ -depleted igneous rocks from the Tertiary complex of the Isle of Mull, Scotland. *Earth and Planetary Science Letters*, 32, 11–17.
- Furlong, K. P., Hanson, R. B. and Bowers, J. R. (1991): “Modeling thermal regimes,” *Reviews in Mineralogy and Geochemistry*, 26, 437–505.
- Gerdes, M. L., Baumgartner, L. P. and Person, M. (1995) Stochastic permeability models of fluid flow during contact metamorphism. *Geology*, 23, 945–948.
- Gerdes, M. L., Baumgartner, L. P., and Person, M. (1998). Convective fluid flow through heterogeneous country rocks during contact metamorphism. *Journal of Geophysical Research: Solid Earth*, 103, 23983–24003.
- Hanson, R. B. (1995) The hydrodynamics of contact metamorphism. *Geological Society of*

- America Bulletin, 107, 595–611.
- Henry, D. J., Guidotti, C. V. and Thomson, J. A. (2005) The Ti-saturation surface for low-to-medium pressure metapelitic biotites: Implications for geothermometry and Ti-substitution mechanisms. *American Mineralogist*, 90(2-3), 316–328.
- Higashino, F., Kawakami, T., Satish-Kumar, M., Ishikawa, M., Maki, K., Tsuchiya, N., et al. (2013) Chlorine-rich fluid or melt activity during granulite facies metamorphism in the Late Proterozoic to Cambrian continental collision zone—An example from the Sør Rondane Mountains, East Antarctica. *Precambrian Research*, 234, 229–246.
- Holness, M. B. (1997). Fluid flow paths and mechanisms of fluid infiltration in carbonates during contact metamorphism: the Beinn an Dubhaich aureole, Skye. *Journal of Metamorphic Geology*, 15(1), 59–70.
- Holness, M. B., and Clemens, J. D. (1999). Partial melting of the Appin Quartzite driven by fracture-controlled H<sub>2</sub>O infiltration in the aureole of the Ballachulish Igneous Complex, Scottish Highlands. *Contributions to Mineralogy and Petrology*, 136, 154–168.
- Holtz, F., Behrens, H., Dingwell, D.B., and Johannes, W. (1995) H<sub>2</sub>O solubility in haplogranitic melts – compositional, pressure, and temperature-dependance. *American Mineralogist*, 80, 94–108.
- Hubbard, S. M., and Shultz, M. R. (2008). Deep Burrows in Submarine Fan-Channel Deposits of the Cerro Toro Formation (Cretaceous), Chilean Patagonia: Implications For Firmground Development and Colonization in the Deep Sea. *Palaios*, 23(4), 223–232.
- Hubbard, S. M., Romans, B. W., and Graham, S. A. (2008). Deep-water foreland basin deposits of the Cerro Toro Formation, Magallanes basin, Chile: architectural elements of a sinuous basin axial channel belt. *Sedimentology*, 55(5), 1333–1359.
- Jamtveit, B., Grorud, H.F. and Bucher-Nurminen, K. (1992) Contact metamorphism of layered carbonate-shale sequences in the Oslo Rift. II: Migration of isotopic and reaction fronts around cooling plutons. *Earth and Planetary Science Letters*, 114, 131–148.
- Labotka, T.C., Nabelek, P.I. and Papike, J.J. (1988) Fluid infiltration through the Big Horse Limestone Member in the Notch Peak contact-metamorphic aureole, Utah. *American Mineralogist*, 73, 1302–1324.
- Leuthold, J., Müntener, O., Baumgartner, L.P., Putlitz, B. and Chiaradia, M. (2013) A Detailed Geochemical Study of a Shallow Arc-related Laccolith; the Torres del Paine Mafic Complex

- (Patagonia). *Journal of Petrology*, 54, 273–303.
- Leuthold, J., Müntener, O., Baumgartner, L.P., Putlitz, B., Ovtcharova, M. and Schaltegger, U. (2012) Time resolved construction of a bimodal laccolith (Torres del Paine, Patagonia). *Earth and Planetary Science Letters*, 325-326, 85–92.
- Michel, J., Baumgartner, L.P., Putlitz, B., Schaltegger, U. and Ovtcharova, M. (2008) Incremental growth of the Patagonian Torres del Paine laccolith over 90 k.y. *Geology*, 36, 459–462.
- Müller, T., Baumgartner, L.P., Foster, C.T. and Bowman, J.R. (2009) Crystal Size Distribution of Periclase in Contact Metamorphic Dolomite Marbles from the Southern Adamello Massif, Italy. *Journal of Petrology*, 50, 451–465.
- Nabelek, P. I. and Labotka, T. C. (1993). Implications of geochemical fronts in the Notch Peak contact metamorphic aureole, Utah, USA. *Earth and Planetary Science Letters*. 119, 539–559.
- Norton, D. and Knight, J.E. (1977) Transport phenomena in hydrothermal systems; cooling plutons. *American Journal of Science*, 277, 937–981.
- Pattison, D. R. M., & Tinkham, D. K. (2009). Interplay between equilibrium and kinetics in prograde metamorphism of pelites: an example from the Nelson aureole, British Columbia. *Journal of Metamorphic Geology*, 27(4), 249–279.
- Putlitz, B., Baumgartner, L.P., Oberhänsli, R., Diamond, L. and Altenberger, U. (2001) The Torres del Paine Laccolith (Chile); intrusion and metamorphism. LPI Contribution, abstract no. 3534.
- Roselle, G.T., Baumgartner, L.P. and Valley, J.W. (1999) Stable isotope evidence of heterogeneous fluid infiltration at the Ubehebe Peak contact aureole, Death Valley National Park, California. *American Journal of Science*, 299, 93–138.
- Suzuoki, T. and Epstein, S. (1976) Hydrogen isotope fractionation between OH-bearing minerals and water. *Geochimica and Cosmochimica Acta*, 40, 1229–1240.
- Tobler, L. (2012) Etude métamorphique et structurale de la région sud-est du parc national Torres del Paine, Chili. Master thesis.
- Valley, J.W. (1986) Stable isotope geochemistry of metamorphic rocks. *Reviews in Mineralogy and Geochemistry*, 16, 445–489.

- Waters, D. J., and Lovegrove, D. P. (2002). Assessing the extent of disequilibrium and overstepping of prograde metamorphic reactions in metapelites from the Bushveld Complex aureole, South Africa. *Journal of Metamorphic Geology*, 20, 135–149.
- Wilson, T.J. (1991) Transition from back-arc to foreland basin development in the southernmost Andes: Stratigraphic record from the Ultima Esperanza District, Chile. *Geological Society of America Bulletin*, 103, 98–111.
- Wohlers, A., and Baumgartner, L. P. (2012). Melt infiltration into quartzite during partial melting in the Little Cottonwood Contact Aureole (UT, USA): implication for xenocryst formation. *Journal of Metamorphic Geology*, 31, 301–312.
- Zhu, C. and Sverjensky, D.A. (1991) Partitioning of F-Cl-OH between minerals and hydrothermal fluids. *Geochimica Et Cosmochimica Acta*, 55, 1837–1858.



## 4 Accurate biotite OH-F-Cl determination using Secondary Ion Mass Spectrometry

Authors: Guillaume Siron, Lukas Baumgartner, Anne-Sophie Bouvier & Torsten Vennemann

Proposed journal: Journal of Analytical Atomic Spectrometry

## 4.1 Introduction

Biotite is an important hydrous phase stable in many different settings in metamorphic and igneous environments. Its chemical formulae can be written as  $K(Mg,Fe,Ti)_3[AlSi_3O_{10}](OH, Cl, F)_2$  (Rieder et al. 1998). The O(4) site can contain substantial  $O^{2-}$  in addition to  $OH^-$ ,  $F^-$  or  $Cl^-$  (Dyar et al. 1993, Cesare et al. 2003, 2008). The O(4) site composition is of particular interest since it can be linked to the chlorine and fluorine composition of the fluid in equilibrium with biotite (Munoz 1984, Zhu and Sverjenski 1991), which allows to track changes in the sources of these fluids. Full determination of O(4) site composition will affect the determination of vacancies on the other sites. Nevertheless, the O(4) site could also contain vacancies. Since normalization is typically completed assuming 11 oxygen, e.g. a completely full O(4) site is assumed, this could lead to significantly different vacancy values of the other sites. Many studies have called upon deprotonation substitutions as important exchange vectors for biotites (Dyar et al. 1993, Cruciani and Zanazzi 1994, Cesare et al. 2003, 2008), highlighting the needs for a full determination of the O(4) site in order to correlate change in the octahedral composition with change in composition of other important phases. To date, only few techniques are available for in-situ determination of F, Cl and OH, nevertheless they do not allow simultaneous measurements of these three components. F and Cl can be measured using Electron Probe Micro Analysis (EPMA), with a precision of about 400 ppm and 50 ppm (1SD) respectively for 30 seconds of counting. The detection limit is about 200 ppm and 40 ppm respectively. Since many hydrous phases have low concentrations of these elements due to their incompatibility with the crystallographic structure, the detection limit and precision can be either too low to be measured or too imprecise to give any reliable information. Additionally, fluorine determination using WDS detector is hampered by the

potentially strong Fe interference using large crystal (LDE), or lower counting rate with other crystal (TAP) that do not exhibit this interference.

In-situ water content measurements can be determined either by Fourier Transform Infrared (FTIR) or Secondary Ion Mass Spectrometry (SIMS). The FTIR technique investigates the characteristic wavelength of O-H bond, allowing to quantify the relative proportions for the different species (i.e. OH<sup>-</sup>, H<sub>2</sub>O, H<sub>3</sub>O<sup>+</sup>, NH<sub>4</sub><sup>+</sup>). The SIMS technique allows to measure either <sup>1</sup>H or <sup>16</sup>O<sup>1</sup>H, normalized to another element to account for changes during the sputtering process. Several isotopes have been tested for normalization, such as <sup>28</sup>Si, <sup>27</sup>Al, <sup>44</sup>Ca (Ottolini et al. 2002, 2006). Both techniques (FTIR and SIMS) require an independent estimation of the water content to calibrate the absolute value. To our knowledge, no set of biotite reference materials (RMs) is available for in situ characterization of F, Cl and OH.

Here we present a complete evaluation of the homogeneity of 5 new RMs as well as the international standard NBS30. We carefully check for potential crystal orientation effects on OH, F, Cl measurements as well as calibration curves to measure these three anions using SIMS for a set of reference materials already characterized for oxygen isotopes (Siron et al. 2016).

## 4.2 Analytical techniques

### 4.2.1 *Electron Probe Micro Analysis (EPMA)*

Major and minor element determinations of biotite were obtained at the Institute of Earth Sciences at the University of Lausanne with a JEOL 8200 Superprobe equipped with five wavelength-dispersive X-ray spectrometers. The mass fractions of Si, Al, Ti, Fe, Mg, Mn, K, Na, Ca, F and Cl were determined. The operating conditions were 15 kV at 15 nA, with a spot size of 10 μm. Counting times were set to 15 s for background before and after peak and 30 s

on the peak, except for Na and K where counting times were 10 s for background (each side) and 20 s on the peak to avoid any diffusion. Natural minerals were used for the calibration. The data were reduced with the CITZAF matrix correction routine (Armstrong 1989). Measurements of twenty to thirty points on three to five grains were made for each of the biotite, using both profiles parallel to the *c*-axis, as well as perpendicular to *c* to investigate the homogeneity of each biotite (Table 1). For more detail see Siron et al. (2016). All the structural formulae were normalized to twenty-two oxygens, without  $\text{Fe}^{2+}/\text{Fe}^{3+}$  ratio corrections. Average for major elements as long as 1SD variations for all RMs are given in table 1.

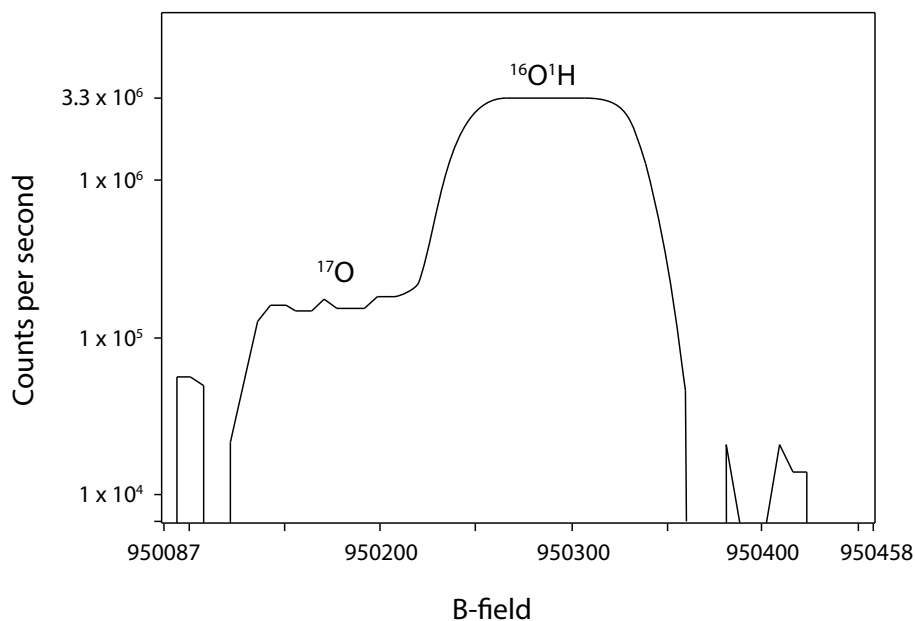


Figure 1: A B-field scan around the mass 17 documenting that the isobaric interference of  $^{17}\text{O}$  can be neatly separate from the analyzed  $^{16}\text{O}^1\text{H}$ .

Table 1: Microprobe analyses of the reference materials in % m/m oxydes. 1SD variations for each Reference Material in brackets. Structural formulae are normalized to 22 oxygens.

	UNIL_B1	1SD	UNIL_B2	1SD	NBS30	1SD	UNIL_B3	1SD	UNIL_B4	1SD	UNIL_B5	1SD
SiO <sub>2</sub>	39.69	(0.26)	40.93	(0.43)	36.36	(0.16)	34.71	(0.37)	38.10	(0.33)	37.58	(0.33)
Al <sub>2</sub> O <sub>3</sub>	10.97	(0.1)	14.44	(0.23)	15.57	(0.23)	14.34	(0.27)	14.98	(0.14)	13.20	(0.26)
TiO <sub>2</sub>	2.12	(0.05)	0.50	(0.04)	3.18	(0.46)	5.54	(0.13)	1.73	(0.15)	0.04	(0.02)
FeO	17.99	(0.12)	6.68	(0.07)	19.99	(0.22)	23.96	(0.29)	10.63	(0.83)	32.04	(0.44)
MgO	13.78	(0.16)	22.08	(0.17)	9.89	(0.22)	6.70	(0.11)	18.55	(0.69)	0.01	(0.02)
MnO	0.63	(0.04)	0.02	(0.01)	0.21	(0.02)	0.16	(0.02)	0.10	(0.02)	1.21	(0.04)
CaO	b.d.l.		0.01	(0.01)	0.02	(0.02)	0.01	(0.01)	0.01	(0.01)	0.01	(0.01)
Na <sub>2</sub> O	0.53	(0.05)	0.38	(0.03)	0.14	(0.03)	0.06	(0.02)	0.09	(0.03)	0.27	(0.08)
K <sub>2</sub> O	9.21	(0.1)	9.38	(0.11)	9.17	(0.08)	8.97	(0.1)	9.95	(0.16)	7.97	(0.14)
F	2.96	(0.1)	0.19	(0.1)	0.13	(0.02)	n.m.		0.08	(0.05)	3.86	(0.11)
Cl	0.05	(0.03)	0.01	(0)	0.06	(0.01)	0.05	(0.01)	0.03	(0.01)	0.29	(0.04)
H <sub>2</sub> O <sup>a</sup>	2.11		4.28		3.58		2.68		3.84		2.05	
O=F	-1.23		-0.08		-0.05				-0.01		-1.61	
Total	98.81	(0.34)	98.88	(0.42)	98.25	(0.39)	97.17	(0.92)	98.02	(0.41)	96.93	(0.46)
Altot	1.969	(0.015)	2.448	(0.047)	2.829	(0.036)	2.666	(0.047)	2.618	(0.028)	2.598	(0.047)
Si	6.044	(0.015)	5.884	(0.036)	5.607	(0.013)	5.508	(0.05)	5.649	(0.027)	6.275	(0.05)
Al <sup>iv</sup> <sup>b</sup>	1.956	(0.015)	2.116	(0.036)	2.393	(0.013)	2.492	(0.05)	2.351	(0.027)	1.725	(0.05)
T site	8.000	(0)	8.000	(0)	8.000	(0)	8.000	(0)	8.000	(0)	8.000	(0)
Al <sup>vi</sup> <sup>c</sup>	0.013	(0.018)	0.332	(0.015)	0.436	(0.037)	0.173	(0.031)	0.267	(0.02)	0.873	(0.031)
Fe	2.291	(0.021)	0.804	(0.011)	2.578	(0.026)	3.162	(0.061)	1.319	(0.108)	4.474	(0.061)
Mg	3.128	(0.031)	4.732	(0.018)	2.273	(0.049)	1.576	(0.006)	4.101	(0.136)	0.003	(0.006)
Mn	0.081	(0.005)	0.002	(0.001)	0.027	(0.002)	0.021	(0.005)	0.012	(0.003)	0.171	(0.005)
Ti	0.242	(0.006)	0.054	(0.004)	0.368	(0.054)	0.657	(0.002)	0.193	(0.017)	0.005	(0.002)
O site	5.756	(0.015)	5.924	(0.013)	5.683	(0.038)	5.590	(0.036)	5.893	(0.017)	5.527	(0.036)
K	1.789	(0.022)	1.720	(0.022)	1.805	(0.016)	1.805	(0.032)	1.881	(0.028)	1.698	(0.032)
Na	0.155	(0.014)	0.106	(0.01)	0.043	(0.008)	0.018	(0.024)	0.026	(0.008)	0.089	(0.024)
Ca	0.001	(0.001)	0.001	(0.001)	0.003	(0.003)	0.001	(0.002)	0.002	(0.002)	0.001	(0.002)
A site	1.945	(0.022)	1.827	(0.024)	1.851	(0.015)	1.824	(0.022)	1.910	(0.024)	1.788	(0.022)
F	1.404	(0.047)	0.059	(0.7)	0.066	(0.008)	n.m		0.039	(0.022)	2.035	(0.057)
Cl	0.020	(0.008)	0.003	(0.001)	0.016	(0.002)	0.015	(0.011)	0.007	(0.002)	0.082	(0.011)
OH												
XMg	0.59	(0.004)	0.86	(0.157)	0.48	(0.005)	0.34	(0.001)	0.76	(0.02)	0.00	(0.001)

<sup>a</sup> H<sub>2</sub>O are from TC/EA measurements, for details see Bauer and Vennemann 2015

<sup>b</sup> Al<sup>iv</sup> is calculate as follow: Altot if Altot + Si < 8 if not 8-Si

<sup>c</sup> Al<sup>vi</sup> is calculate as follow: Altot -Al<sup>iv</sup>

#### 4.2.2 Thermal Conversion Elemental Analyzer (TC/EA)

Water content of the 5 biotite reference materials were measured using Thermal Conversion Elemental Analyzer (TC/EA), following the method described in Bauer and Vennemann (2014). Since it has been demonstrated that grain size influences the measured composition using TC/EA, each biotites RMs were crushed with an agate mortar until small flakes

disappeared. About 2 mg of this mix were weighted into silver cups and closed by folding. Then the cups were placed into an autosampler directly above the TC/EA. The autosampler is connected to a ceramic tube that contains a smaller glassy carbon tube, glassy carbon chips and a graphite cup for the reduction of the sample at 1450°C to form H<sub>2</sub> and CO from H<sub>2</sub>O and C. The gases were then transferred using a He gas carrier via a gas chromatographic column into the mass spectrometer. Both <sup>1</sup>H and D isotopes, as well as water content, are measured using a Finnigan Thermo Delta Plus XL. Water content is determined as the surface area below the hydrogen signal peak and the recorded weight of the samples. In-house standards (kaolinite K17 and biotite G1) were analyzed repeatedly during the session for normalization and possible corrections. Reproducibility for water content measurements is typically in the order of 0.1 wt%. Hydrogen isotopic ratios in delta notation against VSMOW has an uncertainty of ± 2‰. Both water content and hydrogen isotopes composition for all new RMs, along with uncertainties, are given in table 2.

#### 4.2.3 Secondary Ion Mass Spectrometry (SIMS)

##### **Elemental analysis**

OH, F and Cl content of micas were measured with the IMS 1280HR facility at the SwissSIMS laboratory using a 1nA Cs<sup>+</sup> primary beam at 10kV. A focused high-density primary beam in Gaussian mode was used, with a spot size of about 10µm. To avoid lateral contaminations from the border of the pit, a 20µm raster was used during the 210 seconds of presputtering.

Entrance (50µm) and exit (400µm) slits were set to achieve a mass resolution of about 5000 to discriminate the isobaric interferences for <sup>17</sup>O and <sup>16</sup>O<sup>1</sup>H peaks (figure 1). An electron gun with a normal incidence was used for charge compensation and carefully tuned at the beginning of each session.

The analyses were done in mono-collection mode, using magnetic peak switching, to measure successively  $^{16}\text{O}^1\text{H}$ ,  $^{19}\text{F}$ ,  $^{28}\text{Si}$ ,  $^{30}\text{Si}$  and  $^{35}\text{Cl}$  during 1 cycle with counting times of 6, 6, 3, 5 and 8 seconds respectively. A waiting time of 3 seconds was used between each of the 15 cycles. Automatic centering of deflectors associated to field and contrast apertures were performed before each analysis. After deflectors centering, mass  $^{28}\text{Si}$  was automatically scanned to ensure a correct position of the magnet for each measured mass.  $^{16}\text{O}^1\text{H}$ ,  $^{19}\text{F}$  and  $^{28}\text{Si}$  were analyzed using a faraday cup (FC2,  $10^{11} \Omega$  resistor) and the axial electron multiplier (EM) was used for  $^{30}\text{Si}$  and  $^{35}\text{Cl}$ .

Table 2: Thermal Conversion Elemental Analyzer data: water content and hydrogen isotopes of biotite reference materials and quartz standards

Sample	$\delta\text{D}$ corrected ‰	water content wt%	no. analyses
<b>UNIL_B2</b> 01-Feb-16	<b><math>-64 \pm 0.22</math> (1sd)</b>	<b><math>4.28 \pm 0.11</math> (1sd)</b>	(n=2)
<b>UNIL_B1</b> 01-Feb-14	<b><math>-88 \pm 0.57</math> (1sd)</b>	<b><math>2.11 \pm 0.01</math> (1sd)</b>	(n=2)
<b>UNIL_B3</b> 01-May-15	<b><math>-47 \pm 0.49</math> (1sd)</b>	<b><math>2.68 \pm 0.03</math> (1sd)</b>	(n=2)
<b>UNIL_B4</b> 01-May-15	<b><math>-64 \pm 0.49</math> (1sd)</b>	<b><math>3.84 \pm 0.01</math> (1sd)</b>	(n=2)
<b>UNIL_B5</b> 01-May-15	<b><math>-166 \pm 0.69</math> (1sd)</b>	<b><math>2.05 \pm 0.07</math> (1sd)</b>	(n=2)
<b>G1_biotite</b> 01-Feb-14	$-60 \pm 4.17$ (1sd)	$3.57 \pm 0.13$ (1sd)	(n=6)
01-May-15	$-62 \pm 1.87$ (1sd)	$3.48 \pm 0.10$ (1sd)	(n=5)
01-Feb-16	$-63 \pm 0.78$ (1sd)	$3.50 \pm 0.03$ (1sd)	(n=2)
Uncertainties refer to 1 standard deviation (1sd) Data are normalized to biotite reference materials G1 Accepted $\delta\text{D}$ values for G1 is $-62\text{‰}$ relative to VSMOW Accepted water content value for G1 is $3.50 \text{ wt}\%$ Bold values are the final values for each RM			

## Cl accumulation test

We tested the potential chlorine accumulation on cleavage plans using a different technique: a focused Gaussian Cs<sup>+</sup> beam with 100µm raster was used, with 300 seconds of presputtering. Contrast aperture was set to 400µm and field aperture to 5000µm. Entrance (120µm) and exit (300µm) slits were set to achieve a mass resolution of about 2200 at 80% in order to discriminate <sup>35</sup>Cl and <sup>34</sup>S<sup>1</sup>H interferences. <sup>35</sup>Cl and <sup>37</sup>Cl were analyzed simultaneously using EMs detector in multi-collection mode during 500 cycles of 6 seconds. Such a long measurement results in a pit depth of approximately 450 nm. For the RM with Cl accumulation inside cleavages, we conducted a second test with a raster of 60µm and 250 seconds of pre-sputtering, and 1000 cycles to have a deeper pit than in the first test. While it is not an optimized depth profiling analysis, it allows a qualitative measurement of the Cl concentration evolution with depth for biotite RMs. This approach is the only possible way to test very fine grained material which are too small to be mounted perpendicular to the surface, and hence no chlorine maps can be obtained for this orientation using EPMA.

Table 3: homogeneity for all Reference Materials, all values represent 1SD

	OH (%)	ppm	F (%)	ppm	Cl (%)	ppm	<i>n</i>	# grains
UNIL_B1	1.92	404	1.31	388	4.51	23	42	7
UNIL_B2	1.55	668	2.56	49	6.74	7	60	9
UNIL_B3	2.03	546	2.81		14.25	28	18	8
UNIL_B4	2.37	910	36.13	289	17.03	51		4
UNIL_B5	4.2	882	5.92	2283	7.68	223	33	5
NBS30	0.74	260	0.32	4	8.23	49	7	4

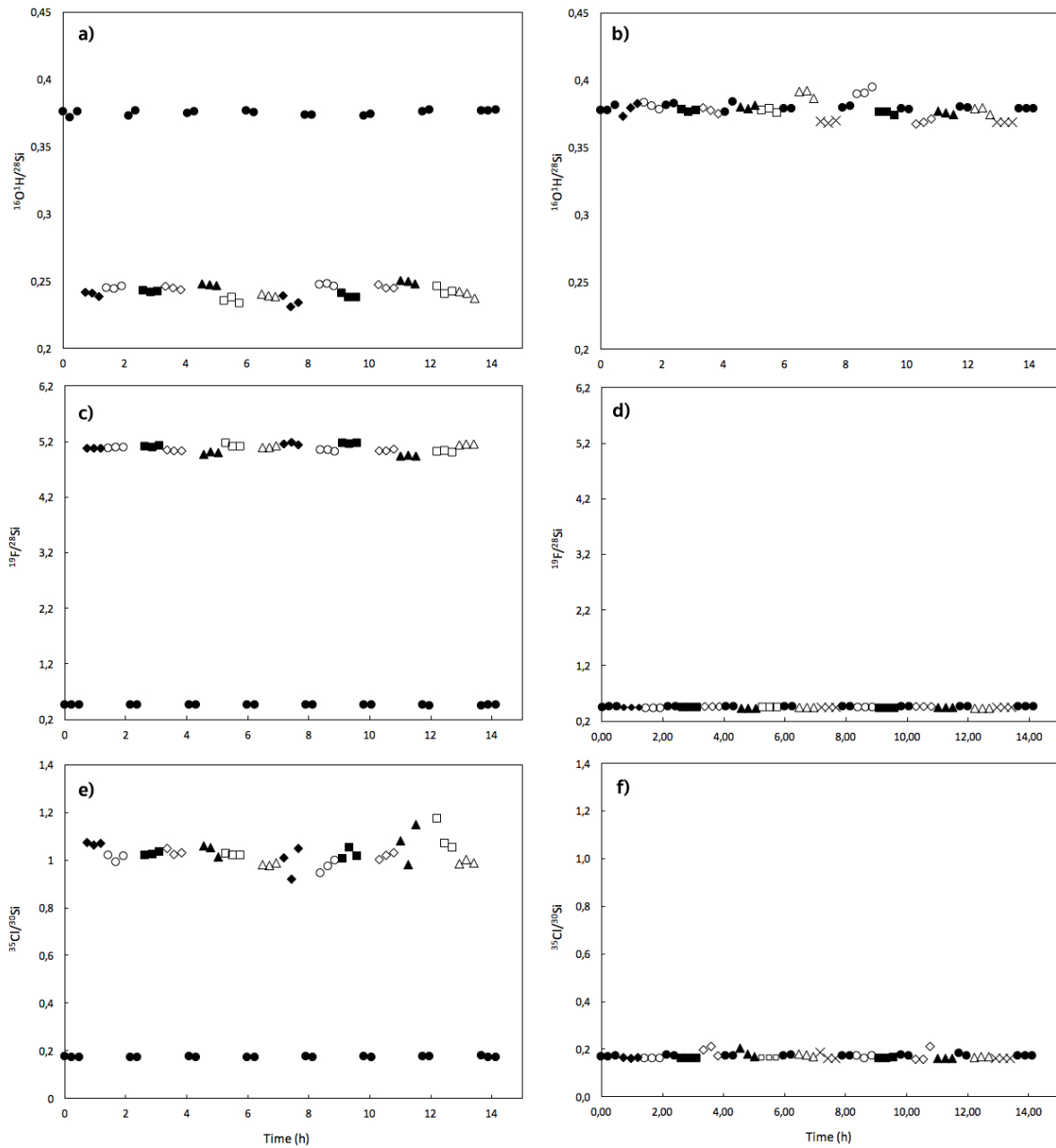


Figure 2: Homogeneity test for UNIL\_B1 (a,  $^{16}\text{O}^1\text{H}/^{28}\text{Si}$ ; c,  $^{19}\text{F}/^{28}\text{Si}$ ; e,  $^{35}\text{Cl}/^{30}\text{Si}$ ) and UNIL\_B2 (b,  $^{16}\text{O}^1\text{H}/^{28}\text{Si}$ ; d,  $^{19}\text{F}/^{28}\text{Si}$ ; f,  $^{35}\text{Cl}/^{30}\text{Si}$ ). For the UNIL\_B1 session, black dots represent analyses in a grain of UNIL\_B2 used as working reference material for this session. Analyses have been made in 7 grains labelled as follow: black diamond is grain 1, white dot is grain 2, black square is grain 3, white diamond is grain 4, black triangles is grain 5, white square is grain 6 and white triangles is grain 7. For the UNIL\_B2 session, black dots represent analyses in the same grain used as working reference material for the session of UNIL\_B1. Analyses have been made in 8 grains labeled as follow: black diamond is grain 1, white diamond is grain 2, black square is grain 3, white diamond is grain 4, black triangles is grain 5, white square is grain 6, white triangles is grain 7 and cross is grain 8.

## 4.3 Results and discussion

### 4.3.1 Homogeneity test of the RMs

Since SIMS analyses rely on the measurements of reference materials with known composition to correct for instrumental bias and potential matrix effect, the homogeneity of these materials is crucial to establish the level of precision of these analyses. A common way to constrain this value is by measuring the reproducibility (1 standard deviation (1SD) for elemental concentrations) of SIMS analyses of as many grains as possible, mounted together on the same mount. All relative (%) and absolute (ppm) variations (1SD), as well as the number of points and grains analyzed for all RMs are given in table 3.

In terms of homogeneity the international standard NBS30 is by far the most homogeneous of the tested RMs, with 0.7% (260 ppm) for water content and 0.3 (4 ppm) for F content. A relatively high Cl content variation with 8.2% (49 ppm) was observed. Unfortunately, NBS30 consists of very small flakes of biotite, hard to polish. It is thus not a suitable internal RM for analysis during an entire session, in which few dozens of analyses have to be made to correct for a potential drift. We rather recommend to mount UNIL\_B1 and UNIL\_B2 with samples, since they consist of bigger flakes (~1mm each) and are very homogeneous (figure 2). UNIL\_B1 is homogeneous at the level of 1.9% (404 ppm) for water content and 1.3% (388 ppm) for F content. It is not suitable for Cl measurements since it contains accumulation of Cl between cleavages (figure 3a and b). We can clearly see spikes at regular spacing (around 50 nm) for both Cl accumulation tests. In comparison, the test for NBS30 shows flat evolution of the  $^{35}\text{Cl}$  and  $^{37}\text{Cl}$  counts per second with depth, resulting in an overall variation for the second test of 0.6% (1 SD) for both isotopes, a value comparable to the uncertainty of the 15 cycles of one elemental analysis. Chlorine accumulation in cleavages explains its larger internal error, i.e. ~2-7% for  $^{35}\text{Cl}$  cps, compared to other reference material. UNIL\_B2 shows a reproducibility

of 1.6% for water (668 ppm) and is the most homogeneous of the tested RMs for Cl and F contents, with variations of 2.6% (49 ppm) and 6.7% (7 ppm), respectively. UNIL\_B3 is fairly homogeneous, with 2.0% (546 ppm) of variations for water content and 2.8% and 14.3% (28 ppm) of variations for F and Cl content respectively. UNIL\_B4 is one of the least homogeneous RM, with variations of water and Cl content of 2.4% (910 ppm) and 17.0% (51 ppm) respectively. F content of UNIL\_B4 display large intra and extra grains variations (36.1%, 289 ppm). Finally, UNIL\_B5 is the least homogeneous RM, with variations of 4.2% (882 ppm) for water content, 5.92% (0.2 wt%) for F content and 7.68% (223 ppm) for Cl content.

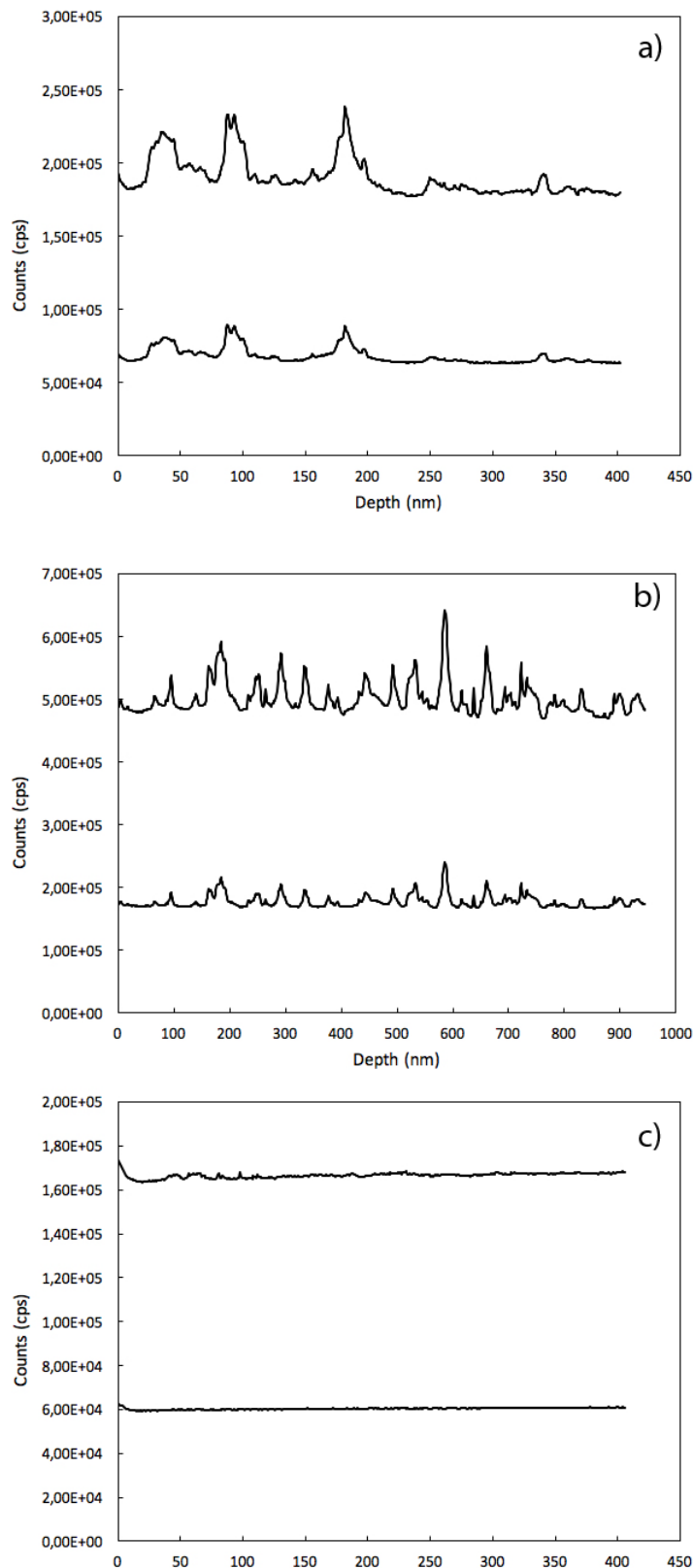


Figure 3: Homogeneity test to identify potential exsolution of chlorine on cleavage plains using depth profiling. a) UNIL\_B1 test with primary beam rastered at 100 $\mu$ m and 500 cycles, the total pit depth is 450 nm; b) UNIL\_B1 test with primary beam rastered at 60 $\mu$ m and 1000 cycles, the total pit depth is 1 $\mu$ m; c) NBS30 test with primary beam rastered at 100 $\mu$ m and 500 cycles, the total pit depth is 450 nm. Note the periodic increase of the Cl-counts for UNIL-B1, which indicates that Cl-accumulations occur along cleavage planes.

### 4.3.2 *Crystal orientation test*

A potential orientation effect has been pointed out by Ottolini et al. (2002, 2006), but the limited amount of data does not allow to definitely conclude that analyses are orientation dependent. In order to test for an orientation effect, several grains for the two most suitable reference materials (UNIL\_B1 and B2) have been mounted with different orientations. We analyzed 4 grains of UNIL\_B1, 3 perpendicular to the surface of the mount with different orientations (grain 2, 3 and 4) and 1 parallel (grain 1), and 2 grains for UNIL\_B2, 1 parallel (grain 1), also used as internal standard to check for potential drift during the session, and 1 perpendicular to the surface of the mount (grain 2). No observable variations between orientation was found (figure 4). The overall variations for  $^{16}\text{O}^1\text{H}/^{28}\text{Si}$  of the 4 grains of UNIL\_B1 was 2.85% (1SD), which is slightly higher than the homogeneity test on 7 grains (1.9%, 1SD), all oriented parallel to the surface of the mount. Nevertheless, we can see the opposite for UNIL\_B2, with a reproducibility (1SD) of 1.3% for the two grains mounted with two different orientations and a value of 1.6% (1SD) for the homogeneity test (9 grains). For  $^{19}\text{F}/^{28}\text{Si}$ , the reproducibility (1SD) for the 4 grains of UNIL\_B1 is 1.8%, slightly higher than the homogeneity test (1.3%, 1SD). The variations are bigger for UNIL\_B2, with a reproducibility of 8.5% (1SD), much higher than the homogeneity test (2.6%, 1SD). Variations for  $^{35}\text{Cl}/^{30}\text{Si}$  for the 4 grains of UNIL\_B1 is 3.7% (1SD), lower than the homogeneity test (4.5%, 1SD). The same trend can be seen for UNIL\_B2, with a reproducibility of 3.1% (1SD) for the two grains with different orientations and a value of 6.7% (1SD) for the homogeneity test.

The 3 grains of UNIL\_B1 mounted perpendicular to the surface of the mounts have deviation from the grain parallel (grain 1) of 2.4%, 5.2% and 3.6% (for grain 2, 3 and 4, respectively) for  $^{16}\text{O}^1\text{H}/^{28}\text{Si}$  values. The deviation for UNIL\_B2 between the two orientations is 1.18%. The deviations between the two orientations for UNIL\_B1 are slightly higher than the homogeneity of this RM (1.9%, 1SD) and values for perpendicular grains are consistently higher than the

grain parallel. Nevertheless, for UNIL\_B2, values are also lower for the grain perpendicular this is the opposite for UNIL\_B1, for which deviation between the two grains with different orientations remains below the variations due to grain to grain variations (i.e. homogeneity test, 1.6% (1SD)).

For  $^{19}\text{F}/^{28}\text{Si}$ , the 3 perpendicular grains of UNIL\_B1 have deviations from the parallel grain of -2.5%, -2.0% and -2.6% (for grain 2, 3 and 4, respectively). They are all above the variations observed during the homogeneity test of 1.3% (1SD), they also behave in the same way, i.e. measured values are lower than the parallel grain. This is also the case for UNIL\_B2 since the perpendicular grain (grain 2) is 14.78% lower than the grain parallel (grain 1). This deviation is outside the variations observed for the homogeneity test of 2.6% (1SD).

For  $^{35}\text{Cl}/^{30}\text{Si}$ , deviations of the 3 perpendicular grains of UNIL\_B1 are -2.3%, 0.3% and -4.6% for grain 2, 3 and 4, respectively, they all lie inside the variations observed during the homogeneity test (4.5%, 1SD). Also, they do not behave in the same way with 1 grain with higher value and the two other grains with lower values than the parallel grain (grain 1). UNIL\_B2 has a deviation between the two grains with different orientation of 2.6%, well below the homogeneity test value of 6.7% (1SD).

The fact both variations and deviations for different orientations is slightly higher compare to the homogeneity of the RMs for some measurements (i.e. for UNIL\_B1 for  $\text{H}_2\text{O}$  content and for both UNIL\_B1 and UNIL\_B2 for F content), but not for all, and not in a consistent way, is a good indication of the absence of orientation effect. Nevertheless, it seems that even with the high number of grains and analyses for the homogeneity test (see Table 3), the value might be slightly underestimated.

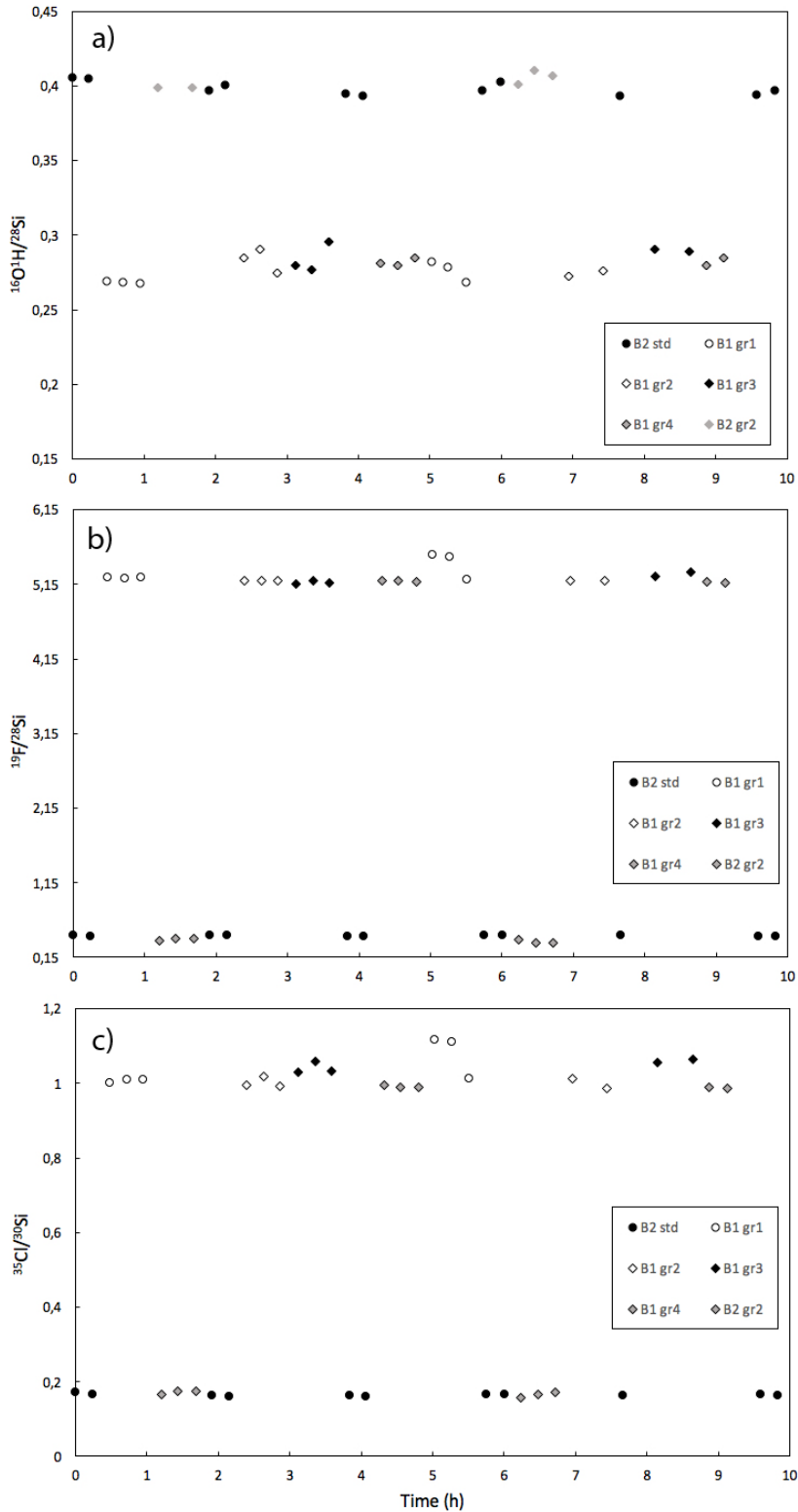


Figure 4: Tests of IMF dependence on crystal the  $^{16}\text{O}^1\text{H}/^{28}\text{Si}$ ; c,  $^{19}\text{F}/^{28}\text{Si}$ ; e,  $^{35}\text{Cl}/^{30}\text{Si}$  ratios measured on the SIMS. No orientation effect was observed. 6 points in a grain of UNIL\_B2 parallel to the surface of the mount have been used as working reference material for this session (black dots). Grey diamonds represent analyses in a grain of UNIL\_B2 perpendicular to the surface of the mount. 3 grains of UNIL\_B1 with different orientations perpendicular to the surface of the mount have been analyzed (grain 2, white diamonds; grain 3, black diamonds and grain 4, grey diamonds). 6 points inside a grain of UNIL\_B1 parallel to the surface of the mount have been analyzed (white dots).

### 4.3.3 Vacuum test

Since  $^{16}\text{O}^1\text{H}$  is synthesized in the analysis chamber during extraction of the ions, vacuum influences the value measured by the detectors for constant  $\text{H}_2\text{O}$  content in biotite. To check for the importance of this effect and establish the pressure limit for analysis, we analyzed first UNIL\_B2 with decreasing vacuum. UNIL\_B2 is the RM with the highest  $\text{H}_2\text{O}$  content, then it should be easier to track changes due to vacuum evolution. Then UNIL\_B1 was tested in alternance with UNIL\_B2 to check for a potential composition effect, as this last RM has lower water content than B2. As can be seen on figure 5, the  $^{16}\text{O}^1\text{H}/^{28}\text{Si}$  ratio decreases by more than 10% between  $2.4 \cdot 10^{-8}$  and  $1.5 \cdot 10^{-8}$  mbar. We did not see any composition related variations due to vacuum conditions. Comparison of  $^{16}\text{O}^1\text{H}/^{28}\text{Si}$  values for different vacuum requires additional correction, increasing the final uncertainty on  $\text{H}_2\text{O}$  content. Acquisition during changing vacuum conditions will also imply drift correction, again, the final uncertainty will increase. To avoid any additional corrections, we recommend to mount biotite into indium to stay always at a vacuum below  $1 \cdot 10^{-8}$  mbar.

Table 4: comparison of relative reproducibility (% 1SD) for the RMs UNIL\_B1 and B2 during the homogeneity test and the orientation test, deviation (%) between the grains parallel and perpendicular to the surface of the mount for UNIL\_B1 and B2 during the orientation test

Element	Reproducibility (% 1SD) homogeneity test		Reproducibility (% 1SD) orientation test (overall)		Deviation (%) between grains parallel and perpendicular, UNIL_B1			Deviation (%) between grains parallel and perpendicular, UNIL_B2
	UNIL_B1	UNIL_B2	UNIL_B1	UNIL_B2	grain 2	grain 3	grain 4	grain 2
OH	1.9	1.6	2.9	1.3	2.4	5.2	3.6	1.2
F	1.3	2.6	1.8	8.5	2.5	2	2.6	14.8
Cl	4.5	6.7	3.7	3.1	2.3	0.3	4.6	2.6

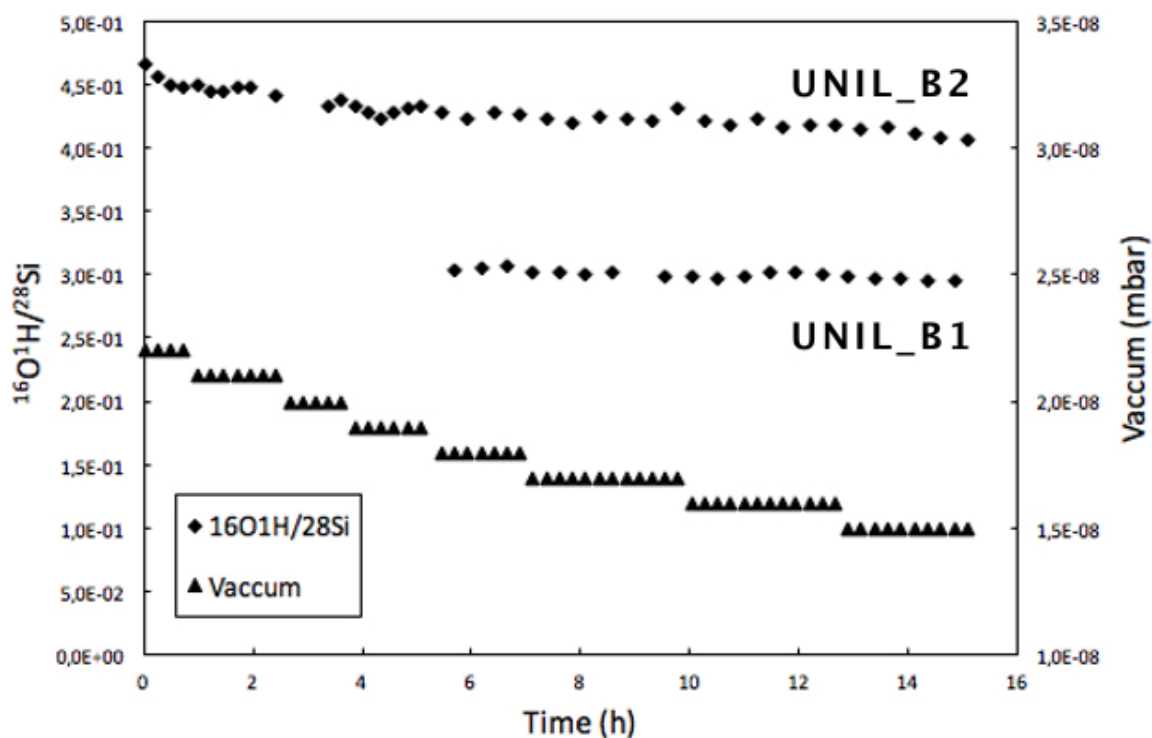


Figure 5: Analyses of UNIL\_B1 and B2 with decreasing pressure (e.g. improving vacuum) inside the analysis chamber during a session. Black triangles represent the vacuum, decreasing from  $2.4 \cdot 10^{-8}$  to  $1.5 \cdot 10^{-8}$  mbar. The  $^{16}\text{O}^{1}\text{H}/^{28}\text{Si}$  ratio of both UNIL\_B1 and UNIL\_B2 decrease with improving vacuum.

#### 4.3.4 F and Cl calibration

A major issue with the determination of major, minor or trace elements using SIMS is the presence of matrix effects (Steele et al. 1981, Bulle and Layne 2014). Matrix effects are related to the differential extraction of element during the sputtering process. It can either result in non-linear correlation between measured ion intensities and reference values or even be a function of other major elements composition of the analyzed material. To circumvent these effects, empirical procedures have been set-up. They mainly rely on working curves between reference values of well characterized materials and measured ion-normalized sensitivity factors, the reference element chosen for this study is Si.

The  $^{19}\text{F}/^{28}\text{Si}$  and  $^{35}\text{Cl}/^{30}\text{Si}$  of all 6 RMs have been characterized during the same session (28<sup>th</sup> of February 2016), with 3 points in each RM, and 3 points in a UNIL\_Q1 quartz (Seitz et al. 2016) for background correction. For both  $^{19}\text{F}/^{28}\text{Si}$  and  $^{35}\text{Cl}/^{30}\text{Si}$ , the value for the quartz

analyses are close to zero, meaning that the difference for the fit is negligible using UNIL\_Q1 background or by forcing the intercept to 0. Matrix effect related to (Fe + Mn) content has been found for F analyses of silicate minerals (Ottolini et al. 2002, 2006), but we did not observe such an effect for biotites. Both F and Cl content do not require any correction for major element variations. They can be determined from a second order polynomial fit (figure 6), with a  $R^2$  of 0.998 and 0.996 respectively.

A linear correlation should be used for low F content, since the polynomial fit gives overestimated F content for UNIL\_B2, B4 and NBS30 that have F content below 0.2 wt%. This allow to reproduce the F content of these RMs within error with a resulting  $R^2$  of 0.81 (caption in Fig. 6a). We recommend to use a linear fit to measure low F content and a polynomial fit for high F content.

A linear calibration can also constrain the Cl content of all RMs, nevertheless it does not reproduce successfully the Cl content of NBS30, at low Cl content (i.e. below 0.03 wt%), the difference between the polynomial fit and the linear fit is within error and does not change significantly the measured Cl content. Additional Cl content in the range of 0.1-0.2 wt% should allow a definitive conclusion on the fit needed to constrain Cl content in biotite using SIMS.

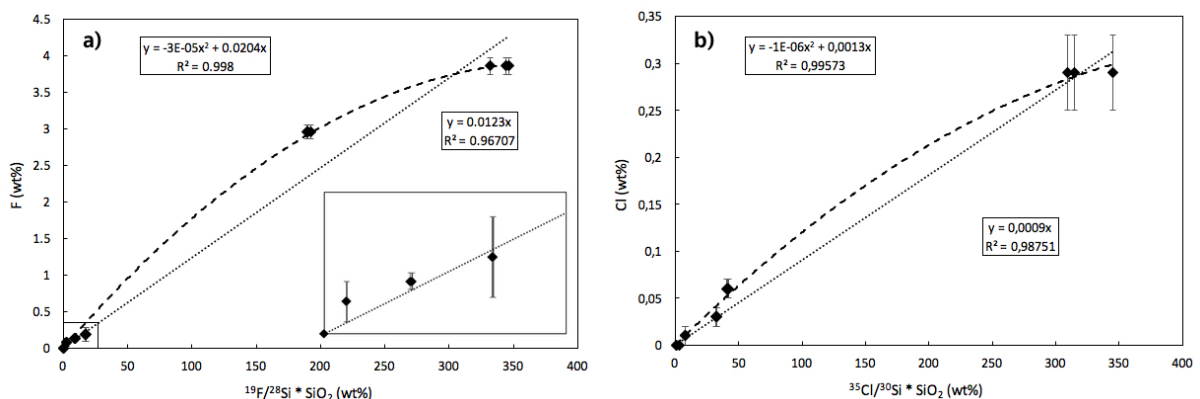


Figure 6: a) Working curve for F content determined using EPMA versus measured  $^{19}\text{F}/^{28}\text{Si} \cdot \text{SiO}_2$  from SIMS. Caption represent a zoom of the low F content RMs (i.e. below 0.2 wt%), showing the successful linear fit only for these 3 RMs. b) Working curve for Cl content from EPMA versus  $^{35}\text{Cl}/^{30}\text{Si} \cdot \text{SiO}_2$  from SIMS measurements. Dashed lines and dot lines represent the second order polynomial and linear fit respectively which successfully reproduce the values of RMs for both measurements. See text for more explanations.

#### 4.3.5 H<sub>2</sub>O calibration

The same approach was attempted for water content measurements using SIMS. Contrary to F and Cl, the reference values for water content in biotites RM does not exhibit a strong relationship with the measured <sup>16</sup>O<sup>1</sup>H/<sup>28</sup>Si ion-intensity (figure 7a). Instead, a multivariate weighted least squares fit has been used (Bevington and Robinson 2002, described in detail in Siron et al. (2016)), using <sup>16</sup>O<sup>1</sup>H/<sup>28</sup>Si and X<sub>Mg</sub> as variables. This computation only accepts uncertainties on the fitted variable (i.e. reference value for H<sub>2</sub>O here), no uncertainties for SIMS analyses were taken into account. The uncertainties for H<sub>2</sub>O reference values of the different RMs were the propagation of the reproducibility (1SD) of both RM and the G1 standard analyzed during the same session, calculated as follow:

$$\sigma_i = \sqrt{(\sigma_{RM})^2 + (\sigma_{G1})^2}$$

$\sigma_i$  represent the final uncertainty for the reference value of H<sub>2</sub>O,  $\sigma_{RM}$  is the reproducibility (1SD) for the two TC/EA measure of the RM,  $\sigma_{G1}$  represent the reproducibility (1SD) of the standards analyzed during the TC/EA session.

Calculation of the multivariate weighted least squares results in a successful fit with a  $\chi^2$  per point (or Mean Square Weighted Deviation, MSWD) of 1.410 using all RMs, including the quartz in-house reference material (UNIL\_Q1). However, as quartz does not closely match the structure of biotite, we decided to do data reduction with only biotite RMs. It results in a better fit, with a  $\chi^2$  per point of 0.672 (figure 7b). This suggests that IMF for H<sub>2</sub>O content is a function of chemistry and structure of the phase analyzed. We also tested a fit without UNIL\_B5, which has sometimes grains with different water content (see homogeneity test section). The resulting

$\chi^2$  per point is 0.790, in the same order of magnitude than for all RMs. It reproduces quite well the reference value of all RMs, including that of UNIL\_B5 (figure 7c). The same argument can be made for UNIL\_B4, which has grains with different  $X_{Mg}$ , especially visible on the figure 1 of Siron et al. (2016).

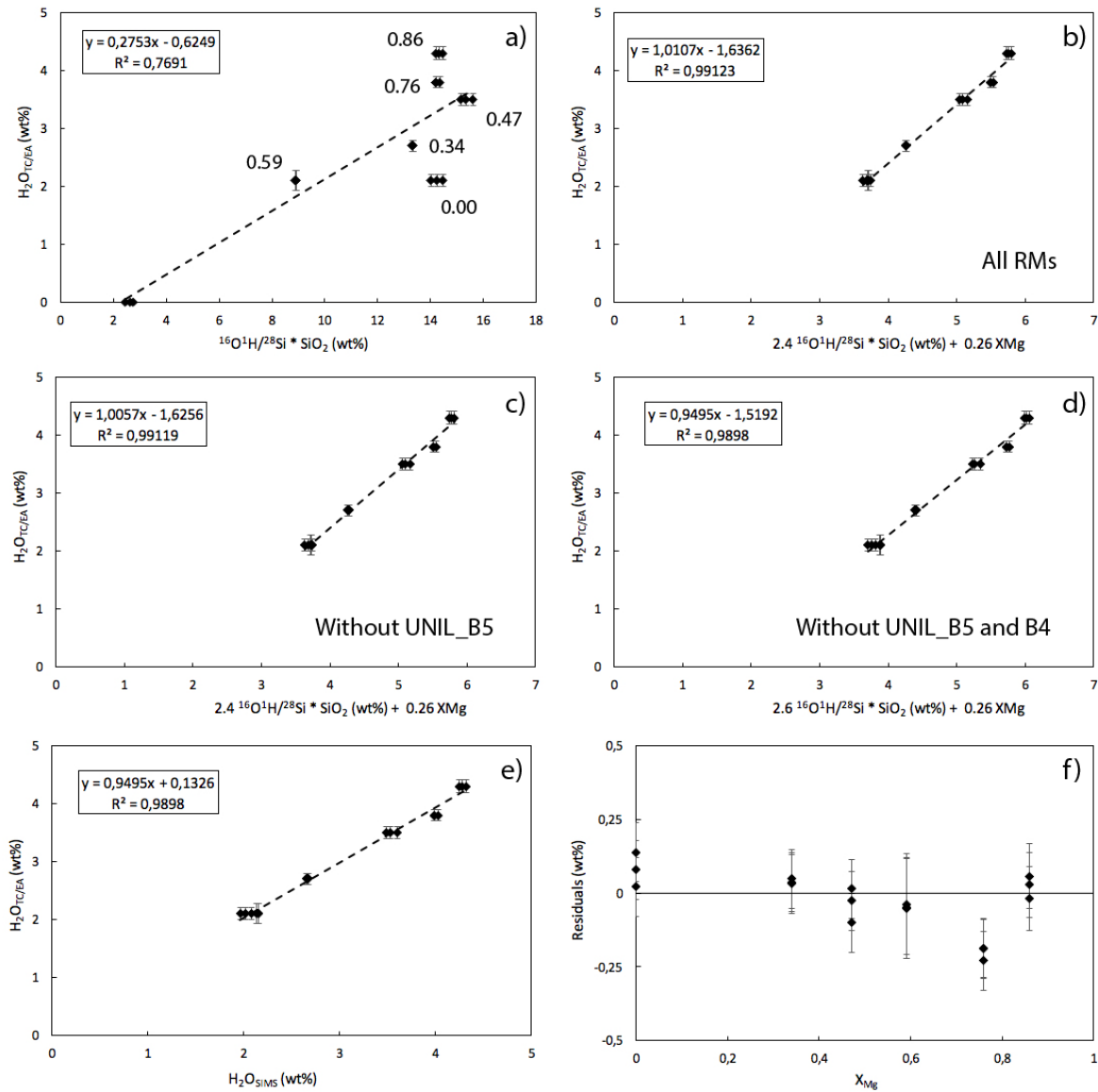


Figure 7: Water content calibration for biotite measurements using SIMS. b) working curves showing a poor correlation between ion-intensity ratio  $^{16}O^1H/^{28}Si * SiO_2$  (wt%), numbers next to each RM are their respective  $X_{Mg}$ ; b) x axis represent the results of the multivariate fit using  $^{16}O^1H/^{28}Si * SiO_2$  and  $X_{Mg}$  as variable for all biotite RMs, without quartz analyses; c) same as b) but the fit were done without UNIL\_B5 RM; d) same as c) but without UNIL\_B5 and B4; d) comparison for all biotite RMs between modelled value using the multivariate analysis and SIMS measurements (x axis) and reference values from TC/EA (y axis).

A fit without UNIL\_B5 and B4 gave a  $\chi^2$  per point of 0.233. It successfully reproduced the reference values for all RMs, within the error, except UNIL\_B4 (figure 7d). The residuals (difference between reference and modelled value) for this last test confirm that all RMs can be modelled within 0.1 wt% error, except UNIL\_B4, which has a modelled value 0.20-0.25 wt% higher than the reference water content. We thus recommend analyzing UNIL\_B1, B2 and B3 as long as NBS30 at the beginning of each session for water content.

#### *4.3.6 Precision and accuracy for H<sub>2</sub>O, F and Cl measurement*

In this paragraph, the term precision will refer to the relative precision during the a single SIMS session and accuracy will refer to the uncertainty for the absolute value for H<sub>2</sub>O, F and Cl content. The first will allow the user to compare biotite compositions analyzed during the same session with a reduced uncertainty for F and Cl content, and biotite with same  $X_{Mg}$  and during the same session for H<sub>2</sub>O content. Nevertheless, to compare the same biotite analyses with other session or with literature values require the use of their absolute values for H<sub>2</sub>O, F and Cl content; these values carry bigger uncertainties since they require a calibration using the external calibrations, e.g. absolute values for RMs, from TC/EA for H<sub>2</sub>O content, and EPMA for F and Cl contents. These reference values have uncertainties that need to be propagated together with the SIMS uncertainties. Additionally, the simple linear or polynomial fit for F and Cl content will also increase the uncertainty on absolute value (i.e. accuracy). The multivariate fit for H<sub>2</sub>O content introduces even more uncertainty since it requires the  $X_{Mg}$  constrain on both RMs and unknown measurements, increasing the final uncertainty for the accuracy on H<sub>2</sub>O content. Typically, due to the homogeneity of the RMs recommended to be used as internal reference materials (i.e. UNIL\_B1 and B2), during a good session, precision for H<sub>2</sub>O content measurement should be slightly better than 0.1 wt%, precision for F and Cl content should be around 50 ppm and 5-10 ppm, respectively. For the same session, accuracy

on H<sub>2</sub>O content is typically between 0.15-0.2 wt%. The uncertainty on the reference value for F and Cl content obtained from EPMA, is 1-2 order of magnitude higher than the precision of the SIMS, the accuracy of the measurement for these elements is virtually determined by the EPMA uncertainty of the primary reference material used during the session. The accuracy of the fluorine content will be the same no matter which of the RMs is used, UNIL\_B1 or B2, since they have the same uncertainty on their reference values, i.e. 0.1 wt%. Chlorine content in the range of 0.01-0.06 wt% will have accuracy determined by UNIL\_B2, i.e. 0.01 wt%, and high chlorine content in the range 0.1-0.2 wt% will have the same accuracy than UNIL\_B5, i.e. 0.04 wt%. Analyzing high chlorine content with SIMS is hence not recommended since the accuracy is in the same order of magnitude as the EPMA analyses, except if the aim is to compare biotite during the same session using only relative SIMS precision.

#### 4.4 Conclusion

In this chapter we show that OH-F-Cl measurements in biotite using SIMS are not affected by crystal orientation effects, allowing the determination of their content in randomly oriented biotites in natural samples. Nevertheless, low water content show a clear correlation with the vacuum inside the analysis chamber. Hence the best possible vacuum should be obtained. This leads us to recommend mounting thin sections or grains into indium in order to achieve a vacuum below  $1 \cdot 10^{-8}$  mbar.

Water, fluorine and chlorine exhibit matrix effects when measured using SIMS. The first two have simple but non-linear correlation between measured ion-intensities and reference values. Accurate measurements of F and Cl content in biotite can be produced using second order polynomial fit of measured  $^{19}\text{F}/^{28}\text{Si}$  and  $^{35}\text{Cl}/^{30}\text{Si}$  for all RMs, except UNIL\_B4 in the case of F content and UNIL\_B1 for Cl content due to heterogeneity visible at the SIMS precision level.

Water content measurements have a more complicated matrix effect, related to the octahedral composition of biotite. Using a multivariate weighted least square procedure, with  $^{16}\text{O}^1\text{H}/^{28}\text{Si}$  (measured with by SIMS) and  $X_{\text{Mg}}$  (determined by EPMA) as variables, water content of all RMs can be reproduced within 0.1 wt%, except UNIL\_B4 which is 0.2-0.25 wt% off the calibration reference value. For that reason, we used UNIL\_B1, B2 and B3 a long with NBS30. In conclusion, we recommend to analyses at the beginning of each session UNIL\_B1, B2, B3 and NBS30 to obtain a H<sub>2</sub>O concentration working curve. If F and Cl content have to be determined simultaneously, UNIL\_B5 has to be analyzed together with the other RMs since it constrains F and Cl at the higher contents (especially for chlorine). We recommend to mount UNIL\_B2 and UNIL\_B1 has working RM in the same mount as the unknown sample to monitor for a potential drift during the session. UNIL\_B1 should be used as primary RM for water content determination, UNIL\_B2 value would be used as check for the accuracy. For F and Cl measurements, UNIL\_B2 should be used as primary RM and UNIL\_B1 as secondary RM. Two points of analyses inside both should be made each 6-10 unknowns.

#### 4.5 References

- Armstrong, J. T. (1989) CITZAF : Combined ZAF and Phi-Rho (Z) Electron Beam Correction Program, California Institute of Technology, Pasadena, CA.
- Bauer, K. K., & Vennemann, T. W. (2014). Analytical methods for the measurement of hydrogen isotope composition and water content in clay minerals by TC/EA. *Chemical Geology*, 363(C), 229–240.
- Bevington, P. R., & Robinson, D. K. (2002). Data reduction and error analysis for the Physical Sciences. 3th edition. McGraw-Hill Education.
- Bulle, F., & Layne, G. D. (2014). International Journal of Mass Spectrometry. *International Journal of Mass Spectrometry*, 361, 41–53. <http://doi.org/10.1016/j.ijms.2014.01.026>

- Cesare, B., Cruciani, G., & Russo, U. (2003). Hydrogen deficiency in Ti-rich biotite from anatectic metapelites (El Joyazo, SE Spain): Crystal-chemical aspects and implications for high-temperature petrogenesis. *American Mineralogist*, 88, 583–595.
- Cesare, B., Satish-Kumar, M., Cruciani, G., Pocker, S., & Nodari, L. (2008). Mineral chemistry of Ti-rich biotite from pegmatite and metapelitic granulites of the Kerala Khondalite Belt (southeast India): Petrology and further insight into titanium substitutions. *American Mineralogist*, 93(2-3), 327–338.
- Cruciani, G., & Zanazzi, P. F. (1994). Cation partitioning and substitution in 1M phlogopite: A crystal chemical study. *American Mineralogist*, 79, 289–301.
- Dyar, D., Guidotti, C. V., Holdaway, M. J., & Colucci, M. (1993). Nonstoichiometric hydrogen contents in common rock-forming hydroxyl silicates. *Geochimica and Cosmochimica Acta*, 57, 2913–2918.
- Munoz, J. L. (1984). F-OH and Cl-OH Exchange in Micas with Applications to Hydrothermal Ore Deposits. *Reviews in Mineralogy and Geochemistry*, 13, 469–493.
- Ottolini, L. P., Cámara, F., Hawthorne, F. C., & Stirling, J. (2002). SIMS matrix effects in the analysis of light elements in silicate minerals: Comparison with SREF and EMPA data. *American Mineralogist*, 87, 1477–1485.
- Ottolini, L., Cámara, F., & Hawthorne, F. C. (2006). Strategies for Quantification of Light Elements in Minerals by SIMS: H, B and F. *Microchimica Acta*, 155(1-2), 229–233.
- Rieder, M., Cavazzini, G., DYakonov, Y. S., Frank-Kamenetskii, V. A., Gottardi, G., Guggenheim, S., et al. (1998). Nomenclature of the micas. *The Canadian Mineralogist*, 36, 41–48.
- Seitz, S., Baumgartner, L. P., Bouvier, A.-S., Putlitz, B., & Vennemann, T. (2016). Quartz Reference Materials for Oxygen Isotope Analysis by SIMS. *Geostandards and Geoanalytical Research*, 1–7.
- Steele, I. M., Hervig, R. L., Hutcheon, I. D., & Smith, J. V. (1981). Ion microprobe techniques and analyses of olivine and low-Ca pyroxene. *American Mineralogist*, 66, 526–546.
- Zhu, C., & Sverjensky, D. A. (1991). Partitioning of F-Cl-OH between minerals and hydrothermal fluids. *Geochimica Et Cosmochimica Acta*, 55, 1837–1858.



## 5 Significance of OH, F and Cl content in biotite during metamorphism of the Western Adamello contact aureole

Authors: Guillaume Siron, Lukas Baumgartner, Anne-Sophie Bouvier, Torsten Venneman

Proposed journal: Contribution to Mineralogy and Petrology

## 5.1 Introduction

The potential for tracing fluid-rock interactions with fluorine and chlorine content in biotite has been recognized over 30 years ago (Munoz 1984, Zhu and Sverjenski 1991, 1992). The fluid-biotite exchange was mainly used to track fluid sources in hydrothermal systems using experimentally determined  $X_{\text{HCl}}/X_{\text{H}_2\text{O}}$  and  $X_{\text{HF}}/X_{\text{H}_2\text{O}}$  ratios between annite and hydrothermal fluids by Munoz (1984) (Panigrahi et al. 2008, Rasmussen and Mortensen 2013). Cl content in biotite (and other minerals) has been used to infer infiltration of highly saline brines in granulite terrains, either interpreted as peak infiltration (Nijland et al. 1993) or at high temperature during cooling (Higashino et al. 2013).

The incompatible behavior of chlorine in minerals should result in a progressive loss of Cl during dehydration reactions. Nevertheless, as documented in Selverstone and Sharp (2015) and Siron et al. (in prep.), the documentation of the loss is not straightforward since biotites in prograde sequences can have low Cl concentrations ( $\sim 0.01\text{wt}\%$ ) which are difficult to measure with high enough precision using electron microprobe. A second potential problem is the retentiveness of biotite for  $\text{Cl}^-$  on its  $\text{OH}^-$  site. That  $\text{Cl}^-$  can be maintained is shown by the studies mentioned above, suggesting that  $\text{Cl}^-$  biotite/fluid exchange could be slow. This is consistent with the observation of Markl and Bucher (1998) in high grade terrains in Norway. They show the coexistence of halide with low-Cl minerals, with the exception of high Cl rim of amphiboles. They suggest that retrograde reactions lead to precipitation of halite due to dessication of the fluid during retrograde hydration reactions.

The water content in biotite has been the focus of a small number of studies since the early 90's (Dyar et al. 1993, Cesare et al. 2003, 2008). These studies were supported by the development of new analytical techniques such as Fourier Transform Infrared (FTIR) or Secondary Ion Mass Spectrometry (SIMS). These studies clearly show that  $\text{OH}^-$ ,  $\text{Cl}^-$ , and  $\text{F}^-$  do not fill completely

the O(4) site. This nonstoichiometry was explained by the need to compensate trivalent or quadrivalent ion substitutions for divalent cation in the octahedral sites (e.g. Cesare et al. 2003, 2008). Such substitutions have been named deprotonation (loss of  $H^+$ ) or oxy-substitution since they lead to the substitution of  $O^{2-}$  for  $OH^-$  in the hydroxyl site. Similarly, complex ion exchanges involving  $Al^{3+}$ ,  $Fe^{3+}$  and  $Ti^{4+}$  have been invoked to explain  $H_2O$  content variations of biotite from metapelites from Western Maine (Dyar et al. 1993), and more recently Cesare et al. (2003, 2008) explained the  $H_2O$  content variations in biotites from Indian granulitic metapelites using the titanium-oxy substitution.

Here we present in-situ secondary ion mass spectrometry measurements of OH, F and Cl in biotite, measured during a single session to minimize analytical uncertainties. The procedure described in Siron et al. (chapter 4), with the aim to determine the behavior of these important anions during prograde metamorphism. Samples from different grades of the Western Adamello contact aureole were analyzed to demonstrate the effect of metamorphic grade, and potentially water activity. By comparing the concentrations of these 3 anions in biotites included in anhydrous minerals with biotite in the matrix we demonstrate that biotite retains its composition with respect to F, Cl, and  $H_2O$  content. Hence we proceed to establish the behavior of water and the halogens in the O(4) site during prograde metamorphism.

## 5.2 Geological setting

The Western Adamello tonalite (WAT) is part of the Adamello batholith located in the Northern Italian Alps (Callegari and Brack 2002; Floess et al. 2015). The batholith is composed of a suite of intrusive rocks of various composition, grouped into 4 super-unit by Bianchi et al. (1970). The age of the intrusive rocks increases from Northeast to Southwest: the Presanella unit (32-31 Ma), the Avio unit (34-32 Ma), the Adamello unit (36-34 Ma) and the Re di Castello unit

(41-38 Ma). The first three units mainly intruded into the Variscan basement at slightly deeper levels, whereas the southernmost were emplaced mostly into Permian to Triassic sedimentary cover (figure 1). The contact aureole of the Western Adamello tonalite (WAT) is mainly composed by polymetamorphic rocks. They were metamorphosed 330 Ma ago, during the Variscan orogeny, at pressure and temperatures of 7-9 kbar and 570-610 °C (Diella et al. 1992). The Variscan basement involved in the aureole is comprised of different lithologies, varying from micaschists, phyllites, to some acidic and mafic gneisses. Exhumation previous to the contact metamorphism induced by the WAT lead to partial re-hydration of the basement (Floess and Baumgartner, 2012). Chlorite, white micas and minor relict biotite define a pervasive foliation in the non-contact metamorphic precursor rocks. They are intercalated with quartz-feldspar-rich layers on a 1cm scale. Retrogression of Variscan garnet by chlorite and clay minerals is common outside the contact aureole. The retrograde minerals were replaced first by biotite, and subsequently by newly formed garnet with increasing contact metamorphic grade (Floess and Baumgartner 2012).

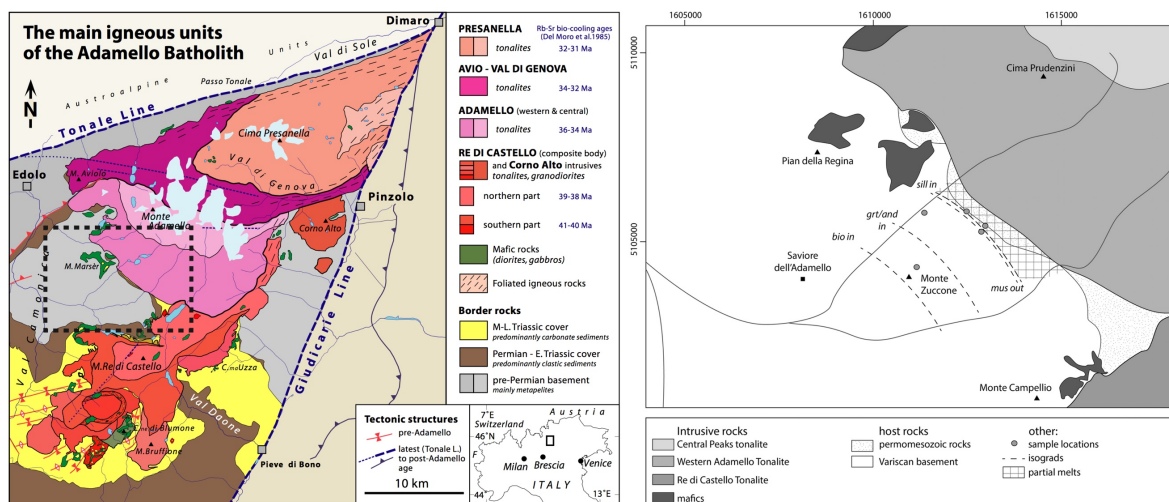


Figure 1 : a) Map of the Adamello massif with the different intrusive units, the dashed box represent the location of the zoomed part showed in b (from Brack et al. 2009). b) Western Adamello contact aureole with the different isograd discussed in the text and the location of the samples studied. Isograd map from Floess and Baumgartner, 2015.

The Tertiary intrusion of the WAT produce a contact aureole with a sequence typical for low to medium pressure contact metamorphism. The mineral sequence observed corresponds to bathozone 2 (Pattison and Tracy, 1991). At about 2200 m from the contact, chlorite reacted to form new biotite, shortly after cordierite is stabilized when variscan paragonite react out to produce plagioclase. At 1700 m, andalusite porphyroblast are visible in the field and grow at the expense of cordierite. Andalusites are poikilitic, with mostly quartz and biotite inclusions, along with some ilmenite. This texture was produced by the reaction cordierite + muscovite = biotite + andalusite + quartz + H<sub>2</sub>O. The andalusite-in isograd is accompanied by the growth of new garnet (Floess and Baumgartner 2012). Closer to the intrusion, muscovite breaks down to form K-feldspar and sillimanite. Pods of first partial melts were observed a few meters up-grade from the first sillimanite and k-feldspar paragenesis at roughly 350m. This sequence of isograds corresponds to the type 1c or 2a in the petrogenetic grid of Pattison and Tracy 1991, it constrains the pressure to about 2.5 kbar. Not all rocks contain aluminosilicates. The observed presence of cordierite at high grade and the absence of andalusite at medium or sillimanite at high grade is most likely due to variations in X<sub>Mg</sub> of the rocks, as suggested by Pattison et al. (1999).

## 5.3 Analytical methods

### 5.3.1 *Electron Probe Micro-analysis (EPMA)*

Major and minor element analyses of biotite were obtained with a JEOL 8200 Superprobe, equipped with 5 wave length dispersive spectrometers. The concentrations of the elements Si, Al, Ti, Fe, Mg, Mn, K, Na, Ca, F and Cl were measured with a 15kV/15nA beam with a spot size of 10 µm. Counting times were set for most elements to 15 seconds for background before

and after peak and 30 seconds on the peak. Counting times were reduced for Na and K to 10 seconds on the background and 20 seconds on the peak. Scapolite (Cl), albite (Na), wollastonite (Ca), orthose (Si, K), andalusite (Al), fayalite (Fe), forsterite (Mg) and MnTi oxide (Mn, Ti) were used as reference standards. The data were reduced with the CITZAF matrix correction routine of Armstrong (1989). Structural formulae for biotite were normalized to 24 – (OH + F + Cl) oxygens. All iron was assumed as Fe<sup>2+</sup>, no Fe<sup>3+</sup> corrections was attempted.

WDS X-ray maps were acquired with the JEOL 8200 superprobe to test for homogeneity in F, Cl, Mg, Fe and K in biotite grains and aggregates. A current of 200nA and 15kV was used, with a pixel size of 0.12µm and different dwell times (100, 200 and 300ms respectively). No additional heterogeneities were discovered with the higher dwell time values.

### 5.3.2 Secondary Ion Mass Spectrometry (SIMS)

OH, F and Cl content of micas were measured with the IMS 1280HR facility at the SwissSIMS laboratory following the method described in the chapter 3. A focused high-density primary beam in Gaussian mode was used, at a current of 1nA and an acceleration voltage of 10keV. A 20µm raster was used during the 210 seconds of pre-sputtering to avoid lateral contaminations from the border of the pit, mainly for Cl<sup>-</sup>. Analysis were obtained with a 10µm raster. This resulted in a spot size slightly bigger than 10µm.

Entrance (50µm) and exit (400µm) slits were set to achieve a mass resolution of about 5000 to discriminate the isobaric interferences for <sup>17</sup>O and the <sup>16</sup>O<sup>1</sup>H peaks, which was used for the analysis of the H-content in biotite. An electron gun with a normal incidence was used for charge compensation and carefully tuned at the beginning of each session.

The analyses were done in mono-collection mode, using magnetic peak switching, by cycling 15 times over the masses <sup>16</sup>O<sup>1</sup>H, <sup>19</sup>F, <sup>28</sup>Si, <sup>30</sup>Si and <sup>35</sup>Cl. Automatic centering of deflectors associated to field and contrast apertures were performed before each analysis. After deflectors

centering, mass  $^{28}\text{Si}$  was automatically scanned to ensure the correct position of the magnet for each measured mass.  $^{16}\text{O}^1\text{H}$ ,  $^{19}\text{F}$  and  $^{28}\text{Si}$  were analyzed using a faraday cup (FC2,  $10^{11} \Omega$  resistor) and the axial electron multiplier (EM) was used for  $^{30}\text{Si}$  and  $^{35}\text{Cl}$ .

## 5.4 Results

### 5.4.1 Petrography

Five samples were selected from the Western Adamello contact aureole for this study from different metamorphism zones, ranging from the biotite zone without cordierite to the partial melting zone, after muscovite breakdown. The Ti-bearing phase is ilmenite in all samples, but there is no graphite present. The lack of graphite suggests that fluid was relatively oxidized. The complete mineral assemblage, distance to the intrusion and estimated temperature for each sample are summarized in table 1.

Sample 09DF032 (biotite zone) is a metapelite which shows a partial retrogression of Variscan garnet. The prograde biotite rimming the garnet is interpreted to have replaced retrograde chlorite. It is slightly darker than matrix biotite (figure 2a and b). White micas mark a well-developed, pervasive foliation. Sample 09DF067 is a metapelite that exhibit typical framboidal garnets (Floess and Baumgartner, 2012). It contains poikiloblastic andalusite (figure 2c and d). Andalusite inclusion trails delineate the Variscan schistosity and some micro-folds (figure 2e and f). Cordierite grew before andalusite since it is included in some places. Sample 09DF096 is a metapelite with newly grown, randomly oriented, biotite crystals (figure 3a and b). It has nicely preserved cordierite with biotite inclusions, but does not contain andalusite. Sample 09DF097 is a gneiss with evidence of new growth of biotite. Minor alteration is evidenced by some pinnitized cordierite (figure 3c and d). It contains abundant quartz-feldspar layers, but

no garnet was found in the mica-rich layers. The absence of andalusite in both 09DF096 and 09DF097 is due to the low  $X_{Mg}$  (around 0.3) compared to the two other samples above the andalusite-in isograd (09DF067 and 09DF042) that have higher  $X_{Mg}$  of about 0.5 (see Pattison, 1999 for discussion). Sample 09DF042 is a metapelite with no muscovite. It shows evidences of partial melting. It contains abundant relict andalusite with biotite inclusions. New sillimanite grew within the mica layers and is aligned with the mica-rich layers.

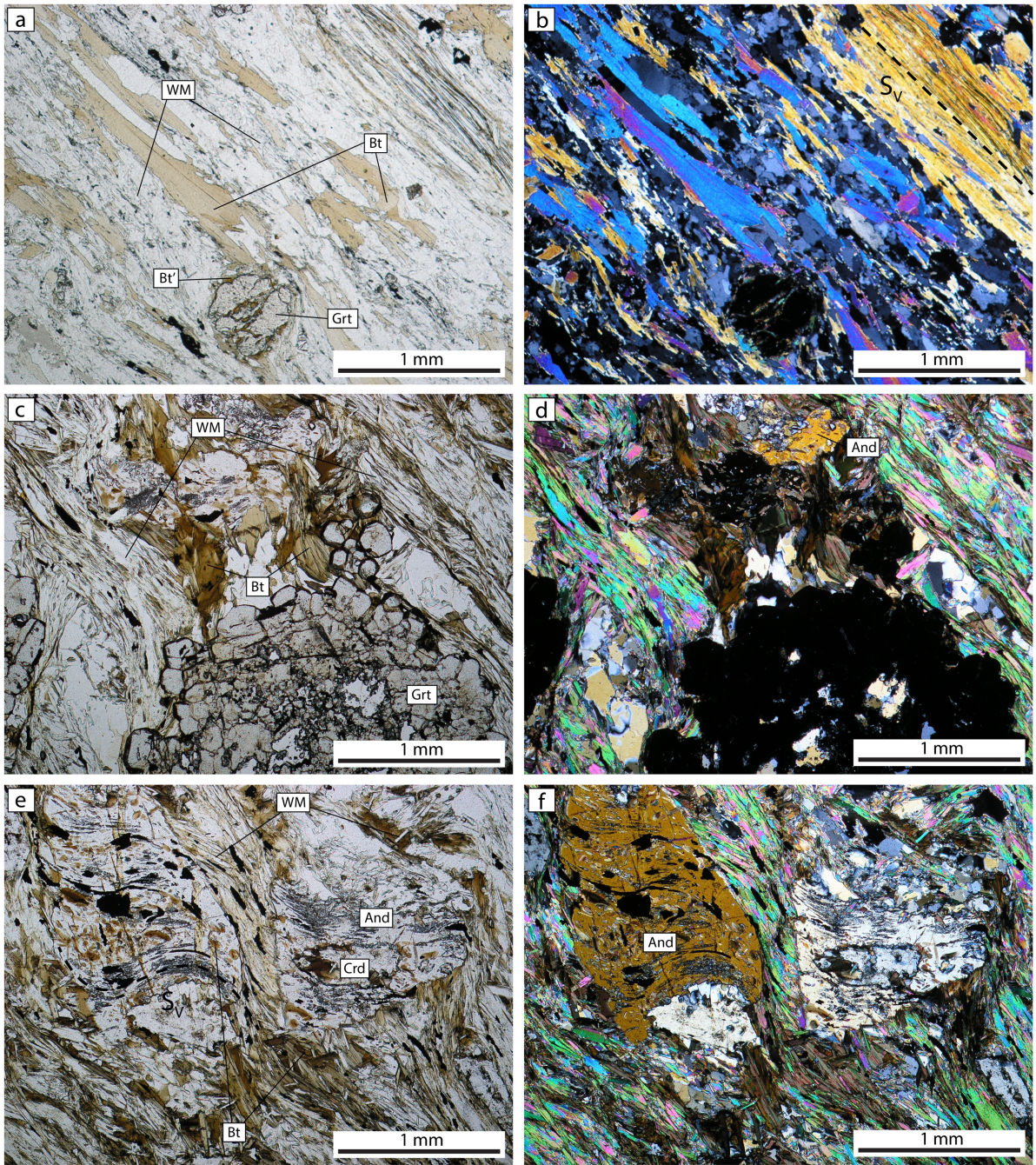


Figure 2 : Natural and cross polarized light photomicrograph of samples from: the biotite zone, 09DF032 (a, b); the andalusite zone, 09DF067 (c, d, e, f). a) Photomicrograph showing the recrystallization of biotite surrounding garnet due to pre-contact metamorphic chloritization of garnet. This biotite (Bt') has a different color, when compared with the newly grown biotite (Bt) in the matrix from chlorite breakdown reaction. b) Photomicrograph in cross polarized light of a) showing white micas that define a pervasive Variscan foliation ( $S_v$ , dashed line in the upper right corner). c) Photomicrograph showing typical framboidal garnet in the lower half, white micas define a pervasive Variscan foliation. The newly grown biotites are randomly oriented. d) Cross polarized light microphotograph of c) showing andalusite on the upper part of the picture, inclusion of biotite and quartz are visible. e) Photomicrograph of inclusion trails inside andalusite that mark the Variscan pervasive foliation together with white micas. Right porphyroblast of andalusite has overgrown cordierite. e) Cross polarized light photomicrograph of e) showing randomly oriented newly grown biotite. WM: white mica, Bt: biotite, Bt': biotite from garnet retrogression, Grt: garnet, Crd: cordierite, And: andalusite.

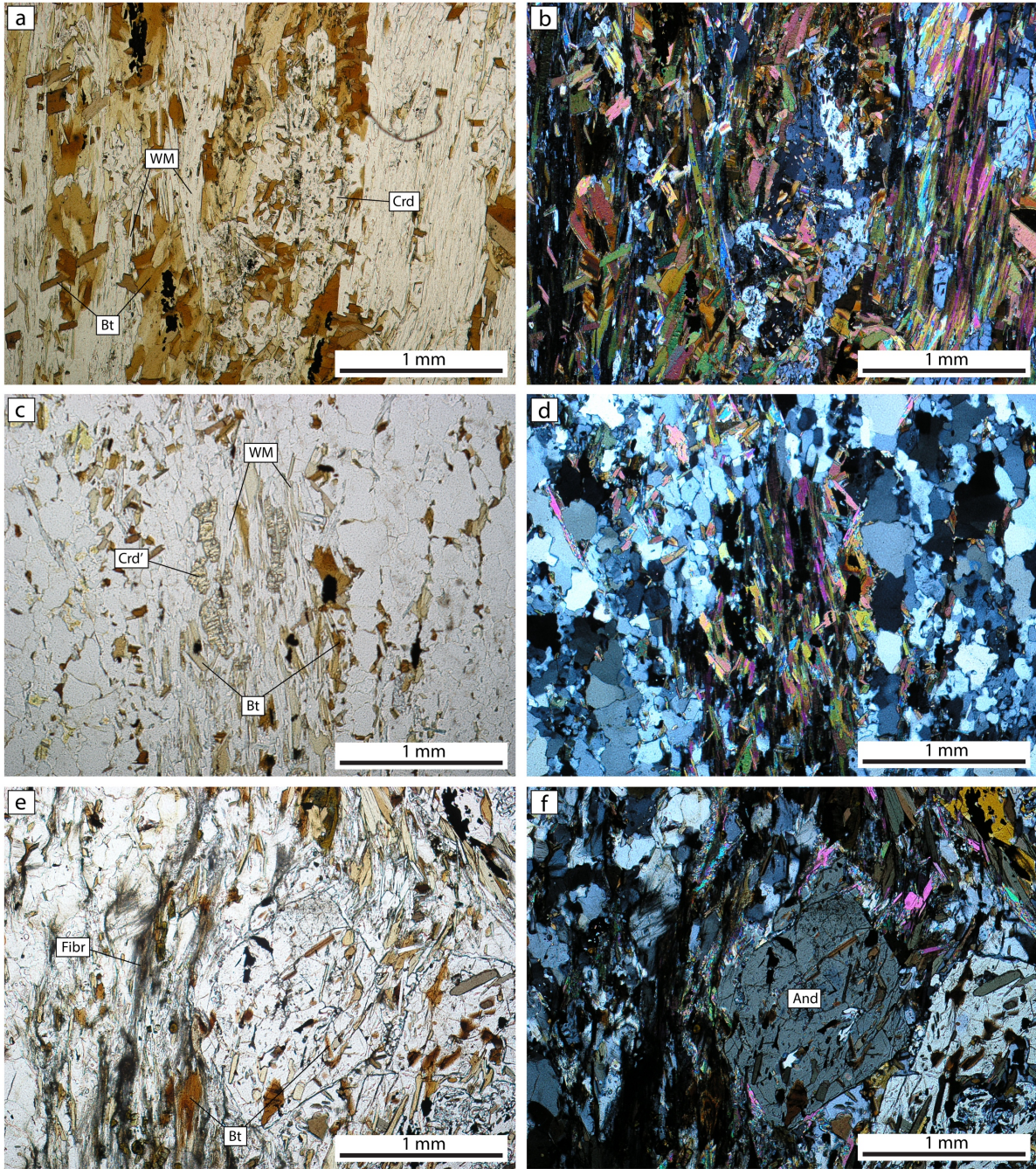


Figure 3 : Plane and cross polarized light photomicrograph of samples from the cordierite-muscovite-biotite zone, 09DF096 (a, b) and 09DF097 (c, d), and from the partial melting zone, 09DF042 (e, f). a) Photomicrograph showing elongated cordierite and white micas defining a pervasive foliation. Newly grown biotites are randomly oriented. b) Photomicrograph in cross polarized light of a). c) Photomicrograph showing typical pinitization of cordierite. d) Cross polarized light photomicrograph of c) showing the appearance of the gneissic sample, with large amounts of quartz-feldspar-rich layers; e) Photomicrograph of fibrolite that grows in the matrix together with biotite. e) Cross polarized light photomicrograph of e) showing andalusite porphyroblast with inclusion of biotite and quartz. WM: white mica, Bt: biotite, Crd: cordierite, Crd': altered cordierite (pinitized), And: andalusite, Fibr: fibrolite.

#### 5.4.2 *X-ray maps of F and Cl*

WDS X-ray maps along with quantitative analysis were acquired for the sample 09DF067 to compare the biotites in inclusion in andalusite with biotites in the matrix. The biotites inside andalusite are homogeneous in both Cl and F (figure 4); no variations are discernable at the precision of the images. Biotites in the matrix show an enrichment of Cl along major cleavages, and Cl accumulation along grain boundaries (figure 5c and d). Fluorine maps are very homogeneous and show no visible variations in the matrix (figure 5e and f). The accumulation of Cl at the grain boundary could be the result of exsolution of chlorine during retrograde metamorphism, desiccation of residual fluids trapped on grain boundaries (Markl and Bucher, 1998) or late stage brine infiltration. In the two later cases, only a very local enrichment is manifested, and no exchange with the biotite is apparent. If Cl exsolved from the crystal lattice, it requires a fast diffusion, which would allow the biotite to exchange completely to eliminate any retrograde zonation. To discriminate between the different hypotheses, we analyzed the F and Cl composition of biotites included in the andalusite and the adjacent matrix using high precision SIMS analyses, since the concentrations were too small to accurately analyze the biotites with electron microprobe.

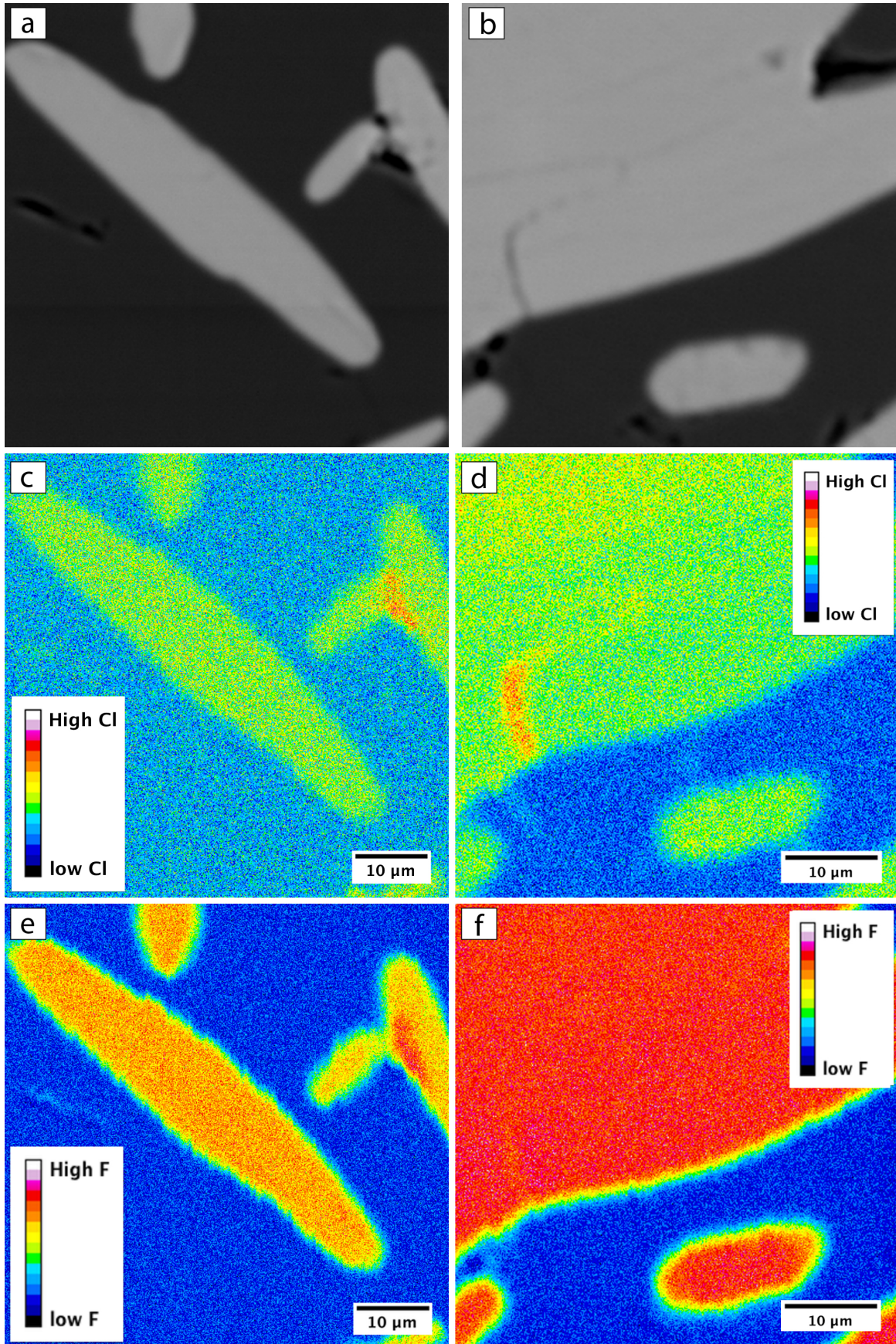


Figure 4 : BSE images showing the texture of two biotite crystals included in andalusite for sample 09DF067 (a and b). WDS X-ray maps of Cl (c and d) and F (e and f) for the same biotite shown the BSE images.

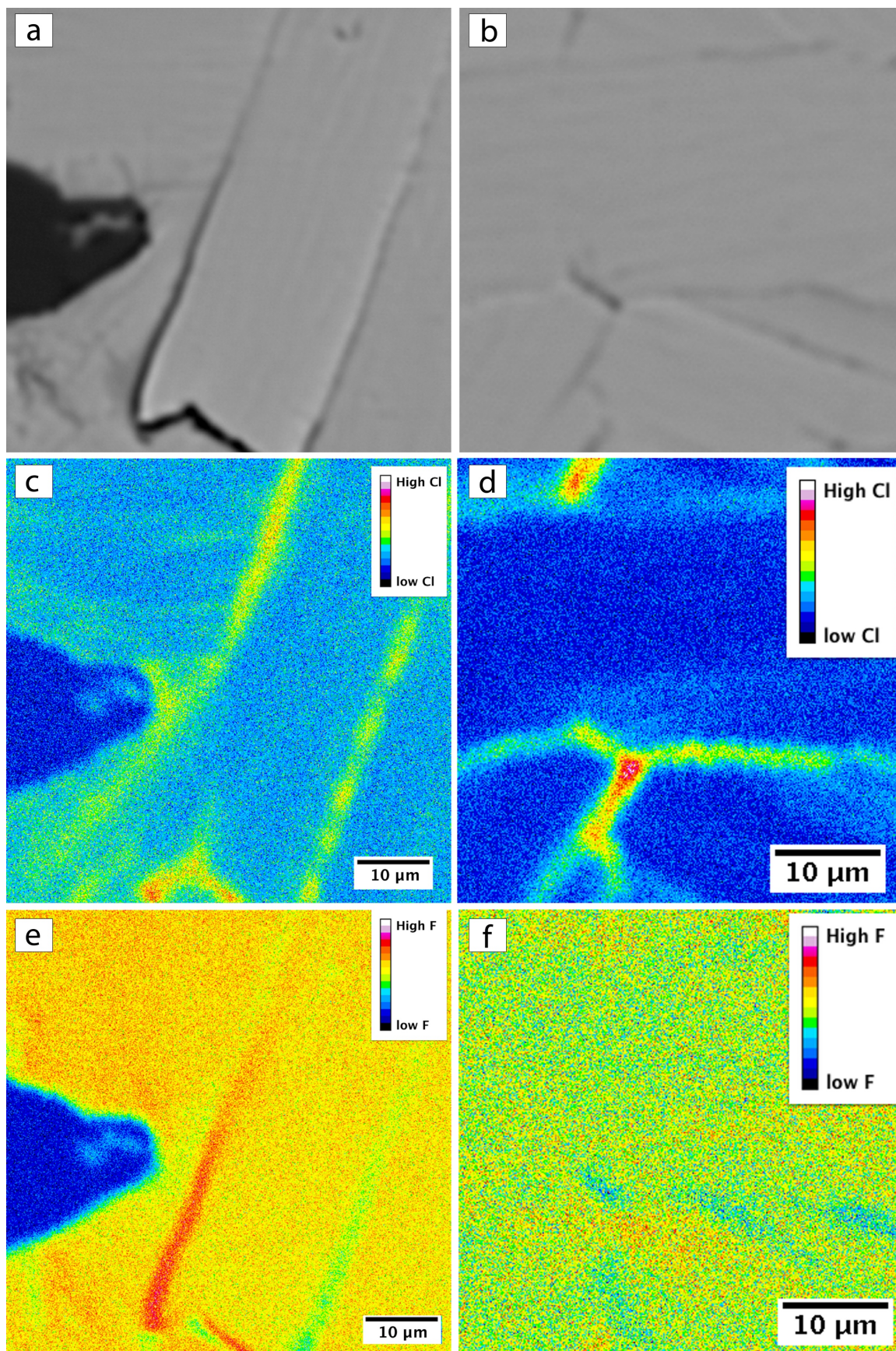


Figure 5 : BSE images showing the texture of the two biotite in the matrix inside andalusite for sample 09DF067 (a and b). WDS X-ray maps of Cl (c and d) and F (e and f) for the same biotite crystals than the BSE images.

### 5.4.3 $H_2O$ , F and Cl content of biotite by SIMS analysis

The small uncertainty of SIMS analyses allows to compare quantitatively the very low F and Cl content of texturally different biotites. For this session, analytical precision for  $H_2O$ , F and Cl content were better than 0.06 wt%, 50 ppm and 5 ppm respectively.  $H_2O$ , F and Cl content as long as respective variations for all samples are summarized in table 3.

Sample 09DF067 has Cl contents of biotite in inclusion between 145 and 155 ppm (white dots, figure 6a), whereas biotite in the matrix range from 140 to 290 ppm (blue dots, figure 6a). Sample 09DF042 has Cl content variations between 390 and 400 ppm for biotites in inclusion (white diamonds, figure 6a) and between 285 and 370 ppm for biotite in the matrix (red diamonds, figure 6a). The larger variability of the Cl content of biotite in the matrix for sample 09DF067 is likely only due sample bias due to the population size differences (e.g. 16 analyses in the matrix, 4 analyses in andalusite). The variations of inclusion composition and matrix biotite in sample 09DF042 are the same, even though the number of points were 5 in the inclusions and 22 in the matrix. In both cases, there is no correlation with  $X_{Mg}$  that would support the Mg-Cl avoidance rule. Indeed, it had been suggested that iron-rich biotites have higher chlorine content than Mg-rich ones, assuming equivalent  $HCl^{\circ}$  activity in the fluid (Munoz 1984). The Cl content is the same for biotite in inclusion and in the matrix. Hence this excludes significant Cl-loss during retrograde metamorphism in matrix biotites.

Fluorine content shows a similar behavior. Sample 09DF067 has variations for F content between 1400 and 1500 ppm for biotite in the inclusions (white dots, figure 6b) and between 1450 and 1700 ppm for biotite in the matrix (blue dots, figure 6b). Sample 09DF042 shows variations between 1700 and 1800 ppm for biotite in inclusion (white diamonds, figure 6b) and between 1700 and 2050 ppm for biotite in the matrix (red diamonds, figure 6b). In this case, the variations for F content in inclusion are smaller than that in the matrix for both samples. Nevertheless, the absolute value for F content does not show a clear trend, which leads again

to the conclusion that F content is not affected by retrograde alteration and does represent prograde or peak values. The differences in the spread is most likely again due to the difference in the number of grains analyzed.

The H<sub>2</sub>O content of biotite does not vary between the matrix and the inclusion biotites. Sample 09DF067 has variations for H<sub>2</sub>O content between 3.40 and 3.71 wt% for biotites in inclusion (white dots, figure 6c) and between 3.31 and 3.98 wt% for biotite in the matrix (blue dots, figure 6c). Sample 09DF042 shows variations between 3.67 and 3.91 wt% for biotites included in andalusite (white diamonds, figure 6c) and between 3.37 and 4.13 wt% for biotites in the matrix (red diamonds, figure 6c). As is the case for F content in biotite, the variations for H<sub>2</sub>O content in included biotite are smaller (0.14 and 0.10 wt%, 1SD, respectively) than for biotites in the matrix (0.20 and 0.22 wt%, 1SD, respectively) for both samples. The H<sub>2</sub>O content for included biotites plot in the middle of the cloud of the H<sub>2</sub>O content of biotites from the matrix for both samples. Hence the water content of biotites does not indicate any water loss or gain post entrapment.

The absence of differences for H<sub>2</sub>O, F and Cl content in biotite between biotite in inclusion in andalusite and in the matrix clearly shows that biotite does not easily adjust its O(4) site composition. It maintains the composition when it crystallized, and hence is not significantly reset during cooling. This is apparently also the case when the sample is infiltrated by fluids during retrograde evolution. Sample 09DF042 has K-feldspar replacement by quartz-muscovite intergrowth documenting some fluid infiltration. Hence diffusive exchange of Cl, F, and H<sub>2</sub>O is slow enough, that they do not re-equilibrate during contact metamorphic time scales.

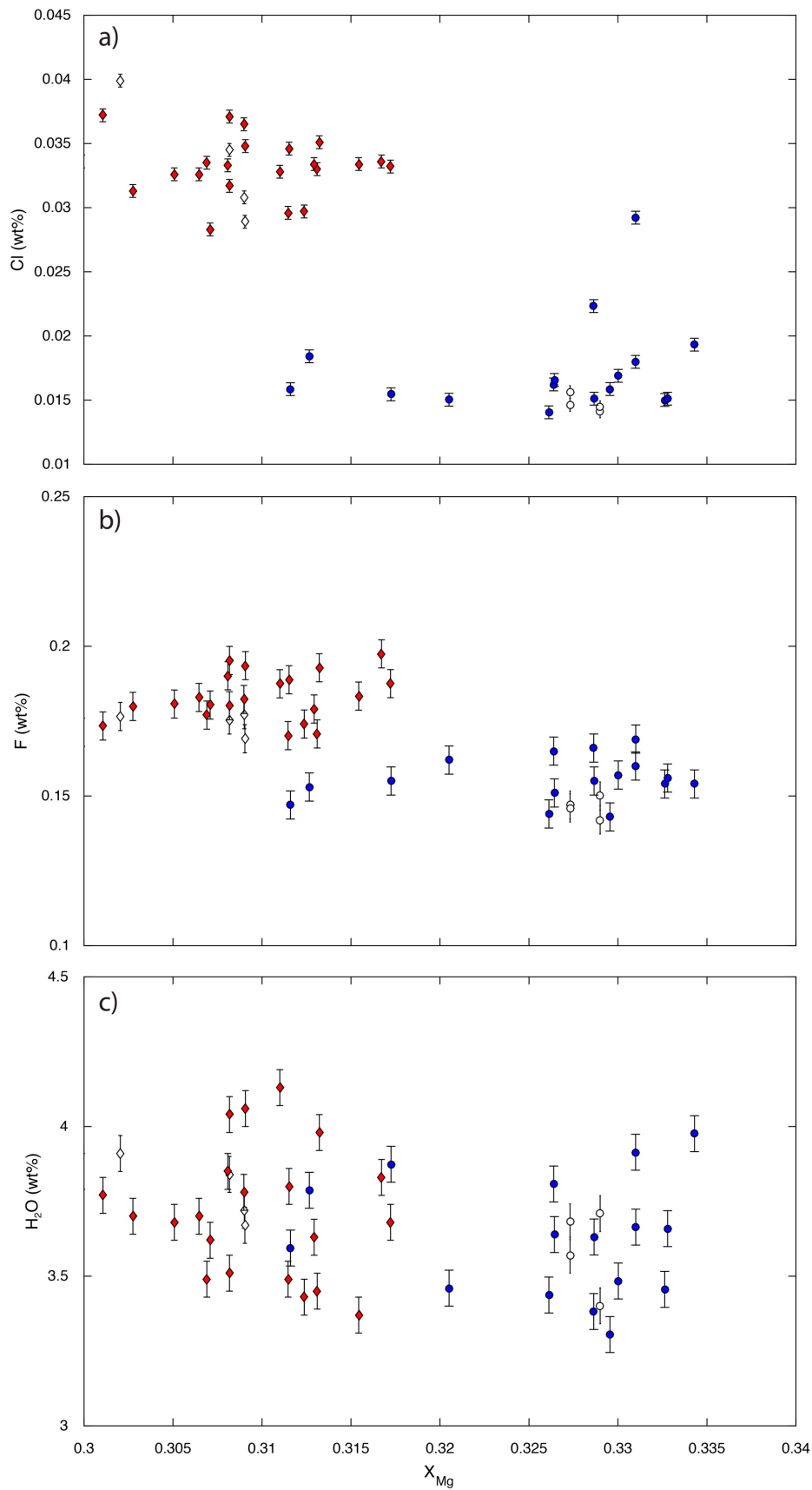


Figure 6 : Comparison SIMS analyses of a) OH, b) F, c) Cl content of biotite in inclusion in andalusite (white symbols) and in the matrix for sample 09DF067 (blue dots) and 09DF042 (red diamonds). See text for further discussion.

	09DF032	1SD	09DF067	1SD	09DF042	1SD	09DF097	1SD	09DF096	1SD
SiO <sub>2</sub>	37.37	(0.46)	34.79	(0.29)	35.00	(0.21)	36.06	(0.26)	36.33	(0.34)
Al <sub>2</sub> O <sub>3</sub>	18.25	(0.44)	19.74	(0.28)	19.55	(0.31)	19.47	(0.18)	19.72	(0.29)
TiO <sub>2</sub>	1.56	(0.14)	1.81	(0.11)	3.23	(0.17)	3.06	(0.12)	2.66	(0.14)
FeO	19.05	(0.35)	24.17	(0.55)	23.33	(0.34)	18.44	(0.21)	18.22	(0.29)
MgO	10.62	(0.22)	6.57	(0.12)	5.86	(0.16)	9.36	(0.18)	9.96	(0.14)
MnO	0.18	(0.02)	0.17	(0.02)	0.43	(0.03)	0.34	(0.03)	0.20	(0.02)
CaO	0.01	(0.01)	0.01	(0.01)	0.01	(0.01)	0.01	(0.01)	0.01	(0.01)
Na <sub>2</sub> O	0.17	(0.02)	0.30	(0.1)	0.17	(0.02)	0.17	(0.02)	0.23	(0.03)
K <sub>2</sub> O	9.23	(0.17)	8.71	(0.16)	9.42	(0.11)	9.29	(0.21)	9.16	(0.18)
H <sub>2</sub> O <sup>a</sup>	3.83	(0.11)	3.61	(0.2)	3.74	(0.2)	3.60	(0.15)	3.44	(0.07)
F <sup>a</sup>	0.16	(0.01)	0.15	(0.01)	0.18	(0.01)	0.13	(0.01)	0.16	(0)
Cl <sup>a</sup>	0.03	(0.01)	0.02	(0)	0.03	(0)	0.02	(0)	0.05	(0)
O = F	-0.06	(0)	-0.06	(0)	-0.08	(0)	-0.05	(0)	-0.07	(0)
Total	100.38	(0.34)	99.98	(0.45)	100.87	(0.51)	99.89	(0.5)	100.07	(0.83)
Altot	3.214	(0.082)	3.585	(0.041)	3.515	(0.051)	3.458	(0.033)	3.488	(0.046)
Si	5.583	(0.056)	5.364	(0.034)	5.339	(0.029)	5.435	(0.03)	5.452	(0.027)
Al <sup>iv</sup> <sup>b</sup>	2.417	(0.056)	2.636	(0.034)	2.661	(0.029)	2.565	(0.03)	2.548	(0.027)
Sum	8.000	(0)	8.000	(0)	8.000	(0)	8.000	(0)	8.000	(0)
Al <sup>vi</sup> <sup>c</sup>	0.798	(0.041)	0.949	(0.064)	0.855	(0.06)	0.894	(0.05)	0.940	(0.026)
Fe	2.380	(0.05)	3.116	(0.082)	2.976	(0.047)	2.324	(0.03)	2.286	(0.028)
Mg	2.365	(0.044)	1.509	(0.025)	1.332	(0.035)	2.103	(0.039)	2.229	(0.034)
Mn	0.023	(0.002)	0.022	(0.002)	0.056	(0.003)	0.043	(0.003)	0.026	(0.002)
Ti	0.175	(0.015)	0.210	(0.013)	0.371	(0.02)	0.346	(0.014)	0.301	(0.015)
Sum	5.741	(0.046)	5.806	(0.064)	5.589	(0.066)	5.710	(0.044)	5.781	(0.037)
K	1.759	(0.036)	1.714	(0.03)	1.833	(0.024)	1.787	(0.04)	1.753	(0.027)
Na	0.025	(0.003)	0.045	(0.014)	0.025	(0.003)	0.025	(0.003)	0.034	(0.004)
Ca	0.001	(0.001)	0.001	(0.002)	0.001	(0.001)	0.002	(0.002)	0.002	(0.001)
Sum	1.786	(0.036)	1.760	(0.028)	1.859	(0.023)	1.815	(0.04)	1.788	(0.027)
OH	3.812	(0.102)	3.715	(0.186)	3.803	(0.19)	3.585	(0.153)	3.440	(0.079)
F	0.074	(0.011)	0.062	(0.014)	0.090	(0.013)	0.060	(0.009)	0.077	(0.019)
Cl	0.007	(0.003)	0.005	(0.002)	0.008	(0.002)	0.005	(0.002)	0.013	(0.001)
Sum	3.893	(0.103)	3.782	(0.186)	3.901	(0.187)	3.651	(0.156)	3.530	(0.081)
X <sub>Mg</sub>	0.498	(0.008)	0.326	(0.007)	0.309	(0.005)	0.475	(0.005)	0.494	(0.006)

Table 1: biotite average compositions for the 5 samples analyzed, <sup>a</sup> is from SIMS analyses, <sup>b</sup> Al<sup>iv</sup> is calculate as follow: Al<sup>tot</sup> if Al<sup>tot</sup> + Si < 8 if not 8-Si, <sup>c</sup> Al<sup>vi</sup> is calculate as follow: Al<sup>tot</sup> - Al<sup>iv</sup>

#### 5.4.4 Variations of Cl and F content

It is interesting to note that the Cl content for all samples does not correlate inversely with X<sub>Mg</sub> (figure 7a) nor does it correlate with tetrahedral Al (figure 7b). Each sample has a quite homogeneous chemical composition (0.005-0.008 (1SD) for X<sub>Mg</sub>, 0.027-0.056 (1SD) for Al<sup>iv</sup>, see table 1). Nevertheless, the changes between samples are much larger, thus a correlation with these compositional variables should be visible and this was expected based on previous work

by Henry et al. (submitted). The correlations were observed in biotite containing up to more than 2wt% of Cl. In contrast the biotite crystals of the Adamello contact aureole contain less than 0.05wt%. The crystallographic control exerted is due to deformation of the crystal lattice around the large Cl<sup>-</sup> ion. For example, including Cl<sup>-</sup> is favored in connection with an Fe<sup>2+</sup> on the octahedral site. At the trace concentrations measured here, chlorine could easily be linked to the abundant Fe<sup>2+</sup> on octahedral sites, without significantly influencing the energetics of the other cations. Hence, we suggest that the absence of any correlation with biotite major element concentration is due to coupling Cl<sup>-</sup> with Fe<sup>+</sup> and as long as the Fe-concentration is significantly higher than the Cl-concentration there will be no noticeable crystal chemical effect. This is in good agreement with the observation of a threshold composition in Cl below which no correlation has been observed with X<sub>Mg</sub> and Al<sup>IV</sup> (Henry et al., submitted).

Table 2: variations for H<sub>2</sub>O, Cl and F content in biotite for the 5 samples described in the text

	<i>n</i>	H <sub>2</sub> O (wt%)	1SD (wt%)	variations (wt%)	F (wt%)	1SD (wt%)	variations (wt%)	Cl (wt%)	1SD (wt%)	variations (wt%)
09DF032	27	3.83	0.11	0.44	0.156	0.009	0.040	0.0288	0.0081	0.0291
09DF067	20	3.62	0.19	0.67	0.154	0.008	0.027	0.0169	0.0035	0.0152
matrix	16	3.63	0.20	0.67	0.156	0.007	0.026	0.0333	0.0023	0.0089
inclusions	4	3.59	0.14	0.31	0.146	0.003	0.008	0.0335	0.0042	0.0110
09DF096	15	3.44	0.07	0.21	0.158	0.004	0.014	0.0483	0.0020	0.0074
09DF097	12	3.60	0.15	0.46	0.129	0.005	0.018	0.0228	0.0026	0.0079
09DF042	27	3.74	0.20	0.76	0.182	0.009	0.036	0.0333	0.0026	0.0116
matrix	22	3.72	0.22	0.76	0.184	0.009	0.035	0.0174	0.0038	0.0152
inclusions	5	3.80	0.10	0.24	0.174	0.004	0.008	0.0147	0.0007	0.0015

There is no dependence of chlorine concentration in biotite as a function of temperature neither. Indeed, Cl concentrations seems to be dependent on the individual sample (figure 7c). The Cl content varies from 140 ppm to 525 ppm. The absence of a trend of Cl-concentrations with increasing temperature is indeed surprising: since chlorine partitions strongly into the fluid phase we expected that chlorine is progressively lost due to dehydration reactions. A Rayleigh

fractionation trend was expected, similar to other incompatible elements. In contrast, we found that the absolute value of the Cl content in biotite is strongly dependent on the sample bulk chemistry rather than a function of the temperature. This kind of behavior is to be expected of biotite indeed obtains its composition upon crystallization, and any further exchange is prevented by the slow exchange kinetics, as suggested by the comparison between the composition of inclusions and matrix biotite.

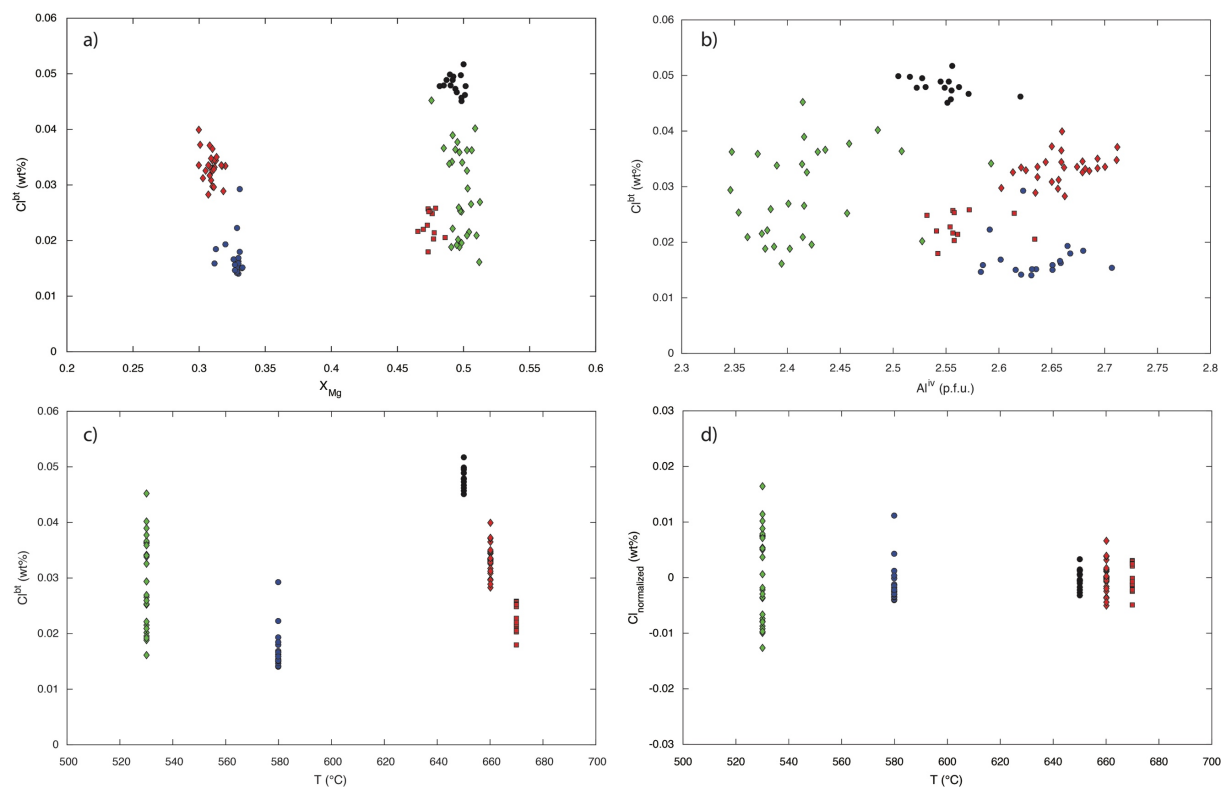


Figure 7 : Cl content for samples 09DF032 (green diamonds), 09DF067 (blue dots), 09DF096 (black dots), 09DF042 (red diamonds) and 09DF097 (red squares) vs  $X_{Mg}$  (a), tetrahedral aluminum (b) and temperature (c). d) Normalized Cl content (difference between measured Cl content and sample mean) vs temperature.

Chlorine content for the two samples from lower grade (09DF032 and 09DF067) show significantly higher absolute variations (i.e. 291 and 152 ppm, respectively) than those from higher grade samples (between 76 and 116 ppm). This homogenization trend with increasing temperature is clearly visible when Cl content in biotite is normalized to the mean of the Cl contents for each sample (figure 7a). Generally, the variation decreases with metamorphic

grade, with the exception of sample 09DF042, which has a slightly higher variation (116 ppm) compare to the two other high grade samples 09DF096 and 09DF097 (74 and 79 ppm respectively). The number of analyses in the sample 09DF042 is significantly higher than for samples 09DF096 and 09DF097 (27 analyses compare to 15 and 12, respectively) and hence this might be due to increased sample size.

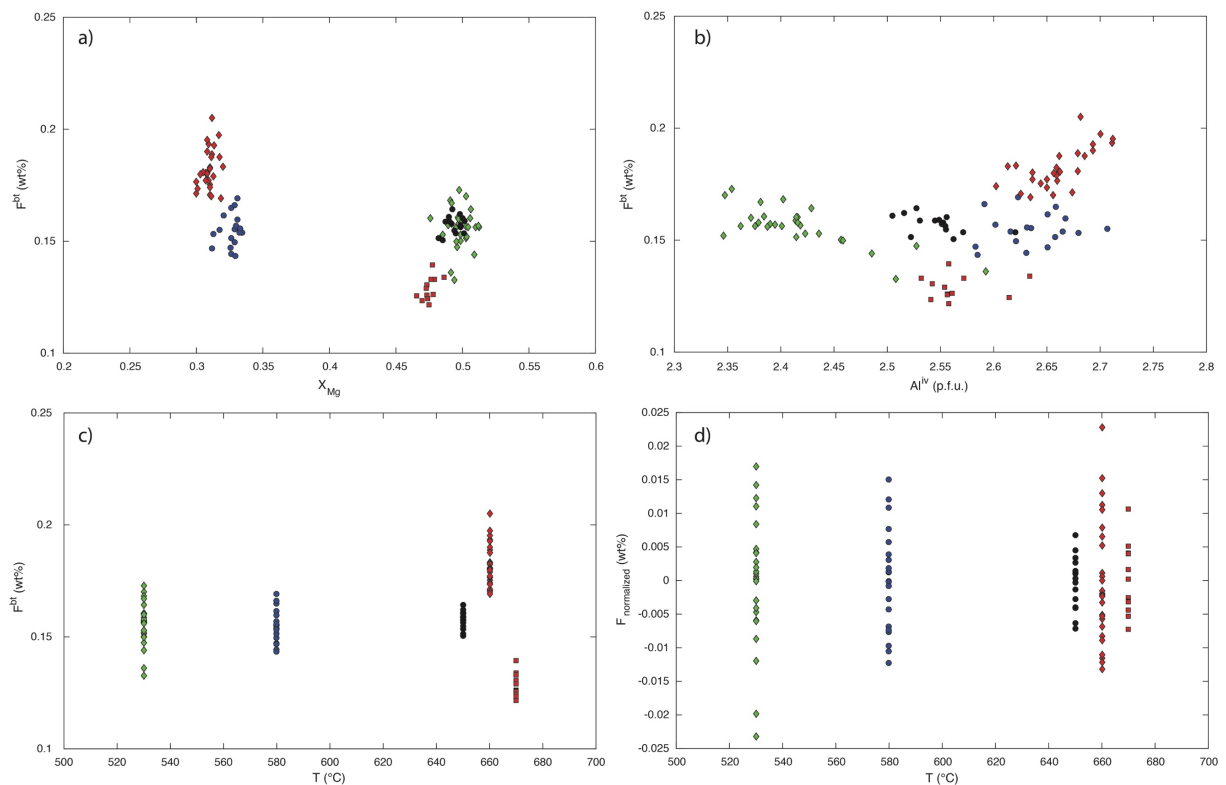


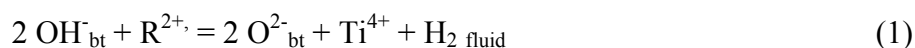
Figure 8 : F content for samples 09DF032 (green diamonds), 09DF067 (blue dots), 09DF096 (black dots), 09DF042 (red diamonds) and 09DF097 (red squares) vs  $X_{Mg}$  (a), tetrahedral Al (b) and temperature (c). d) Normalized F content (difference between measured F content and sample mean) vs temperature.

The F content does not show any correlation with  $X_{Mg}$  (figure 8a) or tetrahedral Al (figure 8b) for the biotites of the Western Adamello contact aureole. This absence of crystallographic control for F content is in good agreement with the similar behavior of the Cl content, and we would argue that again this is due to the small concentrations of fluorine measured. Again, there is no temperature trend visible (figure 8c) and the absolute value varies from sample to sample most likely only due to bulk chemistry. The variability of the fluorine content in biotite is

similar for all metamorphic grades (figure 8d). It varies for 150 to 400 ppm. The lower value for the sample 09DF096 is likely due to the small number of analyses, i.e. only 15 biotite analysis were obtained. Fluorine is also refractory on the O(4) site in biotites during contact metamorphism.

#### 5.4.5 Substitution for OH content

The F-OH and Cl-OH exchanges maintain the charge balance on the hydroxyl site. As noted above these two exchanges can be influenced by other cations in the structure of biotite due to crystal lattice distortion. Additional exchange vectors have been proposed for the O(4) site. These are charge-balance based exchanges due to the incorporation of tri- or quadri-valent cations into the octahedral site, replacing bi-valent cations such as Fe or Mg (Dyar et al. 1993, Cesare et al. 2003, 2008). These substitutions lead to an increase of  $O^{2-}$  in the O(4) site, replacing monovalent  $OH^-$  by bi-valent  $O^{2-}$ . An example is the well-known Ti-oxy substitution:



This and similar reactions have been referred to as deprotonation reactions, or oxy-substitutions. Their presence can be inferred from linear correlations between tri- or quadri-valent exchanges and the measured occupancy of the O(4) site by  $F^-$ ,  $Cl^-$ , and  $OH^-$ . In the case of the samples from the Western Adamello contact aureole, the sum of monovalent anions in the O(4) site (p.f.u.) does not show any systematic relation with the Ti content (p.f.u.), as can be seen on figure 9. Note that the sample with the highest Ti content (09DF042) has a sum of monovalent anions ( $OH^- + F^- + Cl^-$ ) closest to 4, e.g. 3.90. This indicates that reaction (1) is not responsible for the Ti, or for that matter, decrease in sum of halogens plus hydrogen in the other samples. The aluminum cation can also enter the octahedral sites as  $Al^{3+}$ . The ( $OH^- + F^- + Cl^-$ )

content of biotites of the Western Adamello contact aureole is clearly not a function of  $Al^{3+}$  either. For the 5 selected samples the  $Al^{tot}$  (p.f.u.) of biotites has no influence on the non-stoichiometry of the hydroxyl site (figure 9b). Only  $Al^{3+,vi}$  potentially participates in an oxy-substitution exchange. We calculated biotite formulas according to 24 oxygens, to determine  $Al^{3+,vi}$ . Uncertainties for  $Al^{3+,vi}$  are quite large, since it is based on the occupation of the tetrahedral site, containing mainly Si content. Nevertheless, no trend was observed between the  $Al^{vi}$  content average for the 5 samples and the average sum ( $OH^- + F^- + Cl^-$ ).

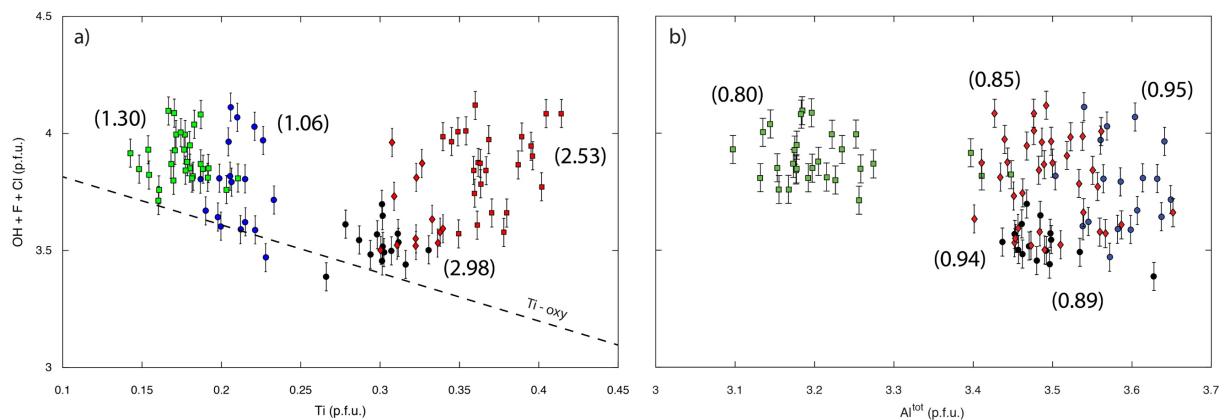


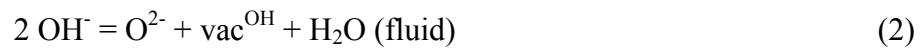
Figure 9: a) Sum of OH, F and Cl content of the hydroxyl site (p.f.u.) vs Ti content (p.f.u.), both normalized to 22 oxygens, for samples 09DF032 (green diamonds), 09DF067 (blue dots), 09DF096 (black dots), 09DF042 (red diamonds) and 09DF097 (red squares). The dashed line represents the titanium oxy-substitution and does not match the variations for the Adamello contact aureole. Samples 09DF032, 09DF067 and 09DF042 are close to full occupancy of this site, whereas most of the biotite of the samples 09DF096 and 09DF097 show significant nonstoichiometry for the hydroxyl site. Numbers in brackets represent  $Fe^{2+}/Fe^{3+}$  ratios for bulk rock chemistry of samples 09DF032 (1.30), 09DF067 (1.06), 09DF042 (2.53) and 09DF097 (2.98). b) Sum of OH, F and Cl content vs total Al from EPMA. As for titanium, no correlation is observed. The numbers in brackets are average calculated octahedral aluminum for each sample, symbols for samples are the same than for a).

Another potential cation that could explain the oxy-exchange is  $Fe^{3+}$  on the octahedral site. But it is most unlikely that variations of the  $Fe^{2+}/Fe^{3+}$  of biotites from the Western Adamello contact aureole could be the explanation for the variations of the O(4) site stoichiometry since the samples 09DF097 and 09DF042 have a comparable bulk rock  $Fe^{2+}/Fe^{3+}$  (2.98 and 2.53 respectively) and very different sums of monovalent anions (3.651 and 3.901, respectively). On the opposite, the low-grade samples 09DF032 and 09DF067 have high bulk rock  $Fe^{2+}/Fe^{3+}$ , i.e.

1.30 and 1.06 respectively, but the same average ( $\text{OH}^- + \text{F}^- + \text{Cl}^-$ ) content than 09DF042 (3.893 and 3.782, for 09DF032 and 09DF067 respectively).

Based on these observations, it is most unlikely that  $\text{Ti}^{4+}$ ,  $\text{Fe}^{3+}$  or  $\text{Al}^{3+}$  substitutions in biotite could explain the variations of the non-stoichiometry of the O(4) site in the biotites of the Western Adamello contact aureole.

An alternative exchange vector involves the water fugacity of a potential fluid. The reaction can be written as:



Here  $\text{vac}^{\text{OH}}$  refers to vacancy in the O(4) site of biotite. This exchange can operate in the condition of absence of an actual fluid phase, and will depend on the water fugacity on the grain boundaries. It is impossible to estimate water fugacity in these rocks independently, but we can evaluate the presence or potential absence of a fluid phase for these samples by considering the reactions occurring during biotite formation. The 3 samples that have the highest  $\text{H}_2\text{O}$  content with nearly filled O(4) sites (09DF032, 09DF067 and 09DF042) are all the result of dehydration reactions. The newly grown biotite of 09DF032 are from chlorite breakdown reaction that produced a significant amount of fluid, while 09DF067 has biotite formed by the reaction:



And finally, the biotites from the sample 09DF042 are recrystallizing during the muscovite breakdown reaction. On the other hand, the two samples with low  $\text{H}_2\text{O}$  content (09DF096 and 09DF097) are recrystallized biotites at the high temperature side of a big divariant field (Ms-

Crd-Bt-Qtz in KFMASH). The production of water at these conditions was very small and the equilibration of F-Cl-OH is likely to occur at water under-saturated conditions ( $a_{\text{H}_2\text{O}} < 1$ ).

**Table 3: positions, estimated temperatures, assemblages of the 5 studied samples**

Samples	Distance to the intrusion (m)	Estimated T (°C)	Mineral assemblage
09DF032	1000	530	WM + Bt + Qtz ± Pl
09DF067	2000	580	Ms + Bt + And + Grt + Crd + Qtz ± Pl
09DF096	400	650	Ms + Bt + Crd + Qtz ± Pl ± Grt
09DF097	350	660	Ms + Bt + Crd + Qtz ± Pl ± Grt
09DF042	350	670	Kfs + Bt + And + Sil + Qtz + Grt ± Pl

## 5.5 Discussion

The case of the WAT contact metamorphic samples is a definite test for chlorine behavior during metamorphism. The collected samples are from several different metamorphic zones, had a similar protolith, and were produced by different dehydration reactions. Most of them produced significant fluid amounts. Our data clearly shows that chlorine does not follow a Rayleigh fractionation trend. In fact, chlorine varies from sample to sample indiscriminately of the amount of fluid produced, and it seems more dependent on whole rock initial composition. The observation of larger chlorine variations in the lower grade samples suggests that chlorine is progressively homogenized during high grade metamorphism, most likely only by local exchanging between grains. The scale of biotite equilibration recorded by chlorine during prograde reaction is probably similar to that for cations like Al and Ti. Since chlorine is definitively more soluble in fluids than the above tri- and quarto-valent cations it is likely that prograde reactions occur in localized reaction domains, quite isolated from each other in time.

Similar reaction mechanisms were proposed by Skora et al., 2011, to explain the observed behavior of oxygen isotopes during wollastonite formation. They argued that the oxygen isotope mass balance requires a local re-equilibration between the products, without equilibration of the reactants, based on stoichiometry.

The local equilibration on a sub-thin section scale resulted in a large heterogeneity both at the thin section and at the contact aureole scale, compare to a single sedimentary layer that equilibrate with the same saline pore fluid. The progressive homogenization of Cl content in biotite is the result of the increase of equilibration at the thin section scale and continuous recrystallization of the biotites. This is in good agreement with other petrologic arguments, such as the progressive recrystallization and new growth of garnet or the recrystallization of micas. A slow diffusion kinetics of Cl is in good agreement with the high Cl at the grain boundary from X-ray maps. Indeed, chlorine from late stage fluids or desiccation of the initial fluid along the grain boundaries did not enter the bulk biotite crystal. This in agreement with the observations for amphiboles by Markl and Bucher (1998). They found that chlorine equilibration was limited to the last formed amphibole crystals, despite the fact that they reached salt saturation (e.g. their Fig. 2) earlier crystals only show small amounts of chlorine. The chlorine content of biotite represents the available chlorine budget during growth of the biotite grain or during its recrystallization. The local chlorine content is probably the result from local, partial retrogression of the Variscan metamorphic assemblages found in these rocks. This resulted in a heterogeneous protolith with respect to chlorine concentrations. The chlorine concentration in biotite will change only if a fluid with a different salinity infiltrates and recrystallizes the biotites.

In general, fluorine content of biotites show the same behavior. There is no trend with increasing metamorphic grade visible in the contact aureole. Nevertheless, fluorine does not have the same homogenization trend as chlorine with increasing metamorphism. Fluorine

possibly re-equilibrates faster than chlorine. These different behaviors can be explained by the difference in radius for these two anions,  $F^-$  being significantly easier to exchange with  $OH^-$  due to their similar effective ionic radii (1.33 and 1.38 Ångström, respectively), compare to the large  $Cl^-$  (1.81 Ångström).

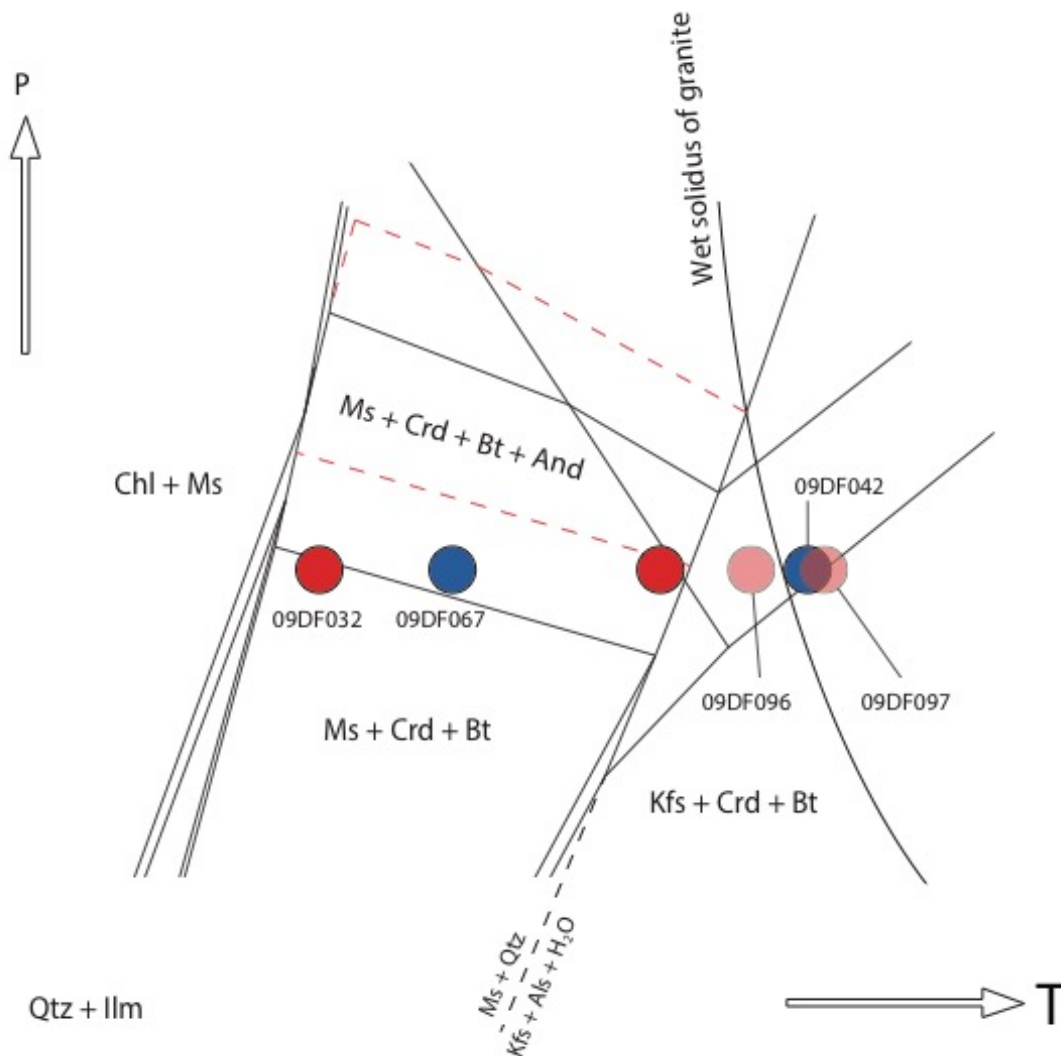


Figure 10: Schematic low pressure P-T phase diagram for typical metapelite composition (in black), representative of the bulk rock composition for samples 09DF067 and 09DF042 (blue circles), very close from samples from Siron et al. (in prep.), using the thermodynamic database from Pattison and Debuhr (2015). Red dotted lines represent the position of the field Ms + Crd + Bt + And for rocks of higher  $X_{Mg}$  such as 09DF032, 09DF096 and 09DF097 (red circles). The red circle without name represent the position of the samples 09DF096 and 09DF097 inferred from mineral assemblage, nevertheless their distances from the intrusion are in contradiction with this temperature. Thus, transparent red dots represent their supposed temperatures as inferred from their distance to the intrusion and temperatures calculated using the geothermometer Ti-in biotite. Mineral abbreviations from Kretz 1983.

The absence of any correlation between the Fe-Mg concentrations on the octahedral site and the O(4) site F-Cl composition is in apparent contradiction with the observation of Mg-Cl and Fe-F avoidance for many hydrous minerals including biotite (Rosenberg and Foit 1977, Munoz and Ludington 1974, Munoz 1984). A possible explanation of this difference is that the authors observed these trends in biotites with much higher fluorine and chlorine contents. Indeed, the low Cl and F contents for biotites of the Western Adamello contact aureole might explain the absence of a crystallographic control on the hydroxyl site composition. Both Cl and F have sufficiently low concentration in comparison to both Fe and Mg, respectively, that lattice scale variations can easily accommodate the trace concentrations of the halogens. Fluorine could preferentially occupy O(4) sites close to Mg-rich octahedral sites, while chlorine could clump with iron. Hence the “avoidance rules” might only be operative at very high halogen concentrations, close to maximum Cl and F values as observed by Henry et al. (submitted).

The recrystallization of biotites at higher temperature can occur even in the absence of new net transfer reactions. This is suggested by the fact that Ti in biotite increases with increasing temperature for the selected samples, in agreement with the work of Henry et al. (2005). Biotite from 09DF096 and 09DF097 have equilibrated under peak conditions since the Ti-in biotite geothermometer (Henry et al. 2005) gives average temperature of 660 and 680 °C, respectively, in agreement with thermal and thermodynamic modelling reported in Floess and Baumgartner, 2015. At these temperatures, muscovite and quartz should have reacted to form K-feldspar and sillimanite at the estimated pressure of 2.5 kbar for the Western Adamello contact aureole, (light red dots, figure 10), unless the absence of a free fluid phase did not allow for the destruction of the reactants, especially muscovite, and transport of nutrients to nucleate and grow new product phases. The low ( $\text{OH}^- + \text{F}^- + \text{Cl}^-$ ) sum would then be the result of the recrystallization of biotites under fluid under-saturated conditions. The average Ti-in biotite temperature for the sample 09DF042 is 670°C, in good agreement with both the presence of K-feldspar and sillimanite and

the thermal model for the Western Adamello published recently (Floess and Baumgartner 2015).

## 5.6 Conclusion

We have shown that OH-F-Cl content in biotite behaves refractively during contact metamorphism. It mostly locks in the chemical activities of these species at the time at which the biotites last recrystallized, hence typically prograde or peak fluid compositions. They are not reset during cooling. Chlorine in particular has a very slow exchange kinetics and is not exchange with increasing grade during metamorphism unless biotite recrystallized due to fluid infiltration or metamorphic reactions. The Cl content of biotite is a strong function of the bulk rock chlorine budget. It reflects the availability of chlorine close to the growing biotite at low grade. In the case of the Western Adamello contact aureole biotite recrystallizes locally reducing progressively the initial large variations shown for the low grade samples. Initial equilibration is at best restricted to grain scale, as manifested by the large variability of chlorine on the thin section scale.

Fluorine does not show the same high variations for low grade samples, but even if it seems to exchange more easily than chlorine, it also requires recrystallization to change the prograde absolute value.

In conclusion, both chlorine and fluorine do not show any Rayleigh fractionation, in contrast to what should be expected and assume for incompatible elements.

Variations of OH<sup>-</sup> content of the biotites depends on the water fugacity in the sample during biotite (re) crystallization. We did not find any trends with octahedral incorporation of highly charged cations (Ti<sup>4+</sup>, Fe<sup>3+</sup> or Al<sup>3+</sup>). In the case of the Western Adamello contact aureole, the OH content seems to be a function of the presence or absence of a free fluid phase, allowing

the composition of the O(4) site to be used as a geohygrometer to monitor change of water activity during metamorphism.

## 5.7 References

- Armstrong, J. T. (1989) CITZAF : Combined ZAF and Phi-Rho (Z) Electron Beam Correction Program, California Institute of Technology, Pasadena, CA.
- Bianchi, A., Callegari, E., & Jobstraibizer, P. (1970). I tipi petrografici fondamentali del plutone dell'Adamello. *Mem Ist Geol Min Univ Padova* 27, 1–189.
- Callegari, E., & Brack, P. (2002). Geological Map of the Tertiary Adamello Batholith (Northern Italy) - Explanatory Notes and Legend. *Mem Sci Geol*, 54, 19–49.
- Cesare, B., Cruciani, G., & Russo, U. (2003). Hydrogen deficiency in Ti-rich biotite from anatectic metapelites (El Joyazo, SE Spain): Crystal-chemical aspects and implications for high-temperature petrogenesis. *American Mineralogist*, 88, 583–595.
- Cesare, B., Satish-Kumar, M., Cruciani, G., Pocker, S., & Nodari, L. (2008). Mineral chemistry of Ti-rich biotite from pegmatite and metapelitic granulites of the Kerala Khondalite Belt (southeast India): Petrology and further insight into titanium substitutions. *American Mineralogist*, 93(2-3), 327–338.
- Diella, V., Spalla, M. I., & Tunesi, A. (1992), Contrasting thermomechanical evolutions in the Southalpine metamorphic basement of the Orobic Alps (Central Alps, Italy). *Journal of Metamorphic Geology*, 10, 203–219.
- Dyar, D., Guidotti, C. V., Holdaway, M. J., & Colucci, M. (1993). Nonstoichiometric hydrogen contents in common rock-forming hydroxyl silicates. *Geochimica and Cosmochimica Acta*, 57, 2913–2918.
- Floess, D., & Baumgartner, L. (2012). Formation of garnet clusters during polyphase metamorphism. *Terra Nova*, 25(2), 144–150.
- Floess, D., & Baumgartner, L. P. (2015). Constraining magmatic fluxes through thermal modelling of contact metamorphism. *Geological Society, London, Special Publications*, 422(1), 41–56.

- Henry, D. J., & Guidotti, C. V. (2002). Titanium in biotite from metapelitic rocks: Temperature effect, crystal-chemical controls, and petrologic applications. *American Mineralogist*, *87*, 375–382.
- Henry, D. J., Guidotti, C. V., & Thomson, J. A. (2005). The Ti-saturation surface for low-to-medium pressure metapelitic biotites: Implications for geothermometry and Ti-substitution mechanisms. *American Mineralogist*, *90*, 316–328. <http://doi.org/10.2138/am.2005.1498>
- Henry, D.J., & Daigle, N.M. (2017, in review) Chlorine incorporation into amphibole and biotite in high-grade iron formations: interplay among temperature, crystallography and metamorphic fluids. *American Mineralogist*.
- Markl, G., & Bucher, K. (1998). Composition of fluids in the lower crust inferred from metamorphic salt in lower crustal rocks. *Letters to Nature*, 1–3.
- Mottana, A., Nicoletti, M., Petrucciani, C., Liborio, G., De Capitani, L., & Bocchio, R. (1985). Pre-alpine and alpine evolution of the South-alpine basement of the Orobic Alps. *Geologische Rundschau*, *74*, 353–366.
- Munoz, J. L. (1984). F-OH and Cl-OH Exchange in Micas with Applications to Hydrothermal Ore Deposits. *Reviews in Mineralogy and Geochemistry*, *13*, 469–493.
- Rasmussen, K. L., & Mortensen, J. K. (2013). Magmatic petrogenesis and the evolution of (F:Cl:OH) fluid composition in barren and tungsten skarn-associated plutons using apatite and biotite compositions: Case studies from the northern Canadian Cordillera. *Ore Geology Reviews*, *50*(C), 118–142.
- Rosenberg P. E., & Foit, F. F. (1977). Fe<sup>2+</sup>-F avoidance in silicates. *Geochimica et Cosmochimica Acta*, *41*, 345-346.
- Panigrahi, M. K., Naik, R. K., Pandit, D., & Misra, K. C. (2008). Reconstructing physico-chemical parameters of hydrothermal mineralization of copper at the Malanjkhanda deposit, India, from mineral chemistry of biotite, chlorite and epidote. *Geochemical Journal*, *42*, 443–460.
- Pattison, D. R. M., & Tracy, R. J. (1991). Phase equilibria and thermobarometry of metapelites. *Reviews in Mineralogy and Geochemistry*, 1–102.
- Pattison, D. R. M., Spear, F. S., & Cheney, J. T. (1999). Polymetamorphic origin of muscovite + cordierite + staurolite + biotite assemblages: implications for the metapelitic petrogenetic grid and for P–T paths. *Journal of Metamorphic Geology*, *17*, 685–703.

- Skora, S, Baumgartner, L.P. & Vennemann, T (2011). Modelling changes in stable isotope compositions of minerals during net transfer reactions in a contact aureole: Wollastonite growth at the northern Hunter Mountain Batholith (Death Valley National Park, USA). *Chemical Geology* 289, 197-209
- Selverstone, J., & Sharp, Z. D. (2015). Chlorine isotope behavior during prograde metamorphism of sedimentary rocks. *Earth and Planetary Science Letters*, 417(C), 120–131.
- Yardley, B. W. D., & Graham, J. T. (2002). The origins of salinity in metamorphic fluids. *Geofluids*, 249–256.
- Zhu, C., & Sverjensky, D. A. (1991). Partitioning of F-Cl-OH between minerals and hydrothermal fluids. *Geochimica Et Cosmochimica Acta*, 55, 1837–1858.

## 6 Conclusion – Perspectives

## 6.2 Summary

The results presented in this thesis show the slow exchange kinetics between the fluid phase and biotite crystals for OH-F-Cl content of the hydroxyl site in this sheet silicate. The concentrations measured for these elements in biotite correspond to the quantitative values frozen in during growth of the biotite grain or later during recrystallization an exchange with a fluid of different composition is possible. This is especially clear for the Cl content in biotite in the the Western Adamello Tonalite contact aureole: the variation of the absolute values for all samples is quite big (100-600 ppm) without any trend related to increasing metamorphic temperature. The variations in Cl content represent the variable alteration of the samples after the Variscan orogeny. The variations at the thin section scale are also bigger at low grade than at higher grade showing that Cl behaves as any other element with slow kinetics at lower temperature.

The fluorine content of biotite shows a similar behavior: It is a function of the initial fluorine availability during biotite growth. It does not exhibit the same homogenization trend, which is interpreted as a faster kinetics for F-OH exchange, in good agreement with the radius size of the two anions (1.33 and 1.53 Ångström, respectively), compare to the large Cl<sup>-</sup> (1.81 Ångström).

Variations of the H<sub>2</sub>O content in biotite has been traditionally explained by charge balance compensation due to incorporation of highly coordinated cations in the octahedral site (Ti<sup>4+</sup>, Fe<sup>3+</sup>, Al<sup>3+</sup>). Nevertheless, this is not the case in the Adamello contact aureole. Here the variations are explained by change in water activity of the system due to fluid under-saturation during recrystallization of the biotites.

The fact that chlorine content in biotite retains its prograde or peak composition has been used in the Torres del Paine contact aureole together with bulk rock hydrogen and oxygen isotopes data to track channelized fluid infiltration from the magmatic intrusion. The fluid flow seems

to be of limited amount since oxygen isotopes does not record any significant trends in the contact aureole. In contrast, hydrogen isotopes show a decrease in the contact aureole due to Rayleigh fractionation behavior and at 150m of the intrusion the  $\delta D$  values increase again toward more magmatic signatures. Using the position of the hydrogen infiltration front, a fluid flux volume of  $4\text{m}^3$  per square meter of contact intrusion has been calculated. This relatively small value is in good agreement with the absence of change for the oxygen isotopes. Chlorine content in biotite shows constant values in the contact aureole, between 0.01 and 0.06 wt%, which represent the initial availability of chlorine for the growing biotites from the chlorite breakdown reaction, supporting the conclusions reached in the Western Adamello contact aureole. Close to the intrusion some samples show high Cl content in biotite (between 0.1 and 0.2 wt%), the rock texture suggested that these biotites have been recrystallized during the muscovite breakdown reaction and their Cl content was re-equilibrated with the high chloride fluid expelled from the intrusion during the crystallization of the first granite pulse. Late stage infiltration result in retrograde muscovite and chlorite + muscovite replacement of biotite and cordierite, but even biotites close to these textures maintain their high Cl content which is in good agreement with the conclusion of a very slow kinetics for Cl-OH exchange.

The basis for this thesis was the development and characterisation of standard materials for the analysis of chlorine, fluorine,  $\text{H}_2\text{O}$ , and oxygen isotopes, so that accurate values could be obtained through SIMS analysis.

The thesis documents that oxygen isotopes measurements using SIMS is hampered by an Instrumental Mass Fractionation (IMF) related to  $X_{\text{Mg}}$  and  $X_{\text{F}}$ . Biotite with relatively low F content (i.e. less than 0.2 wt%) can be modelled using only  $X_{\text{Mg}}$ . Additionally, no crystal orientation effect has been observed at the level of precision of 0.3‰. This allow accurate measurements in natural samples with a spatial resolution of  $10\mu\text{m}$  and with an uncertainty as

low as 0.4‰ ( $2\sigma$ ) for biotite of the same major element composition. For biotite of different composition or from different sessions, the final uncertainty on the absolute value is 0.5‰ ( $2\sigma$ ). The homogeneity of the same set of RMs has been investigated in terms of OH-F-Cl content with the SIMS. As for oxygen isotopes measurements, OH-F-Cl does not show any variations related to crystal orientation of the biotite grains. A potential drawback of the SIMS is the need for high vacuum for H<sub>2</sub>O measurements, it requires a pressure in the analysis chamber better than  $1 \cdot 10^{-8}$  mbar. In order to achieve such high vacuum, it is recommended to mount samples together with working RMs in indium mount rather than in epoxy. H<sub>2</sub>O, fluorine and chlorine content measurement exhibit matrix effect when measured using SIMS. But F and Cl content are simple, but non-linear functions of the measured ion-intensities ( $^{19}\text{F}/^{28}\text{Si}$  and  $^{35}\text{Cl}/^{30}\text{Si}$ , respectively). Accurate determination of the F and Cl content of biotite can be produced using second order polynomial fit for the RMs, except UNIL\_B4 for F content and UNIL\_B1 for Cl content since they are not homogeneous for in-situ measurements. H<sub>2</sub>O content has a more complex matrix effect that involves  $X_{\text{Mg}}$  in addition to the measured  $^{16}\text{O}^1\text{H}/^{28}\text{Si}$  ratio. Determination of the OH content of biotite requires a multivariate analysis, but accurate values can be determined using only 4 RMs, this allow to use only very homogeneous RMs (UNIL\_B1, B2 and B3 and NBS30).

### 6.3 Perspectives

In order to properly measure oxygen isotopes for biotite of high F content additional reference material with a F content comprised between 1 and 2 wt% should be added to the available set of RMs. This in order to test the linear behavior of this additional variable.

It is well known that using Cs<sup>+</sup> as primary beam increase the sensitivity for matrix effect due to the need of a normal electron beam to compensate for charging effect in non-conductive material such as minerals. The matrix effect described in the chapter 4 could be reduced or even

erased using an  $O^{2-}$  primary beam. Nevertheless, this would also impinge the extraction of Cl and F that have high yields with positive  $Cs^+$  source, but a low ion yield with  $O^{2-}$ . Hence this would increase the final uncertainty on the determination of these contents in biotite, and it is questionable if the necessary detection limits could be obtained.

The retentiveness of OH-F-Cl content in biotite has a strong influence on experimental procedures, since published experiments had relatively short duration. It is very unlikely that available experimental data represent equilibrium values between the biotite hydroxyl site composition and the fluid. In order to ensure that equilibrium has been attained, oxides should be put inside capsules to ensure that biotite grew during experiment and that measured composition represent the equilibrium value.

Finally, the potential link between  $H_2O$  content in biotite and water activity raises interest in many environments, and especially for the long-lived debate about the water activity at amphibolite-granulite transition. It is well known that water activity is reduced at these conditions but two very different theories have been called upon to explain these low water activity conditions. The first theory is known as fluid induced partial melting, evidences of  $CO_2$ - and NaCl-rich fluid inclusions, as well as K-feldspar replacement of plagioclase have led to the hypothesis of infiltration of low water activity fluids (either  $CO_2$ -rich or saline brines). The second is called dehydration melting theory since it states that the low water activity is only the result of removal of water from hydrous phase (biotite or amphibole mainly) that encounter dehydration reactions, water being incorporated into the melt phase leading to under-saturated conditions.

The determination of the absolute value for water activity relies on the use of experimentally calibrated stability for low-variant assemblages such as biotite-K-feldspar-orthopyroxene-quartz-melt. The determination of  $a_{H_2O}$  at the amphibolite-granulite transition has been recently revised (Aranovich et al. 2014) toward higher values (0.3-0.6). Nevertheless, the spread for the

different values of water activity is mainly due to discrepancy of the thermodynamic database, especially for biotite mineral. Using an experimentally calibrated OH content in biotite – water activity relationship could potentially reduce the uncertainty on the water activity determination at the amphibolite-granulite transition. The accuracy of this calibration could be tested using natural metacarbonate univariant assemblages, such as phlogopite-diospide-forsterite-tremolite-calcite-dolomite.

## 7 Appendix

## 7.1 Sample description for reference material

UNIL\_B1 is a deep black grain of several centimeters size. It was obtained from the Museum of Natural History of Lausanne and comes from a pegmatite. It was crushed to obtain grains of 1-3 mm size. UNIL\_B2 is from a meta-peridotite from the Western Gneiss Region (Norway). It consists of black grains of 1-2 mm size. UNIL\_B3 is from a diorite of the Ivrea zone, sampled by H. Hunziker (KAW1202). It is composed of black grains of 100-200µm size. UNIL\_B4 is from a biotite pyroxenite, sampled in the Similkameen composite pluton, Washington State (Ingamells and Engels 1976). It has black grains of 200-400 µm . It corresponds to RM LP-6 for Ar-Ar geochronology (Li *et al.* 2008). UNIL\_B5 is from a pegmatite in the southern part of the Brook Mountain, Seward Peninsula, Alaska. It consists of green grains of 0.8-1 mm. The original sample consisted of several grains of 0.5-1 cm size.

## 7.2 List of supplementary data in the dropbox link:

Chapter 2: Full biotite characterization from EPMA, homogeneity test for UNIL\_B1, orientation test and the two sessions of calibration for the matrix effect.

Chapter 4: SIMS homogeneity test for all RMs

Chapter 5: Full analyses of all biotites from the 5 studied samples.

## 7.3 Water activity – OH content in biotite link in metacarbonates from the Ubehebe Peak contact aureole

### 7.3.1 *Introduction*

In chapter 5, I proposed a direct link between the water activity and the hydroxyl concentration in biotites. In order to look at this I analyzed phlogopite in two siliceous dolomite samples from the Ubehebe Peak contact aureole. In these samples the biotites are pure phlogopites ( $X_{Mg} > 0.99$ ), with minor deviation from an ideal biotite formula. This allows to reduce the problems posed by multiple solid solution vectors discussed in detail in chapter 5 for biotites from metapelites, where substitution of, for example,  $Fe^{3+}$ , and  $Ti^{4+}$  in the octahedral site act as potential sources for oxy-components in the OH-site. Two samples were selected that equilibrated with significantly different fluid compositions in order to track the change in the hydroxyl site composition related to the change in water activity.

### 7.3.2 *Geological setting*

The Ubehebe Peak contact aureole is located in the Death Valley National Park (California). It was formed by the intrusion of the 173 Ma old quartz monzonite into a thick, steeply-dipping, Ordovician to Pennsylvania sequence (figure 2). The intrusion is part of a series of alkaline magmas forming the Hunter Mountain Batholith (McAllister 1955, 1956; Roselle et al. 1999). The sediments surrounding the intrusion consist of mostly siliceous dolomite. They have been contact metamorphosed by the monzonite and a series of isograds, the tremolite, forsterite and periclase have been mapped (figure 1a). The forsterite and periclase isograd require the infiltration of a water-rich fluid from the intrusion (Roseelle 1997). The formation of tremolite is triggered by the reaction  $dol + qtz + H_2O = cc + tr + CO_2$  and is in equilibrium with a fluid

with a  $X_{\text{CO}_2}$  of about 0.5. Forsterite nucleation is triggered by the reaction  $\text{tr} + \text{dol} = \text{fo} + \text{cc} + \text{H}_2\text{O} + \text{CO}_2$  with a water-rich fluid ( $X_{\text{CO}_2} \sim 0.05\text{-}0.1$ ).

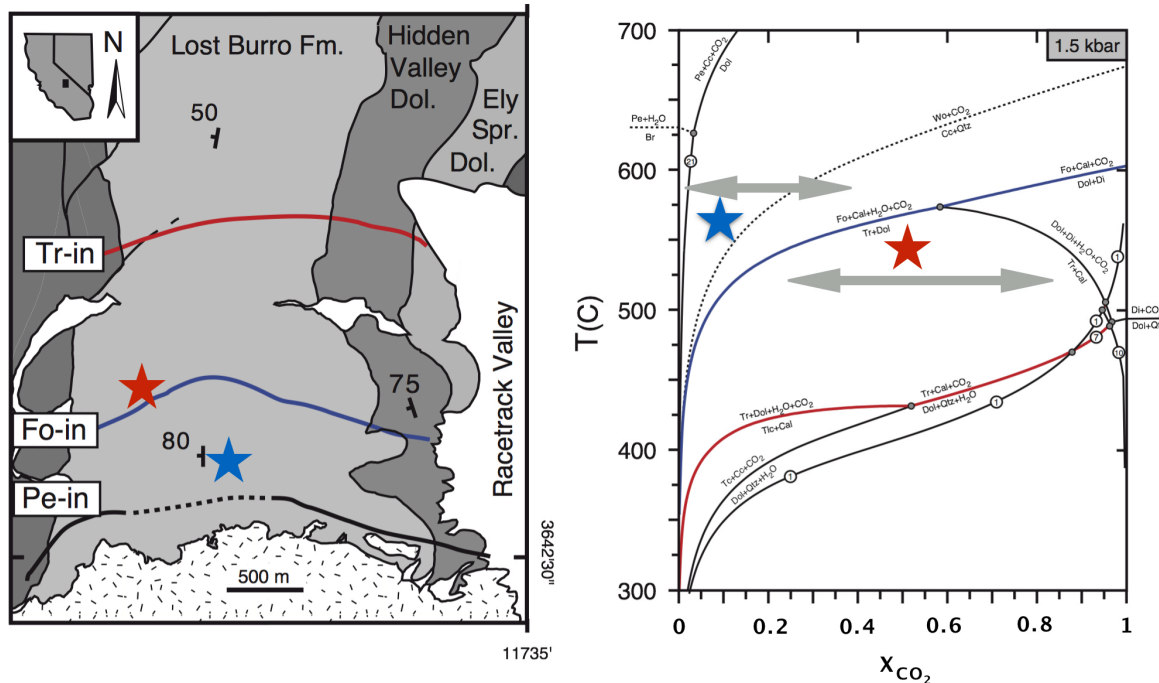


Figure 1: a) geological map of the Ubehebe Peak contact aureole, monzonite intrusion is located at the lowermost part of the figure. The lines represent the different isograds mapped in the aureole by Roselle (1997), as discussed in the text. The stars represent the position of the two samples studied (modified from Roselle 1997). b) Simplified  $T$ - $X_{\text{CO}_2}$  petrogenetic grid for siliceous dolomite. Reaction 1 represent the phlogopite-in reaction. The star colors refers to the figure 1a. Temperature was estimated based on thermometry by Mueller et al., 2008. Arrows illustrate the  $X_{\text{CO}_2}$  composition experienced at peak temperature, as inferred from Roselle 1997 (modified after Roselle 1997).

### 7.3.3 $\text{H}_2\text{O}$ content in phlogopite

The  $X_{\text{CO}_2}$  of the two samples spans large ranges. Nevertheless, it is clear that the forsterite sample (94UB71) was equilibrated with a  $\text{H}_2\text{O}$ -rich fluid and the tremolite sample (95UB218) with a more  $\text{CO}_2$ -rich fluid. The biotite in these two samples are almost pure phlogopite with  $X_{\text{Mg}}$  of 0.993 and 0.997, respectively. The very small amounts of Ti (0.062 and 0.037 per

formula unit, p.f.u.) and some  $\text{Al}^{\text{VI}}$  (0.174 and 0.166 p.f.u.). Variations in  $\text{Fe}^{2+}/\text{Fe}^{3+}$  does not have a measurable effect on the hydroxyl composition, since total Fe content is very small (0.037 and 0.015 p.f.u., respectively). These very pure phlogopite compositions allow us to conclude that any oxy-substitution that would occur would be of extremely minor consequence on the hydroxyl site stoichiometry.

Figure 2 show clearly that the phlogopite equilibrated with a water-rich fluid have significantly higher sum of measured anions ( $\text{OH}^- + \text{F}^- + \text{Cl}^-$ ) compare to the phlogopites from the sample equilibrated with a reduced water activity fluid. This strengthen the conclusion of the chapter 5 for the potentially significant variations of the hydroxyl nonstoichiometry due to the substitution:

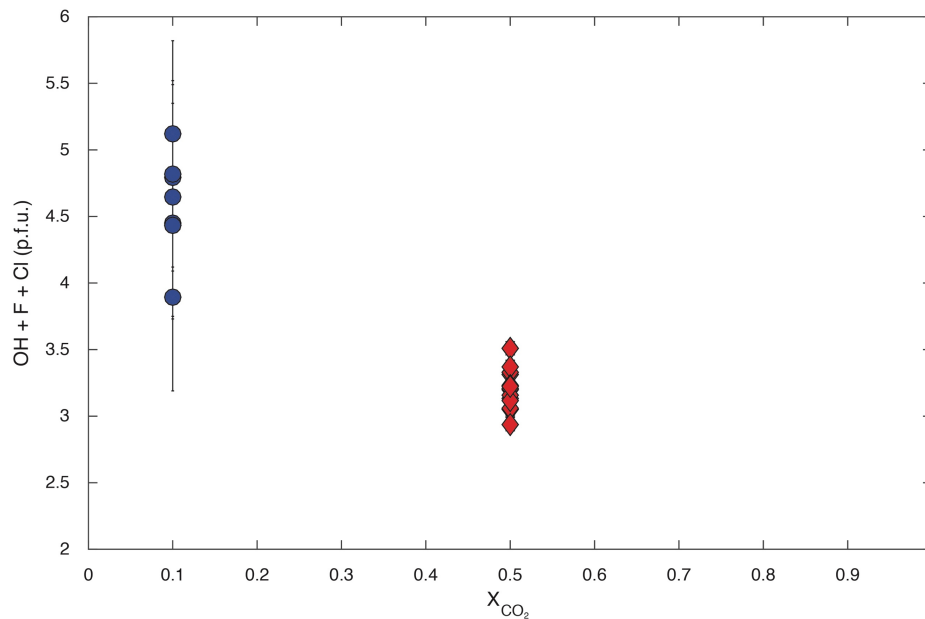


Figure 2: Sum of ( $\text{OH}^- + \text{F}^- + \text{Cl}^-$ ) measured with SIMS vs estimated  $X_{\text{CO}_2}$  for the phlogopites of the two samples from the Ubehebe contact aureole. The color code is the same than for figure 1 (i.e. blue circles represent measurements from sample 94UB71 and red diamond from 95UB218). Error bars represent the 1SD variations of the working reference material mount together with the sample, error is the size of the symbol in the case of the sample 95UB218.

Nevertheless, this conclusion is somewhat weakened by two analytical issues: the high uncertainty on the reference material UNIL\_B2 for the determination of the H<sub>2</sub>O content with the SIMS for the sample 94UB71 and the fact that the sum for the measured anions is above 4 for all phlogopites except one for the water-rich fluid equilibrated sample (fo-containing). The H<sub>2</sub>O content has been overestimated during this session and the analyses will be done again on another mount to avoid any artefact due to sample preparation. Nevertheless, sample 95UB218 shows low sum of hydroxyl anions (between 2.942 and 3.514), the fact that it cannot be explained by any common oxy-substitution due to the low Fe, Ti and Al<sup>VI</sup> contents is another argument for the importance of the substitution mentioned above. In the case of this sample, the uncertainty on H<sub>2</sub>O measurement was in the order of a normal session (i.e. 0.04wt% in this case), this is also reflected by the lower spread of the sum (OH<sup>-</sup> + F<sup>-</sup> + Cl<sup>-</sup>) compare to the sample 94UB71.

#### 7.3.4 Conclusion

The limitations from both the lack of a good constrain on the X<sub>CO<sub>2</sub></sub> for the tremolite sample and the low quality of analyses for the forsterite sample hinder a definite interpretation. Nevertheless, the low absolute value for the phlogopite from the sample 95UB218, equilibrated with a more CO<sub>2</sub>-rich fluid, cannot be explained by the traditionally used oxy-substitution due the low Fe, Ti and Al<sup>VI</sup> contents. Additional analyses on a new mount for sample 94UB71 or another sample equilibrated with a water-rich fluid need to be done to formally conclude on the importance of the link between water activity and H<sub>2</sub>O content in biotite.